

**INVESTIGATION THE EFFECT OF FILM FORMING AMINES  
ON THE CORROSION INHIBITION OF CARBON STEEL**

**M.Sc. Thesis by  
İpek ÖZTÜRK**

**Department : Polymer Science and Technology**

**Programme : Polymer Science and Technology**

**JANUARY 2011**



**INVESTIGATION THE EFFECT OF FILM FORMING AMINES  
ON THE CORROSION INHIBITION OF CARBON STEEL**

**M.Sc. Thesis by  
İpek ÖZTÜRK  
(515071028)**

**Date of submission : 20 December 2010**

**Date of defence examination: 24 January 2011**

**Supervisor (Chairman) : Prof. Dr. Esma SEZER (ITU)**

**Members of the Examining Committee : Prof. Dr. Belkıs USTAMEHMETOĞLU (ITU)  
Assis. Prof. Dr. Sibel ZOR (KU)**

**FEBRUARY 2011**



**İSTANBUL TEKNİK ÜNİVERSİTESİ ★ FEN BİLİMLERİ ENSTİTÜSÜ**

**KARBON ÇELİK KORORZYONUNU ÖNLENMEDE FİLM YAPICI AMİNLERİN  
ETKİLERİNİN İNCELENMESİ**

**YÜKSEK LİSANS TEZİ  
İpek ÖZTÜRK  
(515071028)**

**Tezin Enstitüye Verildiği Tarih : 20 Aralık 2010  
Tezin Savunulduğu Tarih : 24 Ocak 2011**

**Tez Danışmanı : Prof. Dr. Esmâ SEZER (İTÜ)  
Diğer Jüri Üyeleri : Prof. Dr. Belkıs USTAMEHMETOĞLU (İTÜ)  
Doç. Dr. Sibel ZOR (KÜ)**

**ŞUBAT 2011**



## **FOREWORD**

I would like to express my deep appreciation and thanks for my advisor, Professor Esmâ SEZER for her guidance and encouragement through this work.

I would also like to thank to my technical manager Dr. Wolfgang HATER from BK Giulini GmbH for their support during this study.

Finally, I would like to thank to my family and friends for being always with me and whatever supporting me.

This work is supported by Tübitak and ITU Institute of Science and Technology.

December 2010

İpek Öztürk  
Chemical Engineer





## TABLE OF CONTENTS

	<u>Page</u>
<b>FOREWORD</b> .....	<b>v</b>
<b>TABLE OF CONTENTS</b> .....	<b>vii</b>
<b>LIST OF ABBREVIATIONS</b> .....	<b>ix</b>
<b>LIST OF TABLES</b> .....	<b>xi</b>
<b>LIST OF FIGURES</b> .....	<b>xiii</b>
<b>SUMMARY</b> .....	<b>xvii</b>
<b>ÖZET</b> .....	<b>xix</b>
<b>1. INTRODUCTION</b> .....	<b>1</b>
<b>2. LITERATURE SURVEY</b> .....	<b>3</b>
2.1 Corrosion Definition .....	3
2.2 Corrosion Types .....	9
2.3 Corrosion Protection .....	12
2.3.1 Corrosion Protection Methods .....	13
2.3.2 Organic Corrosion Inhibitors .....	14
2.3.3 Filming Inhibitor Technology .....	16
2.4 Corrosion Test Methods .....	22
2.4.1 Non-Electrochemical Measurements .....	22
2.4.2 Electrochemical Measurements .....	23
<b>3. EXPERIMENTAL STUDY</b> .....	<b>31</b>
3.1 Materials.....	31
3.1.1 Seawater Preparation.....	32
3.1.2 Decarbonised Water Preparation.....	33
3.1.3 Deionised Water Preparation .....	34
3.2 Methods.....	34
<b>4. RESULTS AND DISCUSSIONS</b> .....	<b>37</b>
4.1 Measurements in Seawater.....	37
4.1.1 Measurements in the Absence of Inhibitor .....	37
4.1.2 Measurements in Seawater in the Presence of Inhibitors at pH=8 .....	39
4.1.3 Measurements in Seawater in the Presence of $R_uN_2$ at Different pH.....	46
4.1.4 Measurements in Seawater in the Presence of $R_sN_2$ at Different pH.....	48
4.2 Measurements in Decarbonised Water.....	49
4.2.1 Measurements in the Absence of Inhibitor .....	50
4.2.2 Measurements in Decarbonised Water in the Presence of Inhibitors at pH=8 .....	52
4.2.3 Measurements in Decarbonised Water in the Presence of $R_uN_2$ at Different pH.....	57
4.2.4 Measurements in Decarbonised Water in the Presence of $R_sN_2$ at Different pH.....	58
4.3 Measurements in Deionised Water .....	62

4.3.1 Measurements in the Absence of Inhibitor .....	62
4.3.2 Measurements in Deionised Water in the Presence of Inhibitors at pH=8 .....	64
4.3.3 Measurements in Deionised Water in the Presence of $R_uN_2$ at Different pH .....	66
4.3.4 Measurements in Deionised Water in the Presence of $R_SN_2$ at Different pH .....	68
4.4 Adsorption Mechanisms.....	71
4.5 SEM (Scanning Electron Microscopy) Measurements .....	75
<b>5. CONCLUSIONS.....</b>	<b>79</b>
<b>REFERENCES .....</b>	<b>83</b>
<b>APPENDICES .....</b>	<b>89</b>
<b>CURRICULUM VITA.....</b>	<b>99</b>

## LIST OF ABBREVIATIONS

<b>AC</b>	: Alternative Current
<b>BWR</b>	: Boiling Water Reactor
$\beta_a$	: Anodic Tafel Slope
$\beta_c$	: Cathodic Tafel Slope
<b>C<sub>C</sub></b>	: Coating Capacitance
<b>C<sub>dl</sub></b>	: Double Layer Capacitance
<b>CPE</b>	: Constant Phase Element
<b>DHW</b>	: Deutsche Hydrierwerke
<b>E<sub>corr</sub></b>	: Corrosion Potential
<b>EIS</b>	: Electrochemical Impedance Spectroscopy
<b>EN</b>	: Electrochemical Noise
<b>ER</b>	: Electrical Resistance
<b>FFA</b>	: Film Forming Amines
<b>IE</b>	: Inhibitor Efficiency
<b>I<sub>corr</sub></b>	: Corrosion Current
<b>LF</b>	: Low Frequency
<b>LPR</b>	: Linear Polarization Resistance
<b>ODA</b>	: Octadecylamine
<b>PPM</b>	: Part Per Million
<b>R<sub>ct</sub></b>	: Charge Transfer Resistance
<b>R<sub>p</sub></b>	: Polarization Resistance
<b>R<sub>po</sub></b>	: Pore Resistance
<b>R<sub>s</sub></b>	: Solution Resistance
<b>R<sub>S</sub>N</b>	: Saturated Monoamine
<b>R<sub>S</sub>N<sub>2</sub></b>	: Saturated Diamine
<b>R<sub>S</sub>N<sub>3</sub></b>	: Saturated Triamine
<b>R<sub>U</sub>N</b>	: Unsaturated Monoamine
<b>R<sub>U</sub>N<sub>2</sub></b>	: Unsaturated Diamine
<b>R<sub>U</sub>N<sub>3</sub></b>	: Unsaturated Triamine
<b>SEM</b>	: Scanning Electron Microscopy
<b>SCC</b>	: Stress Corrosion Cracking



## LIST OF TABLES

	<u>Page</u>
<b>Table 2.1</b> : Possible reactions in the Fe-H <sub>2</sub> O system between the species most in wet conditions .....	7
<b>Table 2.2</b> : Possible reactions in the Fe-H <sub>2</sub> O system between the species most in dry conditions.....	8
<b>Table 3.1</b> : Formula for 1 kg of 35% artificial seawater .....	33
<b>Table 3.2</b> : The ion content for the 35% w/w artificial seawater .....	33
<b>Table 3.3</b> : Chemical composition of the decarbonised water used during the experiments .....	34
<b>Table 4.1</b> : Polarization parameters for carbon steel in seawater at 25 °C in absence of inhibitors at different pH values.....	39
<b>Table 4.2</b> : Polarization parameters for carbon steel in seawater at 25 °C in absence and with different inhibitors at pH 8 .....	41
<b>Table 4.3</b> : Values of the elements of equivalent circuit required for fitting EIS of carbon steel in seawater in absence and presence of the different inhibitors at pH=8.....	44
<b>Table 4.4</b> : Polarization parameters and the corresponding inhibition efficiency for the corrosion of carbon steel in seawater in absence and with different inhibitors at pH=8.....	46
<b>Table 4.5</b> : Polarization parameters for carbon steel in seawater at 25 °C with R <sub>U</sub> N <sub>2</sub> at varying pH values.....	48
<b>Table 4.6</b> : Polarization parameters for carbon steel in seawater at 25 °C with R <sub>S</sub> N <sub>2</sub> at varying pH values .....	50
<b>Table 4.7</b> : Polarization parameters for carbon steel in decarbonised water at 25 °C in absence of inhibitors .....	51
<b>Table 4.8</b> : Polarization parameters for carbon steel in decarbonised water at 25 °C in absence and presence of inhibitors at pH= 8.....	53
<b>Table 4.9</b> : Values of the elements of equivalent circuit required for fitting the EIS of carbon steel in decarbonised water in absence and presence of different inhibitors at pH=8 .....	55
<b>Table 4.10</b> : Polarization parameters and the corresponding inhibition efficiency for the corrosion of carbon steel in decarbonised water in absence and with different inhibitors at pH=8.....	56

<b>Table 4.11</b>	: Polarization parameters for carbon steel in decarbonised water at 25 °C with $R_{U}N_2$ at varying pH values.....	58
<b>Table 4.12</b>	: Polarization parameters for carbon steel in decarbonised water at 25 °C with $R_S N_2$ at different pH values.....	60
<b>Table 4.13</b>	: Polarization parameters for carbon steel in deionised water at 25 °C in absence of inhibitors .....	64
<b>Table 4.14</b>	: Polarization parameters for carbon steel in deionised water at 25 °C in absence and presence of different inhibitors at pH= 8.....	66
<b>Table 4.15</b>	: Polarization parameters and the corresponding inhibition efficiency for the corrosion of carbon steel in deionised water in absence and with different inhibitors at pH=8.....	66
<b>Table 4.16</b>	: Polarization parameters for carbon steel in deionised water at 25 °C with $R_{U}N_2$ at different pH values .....	68
<b>Table 4.17</b>	: Polarization parameters for carbon steel in deionised water at 25 °C with $R_S N_2$ at different pH values.....	69
<b>Table 4.18</b>	: Values of the elements of equivalent circuit required for fitting the EIS of carbon steel in deionised water in absence and presence of $R_{U}N_2$ and $R_S N_2$ at pH=11.....	71
<b>Table 4.19</b>	: Langmuir isotherm adsorption parameters for $R_S N_2$ in decarbonised water at pH=8 at 25 °C .....	72
<b>Table 4.20</b>	: Concentration and degree of coverage values for $R_S N_2$ in decarbonised water at pH=8 at 25 °C .....	72
<b>Table 4.21</b>	: Langmuir isotherm adsorption parameters for $R_{U}N_2$ in decarbonised water at pH=8 at 25 °C .....	73
<b>Table 4.22</b>	: Concentration and degree of coverage values for $R_{U}N_2$ in decarbonised water at pH=8 at 25 °C .....	74
<b>Table 5.1</b>	: Inhibitor efficiencies of different inhibitors obtained from polarization data in different water qualities 25 °C at pH=8.....	81
<b>Table A.1</b>	: Polarization parameters for carbon steel in decarbonised water at 25 °C with $R_S N$ at different pH values .....	93
<b>Table A.2</b>	: Polarization parameters for carbon steel in decarbonised water at 25 °C with $R_S N_3$ at different pH values.....	94
<b>Table A.3</b>	: Polarization parameters for carbon steel in decarbonised water at 25 °C with $R_{U}N$ at different pH values.....	96
<b>Table A.4</b>	: Polarization parameters for carbon steel in decarbonised water at 25 °C with $R_{U}N_3$ at different pH values .....	97

## LIST OF FIGURES

	<u>Page</u>
<b>Figure 2.1</b> : Simple model describing the electrochemical nature of corrosion Process .....	4
<b>Figure 2.2</b> : Metal corrosion mechanism .....	5
<b>Figure 2.3</b> : E-pH diagram of iron or steel with four concentrations of soluble species, three soluble species and two wet corrosion products (25 °C) .....	6
<b>Figure 2.4</b> : Thermodynamic stability of water, oxygen and hydrogen.....	8
<b>Figure 2.5</b> : Thermodynamic boundaries of the types of corrosion observed on steel. ....	9
<b>Figure 2.6</b> : Factors influencing corrosion fatigue.....	10
<b>Figure 2.7</b> : Various types of corrosion.....	11
<b>Figure 2.8</b> : Distribution of corrosion types in BWR (boiling water reactor) plants in Germany (Evaluation of reportable events 1968 – 2001) ...	12
<b>Figure 2.9</b> : Chemical structure of fatty amines.....	18
<b>Figure 2.10</b> : FFA adsorption on metal surface .....	20
<b>Figure 2.11</b> : Corrosion process showing anodic and cathodic current components. ....	26
<b>Figure 2.12</b> : Nyquist plot with impedance vector.....	27
<b>Figure 2.13</b> : Common electrical elements .....	28
<b>Figure 2.14</b> : The simplified Randles circuit.....	28
<b>Figure 3.1</b> : Generic chemical structure of the different film forming amines .....	31
<b>Figure 3.2</b> : Three electrode type electrochemical cell .....	32
<b>Figure 4.1</b> : Nyquist plot for carbon steel in sea water at 25 °C in absence of inhibitors at different pH values.....	38
<b>Figure 4.2</b> : Potentiodynamic polarization curves for carbon steel in sea water at 25°C in absence of inhibitors at different pH values.....	39
<b>Figure 4.3</b> : Nyquist plot for carbon steel in sea water at 25 °C in absence and with unsaturated filming amines at pH=8 .....	40
<b>Figure 4.4</b> : Nyquist plot for carbon steel in sea water at 25 °C in absence and with saturated filming amines at pH=8 .....	40

<b>Figure 4.5</b>	: Nyquist plot for carbon steel in seawater at 25 °C in absence and presence of different inhibitors at pH=8.....	41
<b>Figure 4.6</b>	: Values of the elements of equivalent circuit required for fitting the EIS of carbon steel in seawater in absence of different inhibitors at pH=8.....	42
<b>Figure 4.7</b>	: Values of the elements of equivalent circuit required for fitting the EIS of carbon steel in seawater in presence of different inhibitors at pH=8.....	43
<b>Figure 4.8</b>	: Potentiodynamic polarization curves for carbon steel in sea water at 25°C in absence and with different inhibitors at pH=8 .....	44
<b>Figure 4.9</b>	: Nyquist plot for carbon steel in sea water at 25 °C with $R_{UN_2}$ at different pH values .....	47
<b>Figure 4.10</b>	: Potentiodynamic polarization curves for carbon steel in sea water at 25°C with $R_{UN_2}$ at different pH values .....	47
<b>Figure 4.11</b>	: Nyquist plot for carbon steel in sea water at 25°C with $R_{SN_2}$ at different pH values .....	49
<b>Figure 4.12</b>	: Potentiodynamic polarization curves for carbon steel in sea water at 25°C with $R_{SN_2}$ at different pH values.....	49
<b>Figure 4.13</b>	: Nyquist plot for carbon steel in decarbonised water at 25 °C in absence of inhibitors at different pH values .....	50
<b>Figure 4.14</b>	: Potentiodynamic polarization curves for carbon steel in decarbonised water at 25 °C in absence of inhibitors at different pH values .....	51
<b>Figure 4.15</b>	: Nyquist plot for carbon steel in decarbonised water at 25 °C in absence and with different inhibitors at pH=8.....	52
<b>Figure 4.16</b>	: Nyquist plot for carbon steel in decarbonised water at 25 °C in absence and presence unsaturated and saturated di- and triamines at pH=8 .....	53
<b>Figure 4.17</b>	: Values of the elements of equivalent circuit required for fitting the EIS of carbon steel in decarbonised water in absence of inhibitors at pH=8.....	54
<b>Figure 4.18</b>	: Values of the elements of equivalent circuit required for fitting the EIS of carbon steel in decarbonised water in presence of different inhibitors at pH=8.....	55
<b>Figure 4.19</b>	: Potentiodynamic polarization curves for carbon steel in decarbonised water at 25 °C in absence with different inhibitors at different pH values .....	56
<b>Figure 4.20</b>	: Nyquist plot for carbon steel in decarbonised water at 25 °C with $R_{UN_2}$ at different pH values .....	57
<b>Figure 4.21</b>	: Potentiodynamic polarization curves for carbon steel in decarbonised water at 25°C with $R_{UN_2}$ at different pH values .....	58
<b>Figure 4.22</b>	: Nyquist plot for carbon steel in decarbonised water at 25 °C with $R_{SN_2}$ at different pH values.....	59



<b>Figure 4.23</b>	: Potentiodynamic polarization curves for carbon steel in decarbonised water at 25°C with $R_S N_2$ at different pH values.....	60
<b>Figure 4.24</b>	: Nyquist plot for carbon steel in deionised water at 25 °C in absence of inhibitors at different pH values.....	62
<b>Figure 4.25</b>	: Nyquist plot for carbon steel in deionised water at 25 °C in absence of inhibitors at pH 11.....	63
<b>Figure 4.26</b>	: Potentiodynamic polarization curves for carbon steel in deionised water at 25 °C in absence of inhibitors at different pH values.....	63
<b>Figure 4.27</b>	: Nyquist plot for carbon steel in deionised water at 25 °C in absence and with different inhibitors at pH=8.....	64
<b>Figure 4.28</b>	: Potentiodynamic polarization curves for carbon steel in deionised water at 25 °C in absence with different inhibitors at different pH values.....	65
<b>Figure 4.29</b>	: Nyquist plot for carbon steel in deionised water at 25 °C with $R_U N_2$ at different pH values.....	67
<b>Figure 4.30</b>	: Potentiodynamic polarization curves for carbon steel in deionised water at 25°C with $R_U N_2$ at different pH values.....	67
<b>Figure 4.31</b>	: Nyquist plot for carbon steel in deionised water at 25 °C with $R_S N_2$ at different pH values.....	68
<b>Figure 4.32</b>	: Potentiodynamic polarization curves for carbon steel in deionised water at 25°C with $R_S N_2$ at different pH values.....	69
<b>Figure 4.33</b>	: Values of the elements of equivalent circuit required for fitting the EIS of carbon steel in deionised water with $R_S N_2$ at pH 11.....	70
<b>Figure 4.34</b>	: Langmuir isotherm adsorption plot of $R_S N_2$ in decarbonised water at 25°C at pH=8.....	73
<b>Figure 4.35</b>	: Langmuir isotherm adsorption plot of $R_U N_2$ in decarbonised water at 25°C at pH=8.....	74
<b>Figure 4.36</b>	: SEM image ( x 500, x 200) of the carbon steel electrode obtained after 1 h immersion a) without inhibitor b) in the presence of $R_U N_2$ c) in the presence of $R_S N_2$ in decarbonised water at pH=8 at 25 °C ..	75
<b>Figure 4.37</b>	: SEM image ( x 500, x 200) of the carbon steel electrode obtained after 1 h immersion a) without inhibitor b) in the presence of $R_U N_2$ c) in the presence of $R_S N_2$ in seawater at pH=8 at 25 °C ..	76
<b>Figure 4.38</b>	: SEM image ( x 500, x 200) of the carbon steel electrode obtained after 1 h immersion a) without inhibitor b) in the presence of $R_U N_2$ c) in presence of $R_U N_2$ d) in the presence of $R_S N_2$ in deionised water at pH=8 at 25 °C ..	77
<b>Figure A.1</b>	: Nyquist plot for carbon steel in decarbonised water at 25 °C with $R_S N_2$ at 3 different pH values ..	91
<b>Figure A.2</b>	: Nyquist plot for carbon steel in deionised water at 25 °C with in absence and presence of $R_U N_2$ and $R_S N_2$ at pH =11 ..	91

<b>Figure A.3</b>	: Potentiodynamic polarization curves for carbon steel in decarbonised water at 25°C with $R_S N$ at different pH values .....	92
<b>Figure A.4</b>	: Nyquist plot for carbon steel in decarbonised water at 25 °C with $R_S N$ at different pH values .....	92
<b>Figure A.5</b>	: Potentiodynamic polarization curves for carbon steel in decarbonised water at 25°C with $R_S N_3$ at different pH values.....	93
<b>Figure A.6</b>	: Nyquist plot for carbon steel in decarbonised water at 25 °C with $R_S N_3$ at different pH values.....	93
<b>Figure A.7</b>	: Potentiodynamic polarization curves for carbon steel in decarbonised water at 25°C with $R_U N$ at different pH values.....	95
<b>Figure A.8</b>	: Nyquist plot for carbon steel in decarbonised water at 25 °C with $R_U N$ at different pH values.....	95
<b>Figure A.9</b>	: Potentiodynamic polarization curves for carbon steel in decarbonised water at 25°C with $R_U N_3$ at different pH values .....	96
<b>Figure A.10</b>	: Nyquist plot for carbon steel in decarbonised water at 25 °C with $R_U N_3$ at different pH values.....	97

# **INVESTIGATION THE EFFECT OF FILM FORMING AMINES ON THE CORROSION INHIBITION OF CARBON STEEL**

## **SUMMARY**

In this study, the behavior of the carbon steel, in presence of different inhibitive formulations based of film forming amines of different structures, by steady-state current-voltage curves and electrochemical impedance spectroscopy measurements was studied. Sea, decarbonised and deionised water qualities were examined in absence of and with inhibitors at varying pH values from 5 to 11 in order to to observe the pH dependency of the inhibitors at corrosion inhibition. Also, at the same pH value (pH 8), 6 different inhibitors were examined at 3 different water quality in order to obtain the relationship between the inhibitor structure and inhibitor efficiency, additionally by the effect of different corrosive media. Moreover, adsorption isotherm plots were observed by using EIS data at decarbonised water which has low electrical conductivity close to that encountered in natural waters at pH=8 in order to understand the corrosion inhibition mechanism. Also, surface structure of some corroded carbon steel electrodes were examined by the scanning electron microscope (SEM) that images the sample surface by scanning it with a high-energy beam of electrons in a raster scan pattern and provides information about the sample's surface topography, composition and other properties such as electrical conductivity.

Because corrosion occurs via electrochemical reactions, electrochemical techniques are ideal for the study of the corrosion processes. The electrochemical impedance spectroscopy (EIS) is one of the most effective and reliable method to extract information about electrochemical characteristics of the electrochemical system. Electrochemical measurements, including potentiodynamic polarization curves and electrochemical impedance spectroscopy (EIS) were performed in a three-electrode cell.

During the work, EIS data is also analyzed by fitting it to an equivalent electrical circuit model. Most of the circuit elements in the model are common electrical elements such as resistors, capacitors, and inductors. From the data obtained, it is intended to develop structure/property relations in order to find optimal corrosion inhibitors.



## **KARBON ÇELİĞİN KOROZYONUNU ÖNLEMEDE FİLM YAPICI AMİNLERİN ETKİLERİNİN İNCELENMESİ**

### **ÖZET**

Bu çalışmada, kararlı durum akım-gerilim eğrileri ve elektrokimyasal impedans ölçümleri kullanılarak, karbon çeliğin korozyonunu önlemede farklı formülasyonlara sahip aminlerin etkileri incelenmiştir. 5 ve 11 arasında değişen pH değerleri arasında, korozyon inhibitörü olarak kullanılan farklı yapıdaki poliaminlerin varlığında ve inhibitörler olmadan korozif ortam olarak seçilen deniz suyu, dekarbonize su ve deiyonize suyunda pH değerine bağlı korozyon önleme etkileri incelenmiştir. Aynı zamanda, pH değeri 8 değerinde sabit tutularak, 3 farklı korozif ortamda 6 farklı inhibitörün korozyon önleme performansları tespit edilmiştir. Böylece değişen inhibitör yapısının farklı su kalitelerindeki etkinlikleri saptanmıştır. İlave olarak, nispeten doğal su kaynaklarında rastlanan düşük iletkenlik değerine sahip olan dekarbonize sudan pH 8 değerinde elektrokimyasal impedans spektroskopisi ile elde edilen veriler ile inhibitörlerin korozyon önleme mekanizmalarını tespit etmek amacıyla adsorpsiyon izotermeleri oluşturulmuştur.

Taramalı Elektron Mikroskobu (SEM) ile inhibitör kullanılmadığı ve inhibitör kullanıldığı durumlardaki karbon çelik malzemenin yüzeyi, yüksek enerjili elektronlarla yüzeyin taranması incelenmiştir. Bu metod ile yüzeylerin engebeli (topografik) yapısıyla, kompozisyonu ve elektriksel iletkenlikleri gibi özellikleriyle ilişkili bilgi elde edilir.

Korozyon olgusu elektrokimyasal reaksiyonlar sonucu oluştuğu için, korozyon prosesinin çalışmaları sırasında elektrokimyasal yöntemler kullanılmıştır. Elektrokimyasal impedans spektroskopisi, elektrokimyasal sistemlerin karakteristikleri hakkında bilgi edinmede kullanılan en etkin ve güvenilir metotlardan biridir. Deneyler sırasında, potansiyodinamik polarizasyon eğrileri ve elektrokimyasal impedans spektroskopisinin kullanıldığı elektrokimyasal ölçümler 3 elektrotlu hücrelerde gerçekleştirilmiştir.

Çalışma sırasında ayrıca EIS dataları eşlenik elektrik devre modelleri oluşturularak da analiz edilmiştir. Oluşturulan devre elemanları genellikle yaygın olarak kullanılan direnç, kapasitör ve indüktör gibi elektrik devre elemanlarıdır. Elde edilen bütün veriler ile yapı / özellik ilişkisine bağlı olarak en uygun korozyon inhibitörün tespiti amaçlanmıştır.



## 1. INTRODUCTION

Corrosion is the destructive attack of a material by reaction with its environment. The serious consequences of the corrosion process have become a problem of worldwide significance. In addition to our everyday encounters with this form of degradation, corrosion causes plant shutdowns, waste of valuable resources, loss or contamination of product, reduction in efficiency, costly maintenance, and expensive overdesign; it also jeopardizes safety and inhibits technological progress.

Corrosion control is achieved by recognizing and understanding corrosion mechanisms, by using corrosion-resistant materials and designs, and by using protective systems, devices, and treatments [1,2].

A synergism, or cooperation, is often present between different inhibitors and the environment being controlled, and mixtures are the usual choice in commercial formulations. The scientific and technical corrosion literature has descriptions and lists of numerous chemical compounds that exhibit inhibitive properties. Of these, only very few are actually used in practice. This is partly because the desirable properties of an inhibitor usually extend beyond those simply related to metal protection. Considerations of cost, toxicity, availability, and environmental friendliness are of considerable importance [3].

Due to stringent environmental regulations and as well as human safety, inorganic corrosion inhibitors such as chromates, nitrites, polyphosphates, zinc salts or oxides incorporated in protective coatings for mild steel are being replaced by organic compounds [4,5].

The present work was designed to gain further understanding of the inhibition mechanism of organic corrosion inhibitors, film forming amines, (FFA). Comparative studies have been carried out to evaluate the efficiency of film forming amines, and to optimize their inhibitive properties against the corrosion of carbon steel.

Because corrosion occurs via electrochemical reactions, electrochemical techniques are ideal for the study of the corrosion processes [6].

In this aim, the work is devoted to study the behavior of the carbon steel, in presence of different inhibitive formulations based of FFA of different structures, by steady-state current-voltage curves and impedance spectroscopy measurements. From the data obtained, it is intended to develop structure/property relations in order to find optimal corrosion inhibitors.

The electrochemical impedance spectroscopy (EIS) is one of the most effective and reliable method to extract information about electrochemical characteristics of the electrochemical system for instance double layer capacitance ( $C_{dl}$ ), determination of the rate of the charge transfer and charge transport processes and solution resistance etc..

In the first part of the study, 3 different water qualities are examined in absence of and with inhibitors at varying pH values from 5 to 11 in order to to observe the pH dependency of the inhibitors at corrosion inhibition.

In the second part of the study, at the same pH value (pH 8), 6 different inhibitors were examined at 3 different water quality in order to obtain the relationship between the inhibitor structure and inhibitor efficiency, additionally by the effect of different corrosive media.

In the last part, adsorption isotherm plots were observed by using EIS data at decarbonised water at pH=8 in order to obtain the corrosion inhibition mechanism. Also, surface structure of some corroded carbon steel electrodes were examined by the scanning electron microscope (SEM) in order to obtain information about the sample's surface topography.



## 2. LITERATURE SURVEY

### 2.1 Corrosion Definition

The corrosion of metals occurs primarily by electrochemical processes involving metal oxidation and simultaneous reduction of some other species. The fundamental understanding of these processes has allowed the development of a number of electrochemical techniques for the study of the corrosion phenomena and assessment of the corrosion rate [2].

Water is used for a wide variety of purposes, from supporting life as potable water to performing a multitude of industrial tasks such as heat exchange and waste transport. The impact of water on the integrity of materials is thus an important aspect of system management. Since steels and other iron-based alloys are the metallic materials most commonly exposed to water, aqueous corrosion has been discussed with a special focus on the reactions of iron (Fe) with water (H<sub>2</sub>O).

The main force behind corrosion is the tendency of iron to break down into its natural state. The iron found in pipe is elemental iron (Fe<sup>0</sup>) which is unstable and tends to oxidize, to join with oxygen or other elements. In nature, this oxidation produces an iron ore such as hematite (Fe<sub>2</sub>O<sub>3</sub>), magnetite (Fe<sub>3</sub>O<sub>4</sub>), iron pyrite (FeS<sub>2</sub>), or siderite (FeCO<sub>3</sub>). In corrosion, the result of this oxidation is rust, Fe(OH)<sub>2</sub> or Fe(OH)<sub>3</sub> [7].

Oxidation of the elemental iron occurs at the anode. First, the elemental iron breaks down (Equation 2.1). In this reaction, elemental iron leaves the pipe, so pits form in the pipe's surface at the anode.

Elemental Iron → Ferrous iron + Electrons



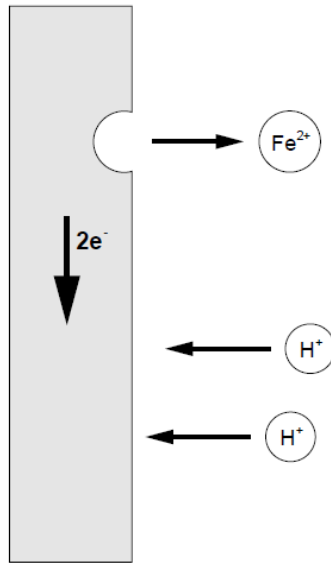


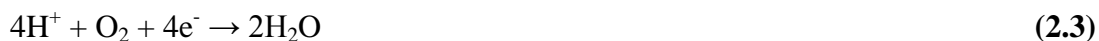
**Figure 2.1** : Simple model describing the electrochemical nature of corrosion process [7].

The reaction produces ferrous iron and two electrons. The electrons are then able to flow through the pipe wall to the cathode [8]. This reaction is rapid in most media, as shown by the lack of pronounced polarization when iron is made an anode employing an external current. When iron corrodes, the rate is usually controlled by the cathodic reaction, which in general is much slower (cathodic control). In deaerated solutions, the cathodic reaction is:



This reaction proceeds rapidly in acids, but only slowly in alkaline or neutral aqueous media. The corrosion rate of iron in deaerated neutral water at room temperature, for example, is less than 5  $\mu\text{m}/\text{year}$ . The rate of hydrogen evolution at a specific pH depends on the presence or absence of low-hydrogen overvoltage impurities in the metal. For pure iron, the metal surface itself provides sites for  $\text{H}_2$  evolution; hence, high-purity iron continues to corrode in acids, but at a measurably lower rate than does commercial iron.

The cathodic reaction can be accelerated by the reduction of dissolved oxygen in accordance with the following reaction, a process called depolarization (Equation 2.3).



Dissolved oxygen reacts with hydrogen atoms adsorbed at random on the iron surface, independent of the presence or absence of impurities in the metal. The oxidation reaction proceeds as rapidly as oxygen reaches the metal surface.

Meanwhile, the ferrous iron reacts with the water (the electrolyte) in the pipe to produce rust and hydrogen ions [7].

Ferrous iron + Water + Oxygen  $\leftrightarrow$  Ferrous hydroxide



The rust builds up a coating over the anode's surface. Ferrous hydroxide may then react with more water to produce another form of rust called ferric hydroxide ( $\text{Fe}(\text{OH})_3$ ).

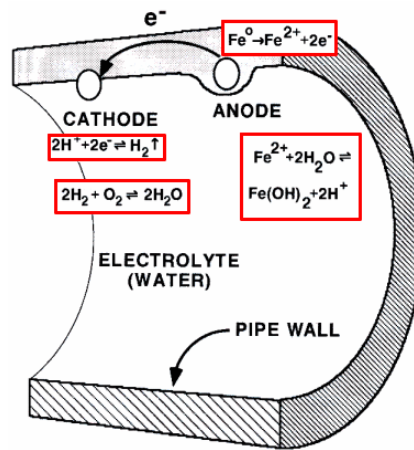


**Figure 2.2 :** Metal corrosion mechanism [8].

Corrosive attack of a metal can take place either uniformly or as a localised attack at specified sites. If the activities of all the local action cells are approximately the same, uniform corrosion occurs resulting in a general thinning of the metal. When some of the local cells are more active than others, localised corrosion such as pitting will occur.

Although corrosion is a dynamic process, thermodynamics can provide a good starting point for discussion. The thermodynamic stability of a metal in a solution is often represented in the form of a Pourbaix diagram, or E-pH, such as the ones shown in Figure 2.3 for iron [9]. Pourbaix diagrams are thermodynamic diagrams which show the ability of metals to be attacked, dissolved or corroded at various pH

and oxidation conditions [10]. Figure 2.3 illustrates the E-pH diagram for iron in the presence of water or humid environments at 25°C, which was calculated by considering all possible reactions associated with iron in wet or aqueous conditions listed in the Table 2.1, excluding therefore drier forms of corrosion products such as magnetite (Fe<sub>3</sub>O<sub>4</sub>) or iron (ferric) oxide (Fe<sub>2</sub>O<sub>3</sub>).

At potentials more positive than -0.6 V and at pH values below about 9, ferrous ion (Fe<sup>2+</sup> or Fe II) is the stable substance (Figure 2.3). This indicates that iron will corrode under these conditions. In other regions of the iron E-pH diagram, it can be seen that the corrosion of iron produces ferric ions (Fe<sup>3+</sup> or Fe III), ferric hydroxide [Fe(OH)<sub>3</sub>], ferrous hydroxide [Fe(OH)<sub>2</sub>], and at very alkaline conditions, complex HFeO<sub>2</sub><sup>-</sup> ions. The solid corrosion products considered are different than earlier, ferric oxide (Fe<sub>2</sub>O<sub>3</sub>) and magnetite (Fe<sub>3</sub>O<sub>4</sub>), both important iron ore constituents [12].

The various stability regions for these drier corrosion products are shown in Table 2.2 where the predominant compounds and ions are also indicated.

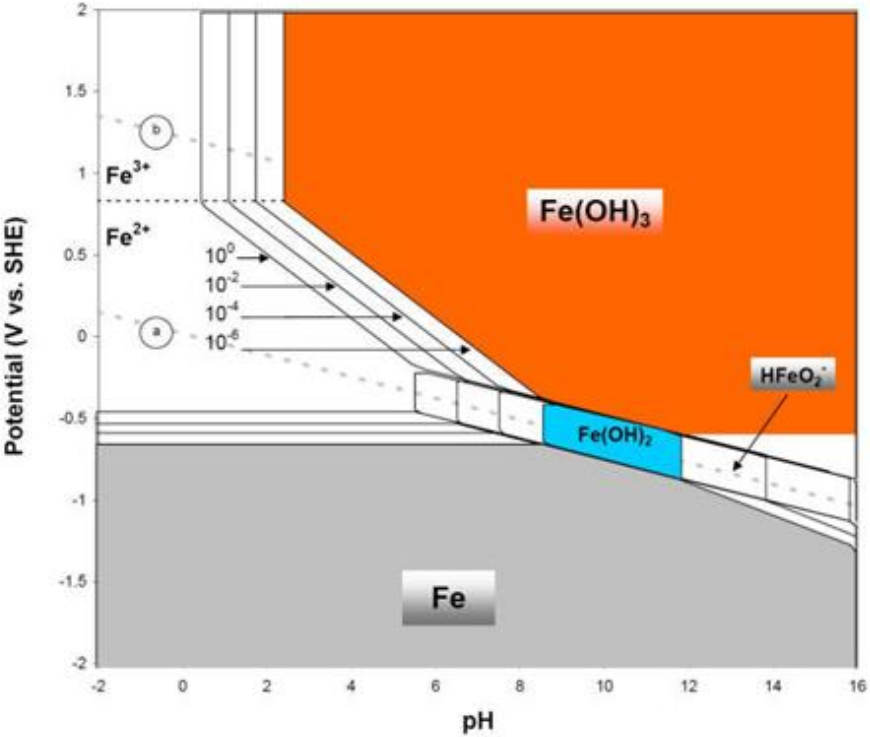


**Figure 2.3 :** E-pH diagram of iron or steel with four concentrations of soluble species, three soluble species and two wet corrosion products (25°C).

**Table 2.1:** Possible reactions in the Fe-H<sub>2</sub>O system between the species most stable in wet conditions.

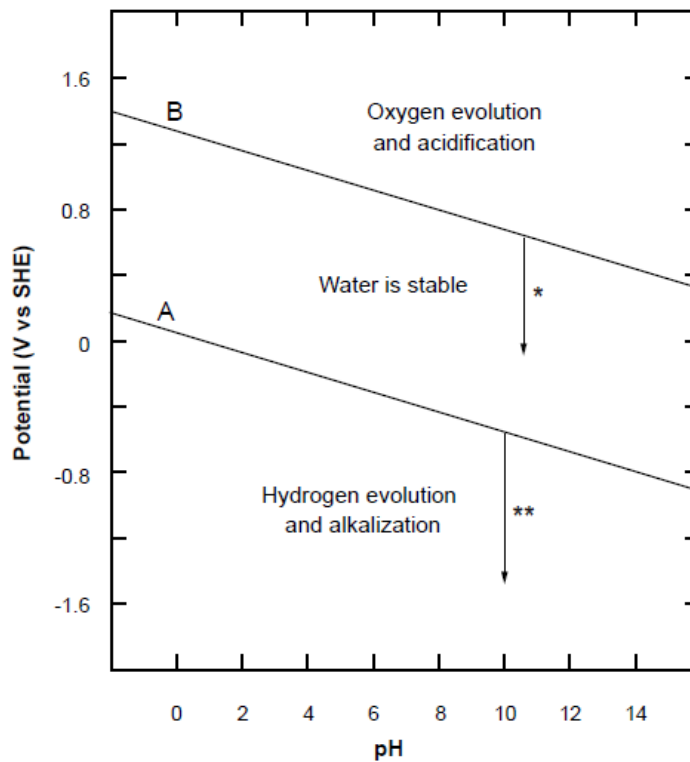
<b>Equilibria</b>
1. $2e^- + 2H^+ = 1H_2$
2. $4e^- + 1O_2 + 4H^+ = 2H_2O$
3. $2e^- + 1Fe(OH)_2 + 2H^+ = 1Fe + 2H_2O$
4. $2e^- + 1Fe^{2+} = 1Fe$
5. $2e^- + 1Fe(OH)_3 + 3H^+ = 1Fe + 3H_2O$
6. $1e^- + 1Fe(OH)_3 + 1H^+ = 1Fe(OH)_2 + 1H_2O$
7. $1e^- + 1Fe(OH)_3 + 1H^+ = 1Fe^{2+} + 3H_2O$
8. $1Fe(OH)_3 + 1H^+ = 1Fe(OH)_2 + 1H_2O$
9. $1e^- + 1Fe(OH)_3 = 1Fe(OH)_3^-$
10. $1Fe^{3+} + 3H_2O = 1Fe(OH)_3 + 3H^+$
11. $1Fe^{2+} + 2H_2O = 1Fe(OH)_2 + 2H^+$
12. $1e^- + 1Fe^{3+} = 1Fe^{2+}$
13. $1Fe^{2+} + 1H_2O = 1FeOH^+ + 1H^+$
14. $1FeOH^+ + 1H_2O = 1Fe(OH)_{2(sln)} + 1H^+$
15. $1Fe(OH)_{2(sln)} + 1H_2O = 1Fe(OH)_3^- + 1H^+$
16. $1Fe^{3+} + 1H_2O = 1FeOH^{2+} + 1H^+$
17. $1FeOH^{2+} + 1H_2O = 1Fe(OH)_2 + 1H^+$
18. $1Fe(OH)_2 + 1H_2O = 1Fe(OH)_{3(sln)} + 1H^+$
19. $1e^- + 1FeOH^{2+} + 1H^+ = 1Fe^{2+} + 1H_2O$
20. $1e^- + 1Fe(OH)_2 + 2H^+ = 1Fe^{2+} + 2H_2O$
21. $1e^- + 1Fe(OH)_{3(sln)} + 1H^+ = 1Fe(OH)_{2(sln)} + 1H_2O$
22. $1e^- + 1Fe(OH)_{3(sln)} + 2H^+ = 1FeOH^+ + 2H_2O$
23. $1e^- + 1Fe(OH)_{3(sln)} + 3H^+ = 1Fe^{2+} + 3H_2O$

In Figure 2.4, A is the equilibrium line for the reaction:  $H_2 \rightarrow 2H^+ + 2e^-$ . B is the equilibrium line for the reaction:  $2H_2O \rightarrow O_2 + 4H^+ + 4e^-$ . \* indicates increasing thermodynamic driving force for cathodic oxygen reduction, as the potential falls below line B. \*\* indicates increasing thermodynamic driving force for cathodic hydrogen evolution, as the potential falls below line A [7].

For corrosion in aqueous media, two fundamental variables, namely corrosion potential and pH, are deemed to be particularly important. Changes in other variables, such as the oxygen concentration, tend to be reflected by changes in the corrosion potential.

**Table 2.2:** Possible reactions in the Fe-H<sub>2</sub>O system between the species most stable in dry conditions [11].

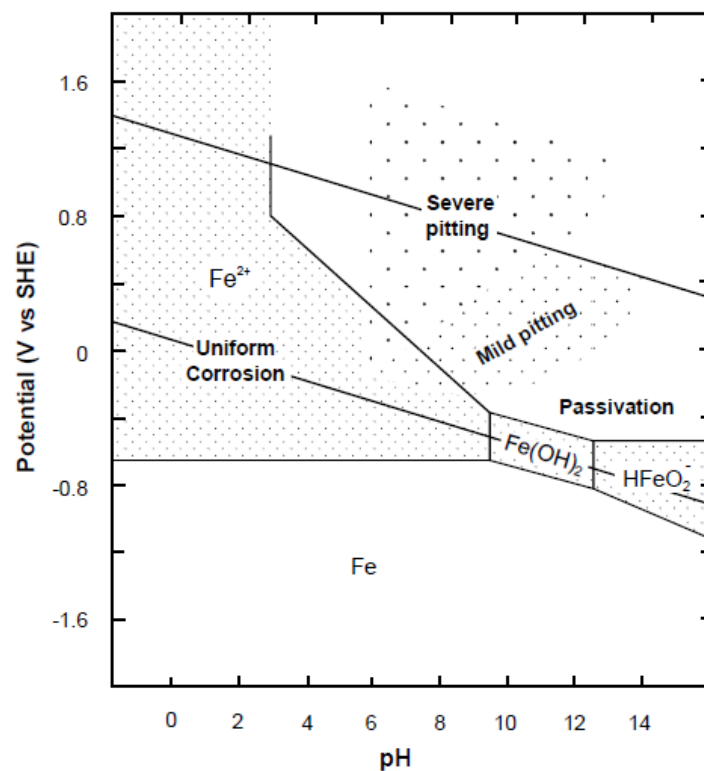
Equilibria
1. $2e^- + 2H^+ = 1H_2$
2. $4e^- + 1O_2 + 4H^+ = 2H_2O$
3. $8e^- + 1Fe_3O_4 + 8H^+ = 3Fe + 4H_2O$
4. $2e^- + 1Fe^{2+} = 1Fe$
5. $2e^- + 1Fe(OH)_3^- + 3H^+ = 1Fe + 3H_2O$
6. $2e^- + 1Fe_2O_3 + 2H^+ = 2Fe_3O_4 + 1H_2O$
7. $2e^- + 1Fe_3O_4 + 8H^+ = 3Fe^{2+} + 4H_2O$
8. $2e^- + 1Fe_2O_3 + 6H^+ = 2Fe^{2+} + 4H_2O$
9. $2e^- + 1Fe_3O_4 + 5H_2O = 3Fe(OH)_3^- + 1H^+$
10. $2Fe^{3+} + 3H_2O = 1Fe_2O_3 + 6H^+$
11. $1e^- + 1Fe^{3+} = 1Fe^{2+}$
12. $1Fe^{2+} + 1H_2O = 1FeOH^+ + 1H^+$
13. $1FeOH^+ + 1H_2O = 1Fe(OH)_{2(sln)} + 1H^+$
14. $1Fe(OH)_{2(sln)} + 1H_2O = 1Fe(OH)_3^- + 1H^+$
15. $1Fe^{3+} + 1H_2O = 1FeOH^{2+} + 1H^+$
16. $1FeOH^{2+} + 1H_2O = 1Fe(OH)_2 + 1H^+$
17. $1Fe(OH)_2 + 1H_2O = 1Fe^{2+} + 2H_2O$
19. $1e^- + 1Fe(OH)_2 + 2H^+ = 1Fe(OH)_{2(sln)} + 1H_2O$
20. $1e^- + 1Fe(OH)_3(sln) + 1H^+ = 1Fe(OH)_{2(sln)} + 1H_2O$
21. $1e^- + 1Fe(OH)_3(sln) + 2H^+ = 1FeOH^+ + 2H_2O$
22. $1e^- + 1Fe(OH)_3(sln) + 3H^+ = 1Fe^{2+} + 3H_2O$



**Figure 2.4 :** Thermodynamic stability of water, oxygen and hydrogen.

Two important variables affecting water-side corrosion of ironbased alloys are the pH and oxygen content of the water. As the oxygen level has a strong influence on the corrosion potential, these two variables exert a direct influence in defining the position on the  $E$ -pH diagram. A higher degree of aeration raises the corrosion potential of iron in water, while a lower oxygen content reduces it.

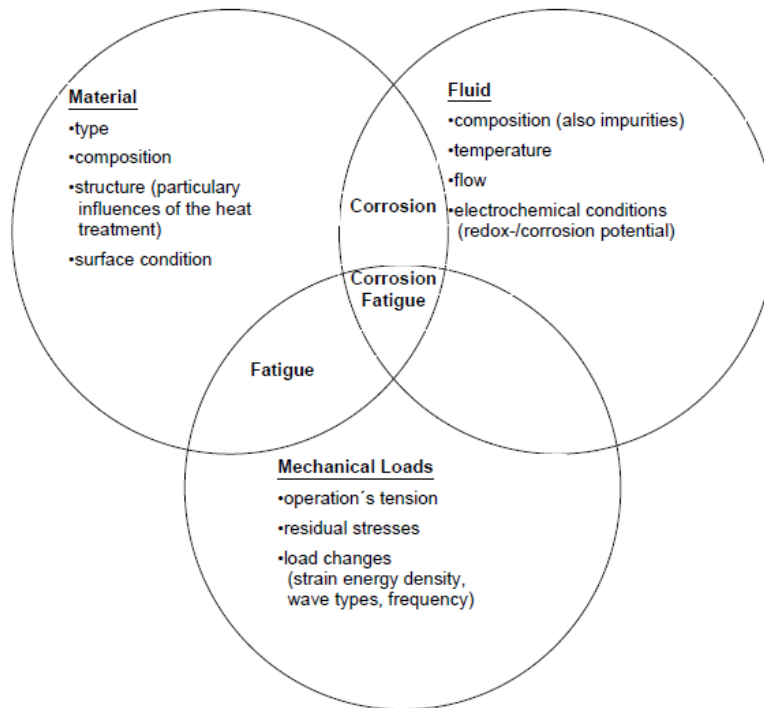
While the  $E$ -Ph diagram provides no kinetic information whatsoever, it defines the thermodynamic boundaries for important corrosion species and reactions. The observed corrosion behavior of a particular metal or alloy can also be superimposed on  $E$ -pH diagrams. Such a superposition is presented in Fig. 2.5. The corrosion behavior of steel presented in this figure was characterized by polarization measurements at different potentials in solutions with varying pH levels.



**Figure 2.5 :** Thermodynamic boundaries of the types of corrosion observed on steel [13].

## 2.2. Corrosion Types

Important influence factors which can favour corrosion processes at safety-relevant components are the operating conditions existing in plants such as water chemistry, assigned materials, mechanical and thermal loads, operational state and geometrical factors (Figure 2.6).



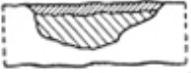




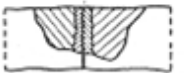



**Figure 2.6 :** Factors influencing corrosion fatigue [14].

Corrosion requires energy. During corrosion, the reacting components go from a higher to a lower energy state and release the energy needed for the reaction. In the dry corrosion the metal and the oxygen combine to produce the oxide on the surface because the reaction leads to a compound (the oxide) at a lower energy level. The oxide layer shields the metal from the oxygen and forms a barrier. The oxide will not react with the oxygen in the air or the metal. The barrier makes it difficult for oxygen in the air to contact the metal and it eventually grows so thick that the movement of electrons and ions across it stop. Provided the oxide layer does not crack, or is not removed, the metal is protected from further corrosion [15].

Corrosion can occur on the outside of a pipe (due to corrosive soil) or on the inside of a pipe (due to corrosive water.) Either outside or inside a pipe, corrosion can have one of several causes. Each cause somehow sets up an anode and a cathode so that corrosion can occur. The creation of the corrosion cell can be through electrolysis, oxygen concentration cells, or through galvanic action [16].

The various types of corrosion are listed in the Figure 2.7.



 <p><b>Uniform corrosion</b></p> <p>The reaction starts at the surface and proceeds uniformly.</p>	 <p><b>Localized corrosion (pitting corrosion)</b></p> <p>The basis metal is eaten away and perforated in places in the manner of holes, the rest of the surface being affected only slightly or not at all.</p>	 <p><b>Wide pitting corrosion</b></p> <p>The corrosion causes localized scarring.</p>
 <p><b>Intergranular corrosion</b></p> <p>Imperceptible or barely perceptible from outside, since the corrosion proceeds at the grain boundaries.</p>	 <p><b>Transgranular or intragranular corrosion</b></p> <p>The grain boundary material is retained, since the corrosion proceeds preferentially within the grain.</p>	 <p><b>Galvanic corrosion</b></p> <p>Increased corrosion in crevices or cracks or at contact surfaces between two metal articles.</p>
 <p><b>Selective corrosion</b></p> <p>Corrosive attack on structural constituents</p>	 <p><b>Exfoliation corrosion</b></p> <p>Occurs in deformed articles. Corrosion follows "fiber orientation".</p>	 <p><b>Interfacial corrosion</b></p> <p>Frequently observed at water-air interfaces.</p>

**Figure 2.7 :** Various types of corrosion [17].

Figure 2.8 contains the distribution of the different corrosion types for all reportable events of all boiling water reactors, BWR of German nuclear power plants which are in operation in the Federal Republic of Germany from 1968 to 2001. As a result one can see that stress corrosion was most frequently identified in BWR plants. Pitting corrosion occurs in the BWR plants with 12% whereas corrosion fatigue occurs with 17% fatigue.

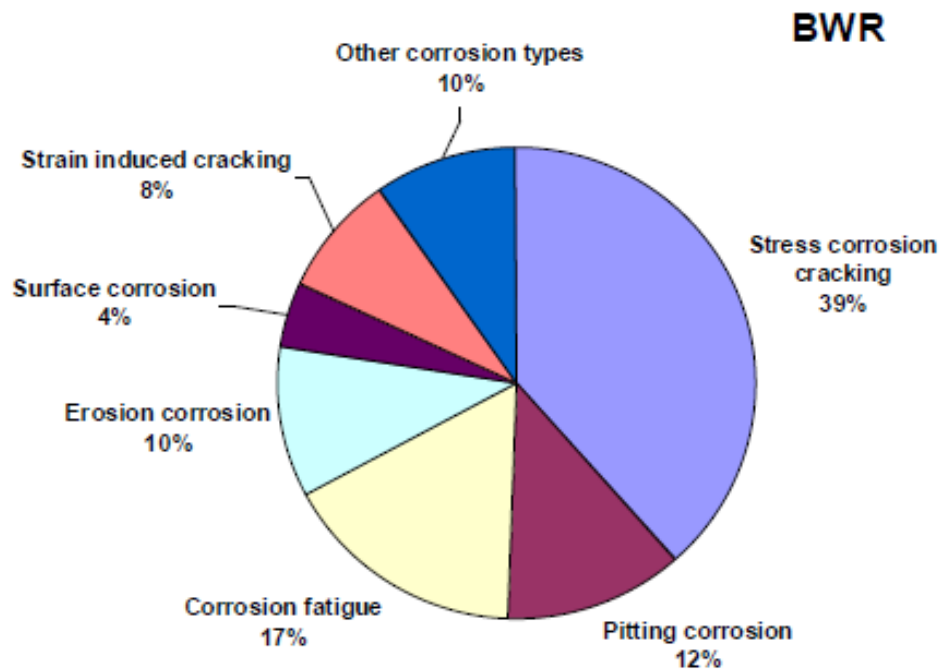


**Figure 2.8 :** Distribution of corrosion types in BWR (boiling water reactor) plants in Germany (Evaluation of reportable events 1968 – 2001) [14].

### 2.3. Corrosion Protection

Hydrogen is considered to be an ideal energy carrier in the future. Considering the inhibition of corrosion of mild steel alloy, the processes of the metal corrosion (active dissolution) and of the hydrogen embrittlement have to be taken into account. The effective inhibitors should suppress both the corrosion and the hydrogen charging, not intensifying any of them. By immersion of mild steel alloy in water solutions, the sources of hydrogen are water decomposition and reaction of water with the metal. Evolved hydrogen may recombine and leave the surface as a gas or may enter the metal causing the hydrogen-induced degradation of the metal. In order to reduce the susceptibility to hydrogen uptake, the modification of solution by addition of inhibitors or the modification of the metal surface may be applied. The requirement for effective inhibition of hydrogen uptake is to inhibit the hydrogen evolution, to promote the hydrogen gas recombination and to inhibit the hydrogen entry. Since hydrogen evolves in corrosion processes, the inhibition of corrosion should have inhibited also the hydrogen evolution. On the other hand, inhibition of hydrogen evolution does not necessarily mean decrease in the hydrogen charging of

the metal. The presence of corrosion inhibitors may substantially affect the hydrogen ingress processes. Therefore, the mutual influence of inhibitors on the corrosion and on the hydrogen evolution should be taken into account [18].

### **2.3.1. Corrosion Protection Methods**

Corrosion can be mitigated by five basic methods: coatings, cathodic protection, materials selection, chemical inhibitors and environmental change [19,20].

When considering the corrosion protection of steel structures, a distinction is made between active and passive measures. Active corrosion protection aims at preventing corrosion or reducing the rate of the corrosion reaction by:

- interfering in the corrosion process, e.g. reducing air pollution
- choosing a suitable material, e.g. using corrosion resistant materials
- using detailing appropriate for corrosion protection

The goal of passive corrosion protection is to shield the steel surface from corrosive substances.

Due to their broad range of application possibilities and their efficiency, the following methods dominate the corrosion protection of steel structures:

- coatings based on liquid or powder coatings
- metallic coatings (zinc, aluminum or zinc-/aluminum alloys) applied by hotdip galvanization or thermal spraying
- combination of metallic coatings and paint systems

Optimal corrosion protection is achieved by combining active and passive corrosion protection methods, based on the appropriate detailing prior to the application of the passive corrosion protection [21].

Inhibitors are chemicals that react with a metallic surface, or the environment this surface is exposed to, giving the surface a certain level of protection. Inhibitors often work by adsorbing themselves on the metallic surface, protecting the metallic surface by forming a film. Inhibitors are normally distributed from a solution or dispersion. Some are included in a protective coating formulation. Inhibitors slow corrosion processes by either:

- Increasing the anodic or cathodic polarization behavior (Tafel slopes)
- Reducing the movement or diffusion of ions to the metallic surface
- Increasing the electrical resistance of the metallic surface [19].

There are various techniques for preventing metallic corrosion. For example, for iron, cathodic protection can be achieved by maintaining its potential and pH within the region of stability of the elemental metal. This can be done via a suitable power source, or by electrical connection to a more reactive metal such as zinc immersed in a solution. Both techniques are widely used.

Certain metal oxides or hydroxides have low aqueous solubilities and are stable in the presence of water. Hence, there may be helpful in stifling further corrosion. Typical examples include  $\text{Fe}_2\text{O}_3$  or  $\text{Al}_2\text{O}_3$ . The formation of such protective films can be accomplished by maintaining the potential and pH within the appropriate region. This method which is known as anodic protection, is not widely used because it is critical dependent on the ability of the protective film to shut down the corrosion reaction. Any failure in the film will result in enhanced corrosion [9].

Broader application of corrosion-resistant materials and the application of the best corrosion-related technical practices could reduce approximately one-third of corrosion costs.

### **2.3.2. Organic Corrosion Inhibitors**

Over the years, as worldwide awareness for environmental issues have grown, gentle processing technologies and the use of renewable resources have become increasingly important [22].

A widespread application like the use of acid solution during pickling and industrial cleaning leads to corrosive attack on mild steel. Therefore, corrosion of mild steel and its inhibition in acidic solutions have attracted the attention of number of investigators as a result of its industrial concern [23, 18].

Due to stringent environmental regulations, high toxicity, unacceptable high level disposal in waste water and as well as human safety, inorganic corrosion inhibitors such as chromates, nitrites, polyphosphates, zinc salts or oxides incorporated in protective coatings for mild steel are being replaced by organic compounds [4,5,24].

Since the 1960s, more advanced treatments using organic compounds (e.g., phosphonates, polyacrylates, amines) have been proposed to improve corrosion protection, their principal advantage being their non-toxic nature. Nevertheless, high concentrations are necessary to obtain good inhibition. More recently, molybdate-based compounds have been considered as an alternative to chromate-based inhibitors. However, these compounds are of low commercial interest because they are very expensive [24].

Study of organic corrosion inhibitors is an attractive field of research due to its usefulness in various industries [25].

Currently, the environmental requirements to the corrosion inhibitors have become more rigid. It was proved that highly hydrophobic compounds are more capable of accumulating in living organisms than their less hydrophobic and, hence, more environmentally dangerous homologs. In connection with this, the water-soluble compounds, which can protect steel against corrosion in two-phase liquids, deserve special attention [26].

Most of the efficient inhibitors used in industry are organic compounds having multiple bonds in their molecules which mainly contain nitrogen and sulphur atoms through which they are adsorbed on the metal surface [18].

The use of corrosion inhibitors are an effective way to reduce metal corrosion. The inhibitors act by adsorbing onto the metal surface, thus providing an barrier to the corrosive environment. The advantages of organic corrosion inhibitors include:

- Presence of film prevents uniform corrosion attack
- Organic inhibitors increase the activation energy on the metal surface (passivation)
- Organic inhibitors have been shown to eliminate corrosion over wide range of pH values
- Inhibitors adsorb and form a thin polymeric layer [27].

Inhibitors are usually used in these processes to control the corrosion of the metals. The protection of mild steel against corrosion can be achieved by adding a small concentration of organic compounds to environment [25].

Compounds with functional groups containing oxygen, nitrogen and sulphur having ability to form complexes with iron. They have been reported to act as effective

inhibitors to the surface of steel by means of their competitive adsorption through the surface complex formation. In practice corrosion or hydrogen evolution can never be stopped but hindered to a reasonable level. Among many methods of corrosion control and prevention the organic inhibitors is the most frequently used. Organic compounds used as inhibitors act through a process of surface adsorption, so the efficiency of an inhibitor depends on:

- (i) The chemical structure of the organic compound
- (ii) The surface charge of the metal, and
- (iii) The type of interactions between the organic molecule and metal surface.

Existing data reveal most inhibitors to act by adsorption on the metal surface through heteroatoms such as nitrogen, oxygen and sulphur, double bonds, triple bonds or aromatic rings which tend to form stronger coordination bonds. Compounds with  $\pi$ -bonds generally exhibit good inhibitive properties, the electrons for the surface interaction being provided by the  $\pi$ -orbitals [18].

Cooling water circuits can present several problems. Corrosion, formation of salt deposits and fouling by micro-organisms can appear when natural waters are used as thermal fluid. These problems can occur jointly, reducing the thermal efficiency of the circuit with significant economic repercussions. To reduce or eliminate these problems, waters used in cooling circuits are treated with inhibitive formulations composed of corrosion inhibitors associated with chemical reagents used to limit the scaling and fouling phenomena. Today, due to new restrictive laws concerning the environment, these compounds must be non-toxic and biodegradable [28].

### **2.3.3. Filming Inhibitor Technology**

As the world develops, greater oil and gas production from marginal sources, there is a need for more effective corrosion inhibitors under more extreme conditions [29]. Compounds derived from fatty acids constitute an important class of corrosion inhibitor. They are used in oil wells and pipelines and in the gas industry [30, 31].

Corrosion of pipelines or equipment results in the necessity to shut down production while corroded pipelines and equipment are replaced. Also, corrosion in pipelines sometimes leads to leaks which in addition to being costly, may create severe environmental hazards [32].

Both anodic and cathodic effects are sometimes observed in the presence of organic inhibitors, but as a general rule, organic inhibitors affect the entire surface of a corroding metal when present in sufficient concentration. Organic inhibitors, usually designated as “film-forming”, protect the metal by forming a hydrophobic film on the metal surface.

Their effectiveness depends on the chemical composition, their molecular structure, and their affinities for the metal surface. Because film formation is an adsorption process, the temperature and pressure in the system are important factors. Organic inhibitors will be adsorbed according to the ionic charge of the inhibitor and the charge on the surface.

Cationic inhibitors, such as amines, or anionic inhibitors, such as sulfonates, will be adsorbed preferentially depending on whether the metal is charged negatively or positively. The strength of the adsorption bond is the dominant factor for soluble organic inhibitors. These materials build up a protective film of adsorbed molecules on the metal surface, which provides a barrier to the dissolution of the metal in the electrolyte. Because the metal surface covered is proportional to the inhibitor concentration, the concentration of the inhibitor in the medium is critical. For any specific inhibitor in any given medium there is an optimal concentration [33].

Compounds with nitrogen and oxygen functional groups as well as multiple bonds or aromatic rings are considered to be one of the effective chemicals for inhibiting the metal corrosion [34].

Nitrogen-based compounds are effective inhibitors for mild steel corrosion in acidic solutions. The presence of the lone pair of electrons on the nitrogen atoms helps to delocalize the electrons and thus stabilize the compound. The presence of non-bonded electron pairs on the nitrogen atom induces greater adsorption of the compounds onto the metal surface thus providing higher inhibition efficiency [30, 31].

In comparison with traditional programs such as all- volatile treatment or solid alkalisation, treatment with film- forming amines is of lesser importance, although numerous steam generators have been successfully treated with film-forming amines for many years – also in some instances where the traditional methods failed to produce satisfactory results.

Film forming amines, often also called polyamines or fatty amines, are defined chemical substances of the class of oligo alkylamino fatty amines, the simplest representative being the well known octadecylamine [28].

The polyamines are, in the main, linear aliphatic molecules of, in biological terms, small molecular mass. They are water soluble, and at physiological pH all the amino groups will be positively charged; hence, these compounds are organic bases, their basicity increasing with the number of amino groups. Unlike inorganic molecules or ions, the positive charges on polyamines are spaced out at intervals and, although the hydrocarbon chains are flexible, will have steric as well as cationic properties [35].

By 1931, Deutsche Hydrierwerke (DHW) in Rodleben/Germany patented and initiated the world's first production of fatty alcohols based on the evolving technology of catalytic, high pressure hydrogenation. The experiences acquired by the DHW since this time in field of hydrogenation technology resulted in a key innovation for the company in 1960: the production of fatty amines from natural raw materials. The initial use for primary amines was in the flotation of potash ore and then followed the establishment of a wide range of fatty amine compounds [22]. Chemical structure of fatty amines are shown in Figure 2.9.

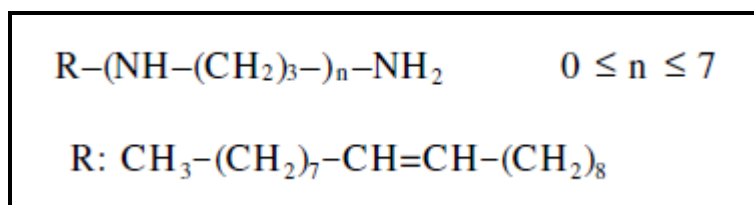


**Figure 2.9 :** Chemical structure of fatty amines [28].

Fatty alkyl amines have typical alkyl chain length of 8-24 carbon atoms, and many of major commercial importance, such as tallow amine, oleylamine, cocoamine and soya amine are naturally derived. Fatty amines are soluble in polar and non-polar solvents, but solubility in water is limited to fatty amines with fewer than 10 carbons per unit chain. Fatty alkyl amines can also be produced synthetically from paraffins or from naturally occurring fatty acids such as cocoamines, soya amines and tallow amines.

Many fatty amines are in fact mixtures of different alkyl chain lengths. For example cocoamine, tallow amine, soya amine and oleylamine contains the following alkyl chains:



Cocoamine	= 7% C <sub>10</sub> + 50% C <sub>12</sub> + 18% C <sub>14</sub> + 6% unsaturated C <sub>18</sub> + 19% others
Oleylamine	= 5% C <sub>18</sub> + 76% unsaturated C <sub>18</sub> + 19% others
Tallow amine	= 29% C <sub>16</sub> + 23% C <sub>18</sub> + 37% saturated C <sub>18</sub> + 11% others
Soya amine	= 16% C <sub>16</sub> + 15% C <sub>18</sub> + 50% unsaturated C <sub>18</sub> + 13% doubly unsaturated C <sub>18</sub> + 6% others [36].

Most alkyl amines are made on an industrial scale by the reaction between ammonia and alcohols or alkyl chlorides and fractionation of the resulting product mixture [37].

Fatty amines and their salts are suitable for use as anticorrosion agents as they can be substantively adsorbed onto metal surfaces from either aqueous or oily systems. The resulting coating firmly adheres to and protects metal surfaces from aggressive liquids or gases. Similarly, in the petroleum industry, fatty amines and their salts give outstanding results in corrosion prevention [22].

The film forming mechanism by which all materials function is the same and requires their adsorption onto the metal through their polar group or head. The nonpolar tail of the inhibitor molecule is oriented in a direction generally vertical to the metal surface. It is believed that the hydrocarbon tails mesh with each other in a sort of 'zipper' effect to form a tight film which repels aqueous fluids, establishing a barrier to the chemical and electrochemical attack of fluids on the base metal. A secondary effect is the physical sorption of hydrocarbon molecules from the process fluids by the hydrocarbon tails of the adsorbed inhibitor molecules. This increases both the thickness and effectiveness of the hydrophobic barrier to corrosion (Figure 2.10).

The film that forms on the metal surface acts as a barrier against corrosive substances such as oxygen, carbon dioxide and carbonic acid. The hydrophobic alkyl group makes the metal surface unwettable with water.

The addition of organic inhibitor compound may reduce the partial anodic (anodic inhibitor), the partial cathodic (cathodic inhibitor) or the two partial reactions (mixed inhibitor).

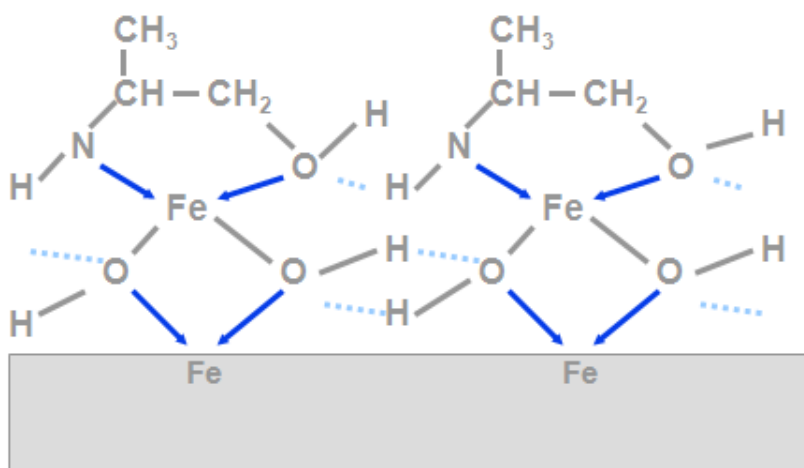


**Figure 2.10 :** FFA adsorption on metal surface [38].

In many cases, the inhibition is related to adsorption of the inhibitor on the metal surface forming a barrier layer which separates the metal from the corrosive media. According to the type of inhibitor species and the nature of metal and alloy, adsorption may be chemical or physical adsorption [39].

The film-forming amine, FFA, can be described most effectively as a surface active chelant. By definition, surface-active chelants are both surfactants and chelants and their use as corrosion inhibitors is not new. It is theorized that proper combination of surface-active and chelating groups in the same molecule will enable surface-active chelants to seek out the metal–water interface, undergo chemisorption with surface metal atoms or ions, and provide an insoluble adherent, protective chelate film on the metal surface.

Corrosion research has indicated that surface chelation provides enhancement of already existent corrosion inhibition properties and that surface-active chelants possessing large hydrophobic substituent groups promote adsorption onto the steel surface and once adsorbed improve the hydrophobic barrier to electrolyte penetration. In addition, this barrier may be enhanced by the ability of the hydrophobic tails of the chelated FFA to attract other hydrocarbon molecules, such as additional FFA molecules or the waterproofing ester, to create an additional water-repellent oil film [38].

The choice of fatty amines as corrosion inhibitors is based on the following: these molecules (a) can be easily synthesized, (b) contain oxygen and nitrogen as active centers, (c) have high solubility in acidic media and (d) are not expensive.

Indeed, the number of alkyl groups greatly influences the inhibition properties and can be related to the flexibility of the molecule, influencing therefore the adsorption process. Then we can conclude that with higher alkyl chain length, the inhibition becomes less effective. This behavior is in agreement with the literature [40,41]. However, other authors state that the inhibition efficiency is improved when the alkyl chain length of the inhibitors was increased in the case of primary aliphatic amines [25].

Tallow is a hard fat consists chiefly of glyceryl esters of oleic, palmitic, and stearic acids (16-18 carbon chains). It is extracted from fatty deposits of animals, especially from suet (fatty tissues around the kidneys of cattle and sheep). Tallow is used for soaps, leather dressings, candles, food, and lubricants. It is used in producing synthetic surfactants. Tallow based alkyl amines are widely used in the synthesis of organic chemicals and cationic and amphoteric surfactants [42].

The combination amine-carboxylic acid gives rise to ammonium carboxylates, also named catanionic surfactants. For reasons of compatibility with the coating, carboxylic acids are often used together with an organic base, typically an amine. The resulting corrosion inhibitor consists therefore of an acid/base couple [4].

The cationic compounds i.e. fatty amines and fatty amine derivatives, differ from anionic and nonionic surfactants in that they have a marked degree of substantivity for nearly all solid surfaces. Their substantivity is a characteristic property which allows them to be adsorbed onto solids and form a firm cationic film on them so that properties can be varied to fit in with any desired application. Thus, materials such as wool, hair, leather, cotton, synthetic fibres, plastics, dye pigments, rocks, metals etc. can be treated with fatty-amine-based cationic formulations to acquire useful properties for quite specific applications [22].

It is known that in the case of long-term standstill (over 7 days) of the power equipment of a cogeneration plant the equipment should be protected from standstill corrosion. The equipment with scale on the surfaces, under the layer of which corrosion processes intensify, requires protection especially urgently. In the presence of moisture standstill corrosion develops even in the absence of scale. Today the metal of power equipment is protected from standstill corrosion by various methods aimed at preventing contact between the metal and air and creating a protective film on the surface of the metal. One such method involves the use of film-forming

amines, octadecylamine (ODA) in particular . This reagent forms a protective film on the surface of the metal, which prevents contact between the metal and aggressive media, for example, humid air. In addition, ODA possesses detergent properties, which makes it suitable for preservation and washing-off of deposits (loose deposits) from power equipment stopped for a long period [43].

## **2.4 Corrosion Test Methods**

Corrosion test methods can be divided into electrochemical and non-electrochemical methods. Among the electrochemical techniques that have been used successfully for corrosion prediction are potentiodynamic polarization methods, electrochemical impedance spectroscopy (EIS), corrosion current monitoring, controlled potential tests for cathodic and anodic protection and the rotating cylinder electrode for studies of velocity effects. Though not literally a test, potential-pH (Pourbaix) diagrams have been used as road maps to help understand the results of other tests [44].

### **2.4.1. Non-Electrochemical Measurements**

A number of non-electrochemical measurement techniques can be used to assess corrosion rate. These techniques can be simplified as weight lost, pitting and crevice rate and stress-strain time determination, resistance measurements, surface measurements and different analytical measurements.

*Weight loss measurement*, considered by some to be the “gold standard” of corrosion testing is certainly the easiest. However, there are important issues to consider even for weight loss measurements. First, since mass can be measured easily only to about 0.1 mg, the sensitivity of weight loss measurements is limited [2].

The non-electrochemical techniques include direct immersion of material samples in the test fluid either in the laboratory or plant. These samples sometimes have an artificial crevice generated with a serrated washer. They may be welded to determine the effects of welds and weld heat affected zones. Real time- time information can be obtained using electrical resistance probes. Heat transfer effects can be evaluated by having a test sample that is exposed to the corrodent on one side and the other side heated or cooled. Stressed samples are used to evaluate stress corrosion cracking tendencies [44].

A technique that has had more application in corrosion rate monitoring than in corrosion science involves the change in *electrical resistance* *\_ER\_* of a probe sample. The reduction of the cross-sectional area of a probe by corrosion is accompanied by a proportionate increase in the electrical resistance, which can be tracked easily. A major advantage of the ER technique is its applicability to a wide range of corrosive conditions including environments having poor conductivity or non-continuous electrolytes such as vapors and gases. However, ER monitoring typically requires a relatively long exposure period for a detectable difference in probe resistance and electrically conductive deposits can affect the measurements [2].

#### **2.4.2. Electrochemical Measurements**

While all laboratory corrosion tests require accelerating corrosion processes, only electrochemical tests can directly amplify the impact of corrosion processes. The main reasons why this is possible is that all electrochemical tests use some fundamental model of the electrode kinetics associated with corrosion processes to quantify corrosion rates. The amplification of the electrical signals generated during these tests has permitted very precise and sensitive measurements to be carried out [45].

The main advantage of electrochemical techniques for studying corrosion over traditional coupon testing is that it allows the rapid determination of the corrosion rate of a sample without requiring long-term testing. Corrosion rate itself can vary with time under a given set of conditions, so electrochemical corrosion measurements only give you a snapshot of how the system behaved under those conditions at that point in time. Long-term testing is still required if you need to know how a metal reacts after 12 months in a given test environment. But short-term electrochemical measurements are more than sufficient in many cases, as they allow you to compare the performance of inhibitors or to decide that a given metal is corroding too rapidly under those conditions to be a valid candidate for the application [46,47,48].

Corrosion testing by weight loss methods is generally a long, tedious affair which often does not produce completely satisfactory results. This is particularly true when the corrosion rate changes with time [49].

**Potentiodynamic polarization methods:** Polarization methods such as potentiodynamic polarization, potentiostaircase, and cyclic voltammetry are often used for laboratory corrosion testing. These techniques can provide significant useful information regarding the corrosion mechanisms, corrosion rate and susceptibility of specific materials to corrosion in designated environments. Polarization methods involve changing the potential of the working electrode and monitoring the current which is produced as a function of time or potential.

**Linear polarization resistance (LPR):** With this widely used technique in corrosion monitoring, the polarization resistance of a material is defined as the slope of the potential-current density ( $\Delta E/\Delta i$ ) curve at the free corrosion potential, yielding the polarization resistance,  $R_p$ , that can be related (for reactions under activation control) to the corrosion current by the Stern-Geary equation (Equation 2.6) [45].

$$R_p = \frac{\beta}{I_{corr}} = \left( \frac{\Delta E}{\Delta I} \right)_{\Delta E \rightarrow 0} \quad (2.6)$$

- $R_p$  is the polarization resistance
- $I_{corr}$  the corrosion current
- The proportionality constant  $\beta$ , for a particular system can be determined empirically (calibrated from separate weight loss measurements) or, as shown by Stern and Geary, can be calculated from  $\beta_a$  and  $\beta_c$ , the slopes of the anodic and cathodic Tafel.

$$\beta = \frac{\beta_a \beta_c}{2.3(\beta_a + \beta_c)} \quad (2.7)$$

An electrochemical reaction under kinetic control obeys Equation 2.8, the Tafel Equation:

$$I = I_0 \cdot \exp\left(2.3 \frac{E - E^0}{\beta}\right) \quad (2.8)$$

In this equation,

- $I$  is the current resulting from the reaction
- $I_0$  is a reaction dependent constant called the Exchange Current
- $E$  is the electrode potential
- $E^0$  is the equilibrium potential (constant for a given reaction)
- $\beta$  is the reaction's Tafel Constant (constant for a given reaction).  
Beta has units of volts/decade [50].

The Tafel equations for both the anodic and cathodic reactions in a corrosion system can be combined to generate the **Butler-Volmer Equation** (Equation 2.9).

$$I = I_a + I_c = I_{corr} \cdot \left( \exp\left(2.3 \frac{E - E_{corr}}{\beta_a}\right) - \exp\left(-2.3 \frac{E - E_{corr}}{\beta_c}\right) \right) \quad (2.9)$$

where

- I is the measured cell current in amps
- $I_{corr}$  is the corrosion current in amps
- E is the electrode potential
- $E_{corr}$  is the corrosion potential in volts
- $\beta_a$  is the anodic Beta Tafel Constant in volts/decade
- $\beta_c$  is the cathodic Beta Tafel Constant in volts/decade [46,47,48].

The following is a list of situations where it appears that the use of linear polarization measurements can supply valuable information.

1. Studies of the effect of environment variables on corrosion rate. These include changes in composition, velocity, and temperatures.
2. Evaluation of inhibitors in controlling corrosion.
3. Comparison of the corrosion rates of various alloys of similar composition in a given environment.
4. Determination of changes in corrosion rate with time, including studies of underground structures as well as materials in aqueous solutions.
5. It also may be possible to evaluate the condition of coatings in service which cannot be inspected by visual methods [49].

At Figure 2.11, a typical linear polarization curve with the vertical axis is potential and the horizontal axis is the logarithm of absolute current is shown. The theoretical current for the anodic and cathodic reactions are indicated as straight lines. The curved line is the total current - the sum of the anodic and cathodic currents. This is the current that is measured when the potential of the metal is swept with the potentiostat [51].

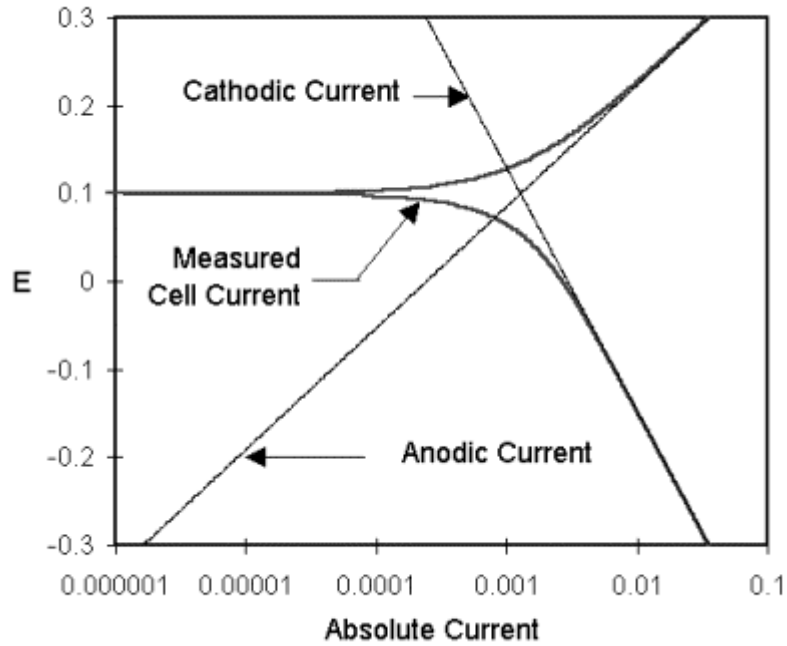


**Figure 2.11** : Corrosion process showing anodic and cathodic current components [52].

**Electrochemical impedance spectroscopy (EIS)** : Electrochemical Impedance Spectroscopy (EIS) is an electrochemical technique with applications in corrosion, biosensors, battery development, fuel cell development, paint characterization, sensor development, and physical electrochemistry. EIS experiment involves the application of a sinusoidal electrochemical perturbation (potential or current) to the sample that covers a wide range of frequencies. This multi-frequency excitation allows (1) the measurement of several electrochemical reactions that take place at different rates and (2) the measurement of the capacitance of the electrode [53].

An important advantage of EIS over other laboratory techniques is the possibility of using very small amplitude signals without significantly disturbing the properties being measured. To make an EIS measurement, a small amplitude signal, usually a voltage between 5 to 50 mV, is applied to a specimen over a range of frequencies of 0.001 Hz to 100,000 Hz. The EIS instrument records the real (resistance) and imaginary (capacitance) components of the impedance response of the system [45]. The excitation signal, expressed as a function of time, has the form:

$$E_t = E_0 \cdot \sin(\omega t) \quad (2.10)$$



where  $E_t$  is the potential at time  $t$ ,  $E_0$  is the amplitude of the signal, and  $\omega$  is the radial frequency. In a linear system, the response signal,  $I_t$ , is shifted in phase ( $\phi$ ) and has a different amplitude,  $I_0$  (Equation 2.11).

$$I_t = I_0 \cdot \sin(\omega t + \phi) \quad (2.11)$$

An expression analogous to Ohm's Law allows us to calculate the impedance of the system as:

$$Z = \frac{E_t}{I_t} = \frac{E_0 \cdot \sin(\omega t)}{I_0 \cdot \sin(\omega t + \phi)} = Z_0 \frac{\sin(\omega t)}{\sin(\omega t + \phi)} \quad (2.12)$$

The impedance is therefore expressed in terms of a magnitude,  $Z_0$ , and a phase shift,  $\phi$ . With Eulers relationship,

$$\exp(j\phi) = \cos\phi + j \sin\phi \quad (2.13)$$

The impedance is then represented as a complex number,

$$Z(\omega) = \frac{E}{I} = Z_0 \exp(j\phi) = Z_0(\cos\phi + j \sin\phi) \quad (2.14)$$

At Equation 2.14, the expression for  $Z(\omega)$  is composed of a real and an imaginary part. If the real part is plotted on the X-axis and the imaginary part is plotted on the Y-axis of a chart, "Nyquist Plot" is observed (Figure 2.12).

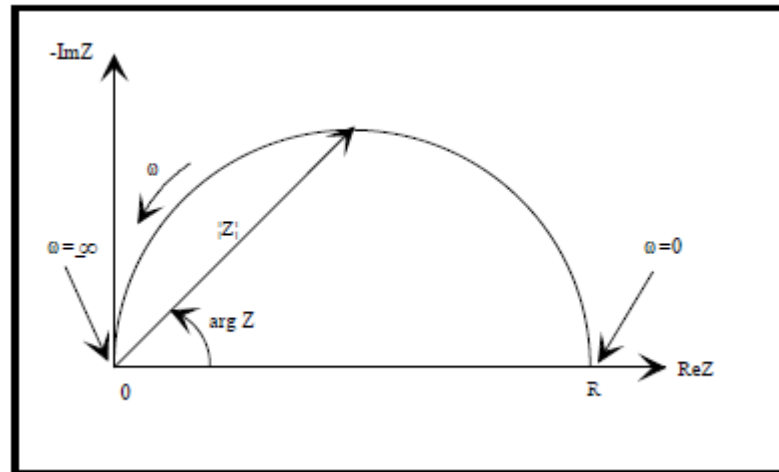


**Figure 2.12 :** Nyquist plot with impedance vector [53].

EIS data is commonly analyzed by fitting it to an equivalent electrical circuit model. Depending upon the shape of the EIS spectrum, a circuit model or circuit description code and initial circuit parameters are assumed and input by the operator [45]. Most

of the circuit elements in the model are common electrical elements such as resistors, capacitors, and inductors.

Component	Current Vs.Voltage	Impedance
resistor	$E = IR$	$Z = R$
inductor	$E = L di/dt$	$Z = j\omega L$
capacitor	$I = C dE/dt$	$Z = 1/j\omega C$

**Figure 2.13 :** Common electrical elements [54].

Constant phase elements, CPEs are widely used in the analysis of EIS corrosion data. The extra fitting parameter associated with the non-ideal capacitance of a CPE improves the fit to the data. The CPE is a mathematical construct of convenience. However, it is not surprising that a physical structure such as an electrochemical interface does not behave exactly like a combination of standard circuit elements, and no rationale need to be given for the use of CPEs. The simplified Randles circuit with a CPE shown in Fig. 2.14 and is commonly used to represent many corroding interfaces. EIS is a particularly useful technique for low conductivity electrolytes as the ohmic resistance is determined explicitly [2].

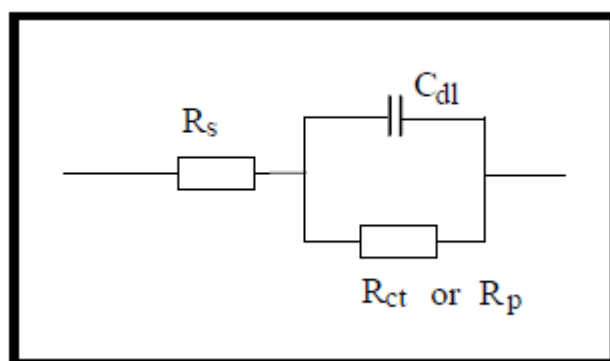


**Figure 2.14 :** The simplified Randles circuit [55].

**Electrochemical noise (EN):** The extensive development in the sensitivity of the equipment for studying electrochemical systems has rendered the study of oscillations in electrochemical processes, that translate into measurable EN, increasingly accessible. The study of corrosion potential fluctuations was applied, for example, to monitor the onset of events characterizing localized corrosion such as pitting or stress corrosion cracking (SCC), exfoliation, erosion-corrosion in either laboratory or diverse and complex industrial environments. No other technique,

electrochemical or otherwise is even remotely as sensitive as EN to system changes and upsets.

During localized corrosion, EN is believed to be generated by a combination of stochastic processes, such as passivation breakdown and repassivation events, and deterministic processes which can be caused by film formation or pit propagation processes [45].



### 3. EXPERIMENTAL STUDY

#### 3.1. Materials

The corrosion inhibitor compounds, selected for the study are based on 3 different chemical families of film forming amines (FFA), that vary in the number of amino groups and the aliphatic alkyl group, generally a fatty alkyl chain. The generic structure of these compounds is presented in Figure 3.1.



With:                    n = number of monomers  
                              R<sup>1</sup> = alkyl chain: CH<sub>3</sub>- (CH<sub>2</sub>)<sub>7</sub>- CH=CH- (CH<sub>2</sub>)<sub>8</sub>  
                              R<sup>2</sup> = alkyl group: -(CH<sub>2</sub>)<sub>3</sub>-

**Figure 3.1** : Generic chemical structure of the different film forming amines [56].

During the study, six compounds different in the number of amino groups are used, e.g. N<sub>2</sub> indicates a diamine, or the type of alkyl chain R, i.e. saturated or unsaturated, which is indicated by a subscript “s” and “u” respectively. As an example R<sub>u</sub>N<sub>2</sub> is a oleylpropylenediamine. The whole species used through the study are R<sub>u</sub>N, R<sub>u</sub>N<sub>2</sub>, R<sub>u</sub>N<sub>3</sub>, R<sub>s</sub>N, R<sub>s</sub>N<sub>2</sub> and R<sub>s</sub>N<sub>3</sub>. All the compounds were supplied from BK Giulini GmbH- Düsseldorf.

For all the experiments, each compound has been studied at the same concentration of 100 mg L<sup>-1</sup>.

Through the study, experiments with six different inhibitors are carried out at five different pH values varying between pH = 5 -11 with 1.5 increment. Sulphuric acid 5 % w/w and NaOH 4 % w/w were used for the adjustment of the pH.

The chemical composition of commercially mild steel metal for working electrode with exposed area of 3.95 cm<sup>2</sup> is as follows (percentage by weight): C=0.35, Mn=0.65, Si=0.25, P=0.035, S=0.035 and Fe to 100. Carbon steel metals were supplied from Imotron Instruments B.V., distributor for Rohrback Cosasco Systems

Inc, Netherlands. For each run, an unused set of electrodes were used and the samples were rinsed in acetone to remove any organic contamination from metal surface before measurements.

A glass cell of capacity 200 mL was used, which contained three electrodes; steel as working, platinum as counter and silver/silver chloride (Ag/AgCl) as reference electrodes.

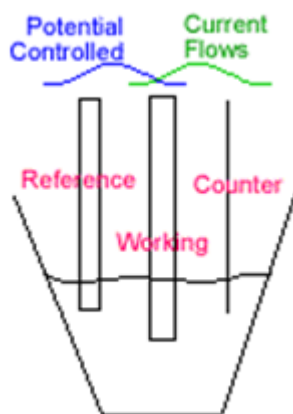


**Figure 3.2 :** Three electrode type electrochemical cell

The measurements were carried out in 3 different aerated solution quality: seawater, decarbonised water and deionised water. The solutions were freshly prepared from analytical grade chemical reagents supplied from Carlo Erba Company using distilled water and used without further purification.

All the tests were carried out at ambient temperature (25 °C), the solutions being in contact with air.

### **3.1.1. Seawater Preparation**

Through the experiments, artificial seawater is prepared as indicated at Table 3.1. For each run, a freshly prepared solution was used. The ion content for the 35% w/w artificial seawater is seen at Table 3.2 and the approximate pH value of this formulation is 8 and conductivity is 60.000  $\mu\text{s}/\text{cm}$ .

**Table 3.1:** Formula for 1 kg of 35% artificial seawater

<b>A. Gravimetric salts</b>		
<b>Salt</b>	<b>Molecular wt</b>	<b>g/kg of solution</b>
NaCl	58.44	23.926
Na <sub>2</sub> SO <sub>4</sub>	142.04	4.008
KCl	74.56	0.677
NaHCO <sub>3</sub>	84.00	0.196
KBr	119.01	0.098
H <sub>3</sub> BO <sub>3</sub>	61.83	0.026
NaF	41.99	0.003
<b>B. Volumetric Salts</b>		
<b>Salt</b>	<b>Molecular wt</b>	<b>moles/kg of solution</b>
MgCl <sub>2</sub> ·6H <sub>2</sub> O	203.33	0.053
CaCl <sub>2</sub> ·2H <sub>2</sub> O	147.03	0.010
SrCl <sub>2</sub> ·6H <sub>2</sub> O	266.64	0.00009
<b>C. Distilled water to 1,000 g</b>		

**Table 3.2:** The ion content for the 35% w/w artificial seawater [57].

<b>Ion</b>	<b>Artificial Seawater (g/kg)</b>
Cl <sup>-</sup>	19.353
Na <sup>+</sup>	10.765
SO <sub>4</sub> <sup>2-</sup>	2.711
Mg <sup>2+</sup>	1.295
Ca <sup>2+</sup>	0.414
K <sup>+</sup>	0.387
HCO <sub>3</sub> <sup>-</sup>	0.142
Br <sup>-</sup>	0.066
Sr <sup>2+</sup>	0.008
H <sub>3</sub> BO <sub>3</sub>	0.026
F <sup>-</sup>	0.001

### 3.1.2. Decarbonised Water Preparation

The decarbonised water advantageously is produced in deionised water by addition of two basic solutions. At Table 3.3, chemical composition of the decarbonised water used during the experiments is indicated.

#### Decarbonised Water I

In 1 L deionised water:

17.64 g CaCl<sub>2</sub> · 2H<sub>2</sub>O

16.24 g MgCl<sub>2</sub> · 6H<sub>2</sub>O

92.00 g NaCl are dissolved.

## Decarbonised Water II

In 1 L deionised water:

6.72 g NaHCO<sub>3</sub> is dissolved.

By filling-up 5 ml decarbonised water I and 5 ml decarbonised water II with deionised water to 1000 ml, 1l decarbonised water is obtained.

**Table 3.3:** Chemical composition of the decarbonised water used during the experiments

Ion	Ca <sup>2+</sup>	Mg <sup>2+</sup>	Cl <sup>-</sup>	HCO <sub>3</sub> <sup>-</sup>	pH	Conductivity (μs/cm)
Concentration in mg.L <sup>-1</sup>	24	9.7	350	24.4	7.0	1.100 -1.200

The choice of this medium was based upon the following criteria:

- (i) its low electrical conductivity is close to that encountered in natural waters,
- (ii) its corrosivity is fairly high and
- (iii) it is an easily reproducible baseline solution [28].

### 3.1.3. Deionised Water Preparation

Deionised water consumed during the study were obtained from a mixed-bed demineralizer in which the cation and anion resin beads are mixed together. The approximate conductivity was around 3 μs/cm with a silica content less than 0,02 ppm.

## 3.2. Methods

Because corrosion occurs via electrochemical reactions, electrochemical techniques are ideal for the study of the corrosion processes [52].

Electrochemical measurements, including potentiodynamic polarization curves, and electrochemical impedance spectroscopy (EIS), were performed in a three-electrode cell using Parstat 2263 Instrument potentiostat/galvanostat, which included Powersuite framework system. The potentiodynamic current–potential curves were swept from –250 to 250 mV at a scan rate of 1.00 mV/s. Impedance measurements were carried out using AC signals of amplitude of ±10 mV (peak to peak) at open circuit potential in the frequency range from 10 mHz to 2 MHz. Prior to the potential sweep, the electrode was left under open-circuit in the respective solution for ~1 h



until a steady free corrosion potential was recorded. The above procedures were repeated two times with success for each water quality, pH value and each inhibitors.

In the first part of the study, 3 different water qualities are examined in absence and presence of  $R_U N_2$  and  $R_S N_2$  at different pH values from 5 to 11 with an increment of 1.5. This is repeated for six inhibitors in decarbonised water. The aim is to observe the pH dependency of the inhibitors on corrosion inhibition.

In the second part of the study, six different inhibitors were examined in three different water at pH= 8, in order to observe the relationship between the inhibitor structure and inhibitor efficiency, additionally by the effect of different corrosive media .

In the last part, as a result of the literature survey, it is also obvious from the name of inhibitors (film forming amines) that fatty polyamines can be adsorbed on the carbon steel surface and block the active sites to decrease the corrosion rate. Therefore, adsorption isotherm plots were observed by using EIS data at decarbonised water at pH 8 for  $R_U N_2$  and with  $R_S N_2$ . Also, surface structure of some corroded carbon steel electrodes were examined by the scanning electron microscope (SEM) in order to obtain information about the sample's surface topography.



## **4. RESULTS AND DISCUSSION**

### **4.1. Measurements in Seawater**

In this part of the work, corrosion phenomena of carbon steel is examined by polarization curves and EIS measurements in absence and presence of  $R_{UN_2}$  and  $R_{SN_2}$  inhibitors at different pH values from 5 to 11 in seawater. Then six inhibitors differing in chemical structure are studied at pH= 8 in order to observe the effect of chemical structure and pH at corrosion inhibition of carbon steel in seawater.

#### **4.1.1. Measurements in the Absence of Inhibitor**

Figure 4.1 reports the Nyquist diagrams plotted at the corrosion potential for the different pH values in seawater in the absence of inhibitors. The impedance diagrams are characterized by a single time constant (a single loop). High frequency intercept of semi-circle on the real axis yields the solution resistance ( $R_s$ ) and low frequency region yield the sum of  $R_s$  and polarization resistance ( $R_p$ ).  $R_p$  values obtained from Nyquist diagram were summarized in Table 4.1 The semicircles are generally associated with the relaxation of the capacitors of electrical double layers with their diameters representing the charge transfer resistance. Loop size of pH 9.5 is larger than the other pH values which means highest polarization resistance and less corrosion rates.

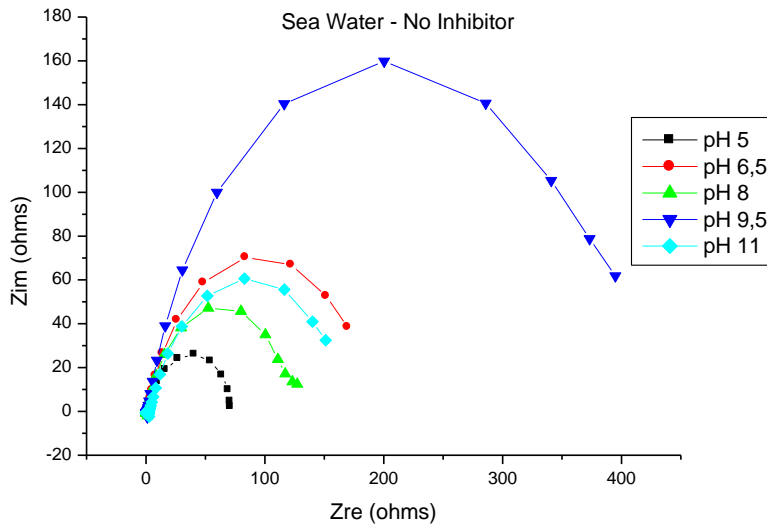


**Figure 4.1 :** Nyquist plot for carbon steel in seawater at 25 °C in absence of inhibitors at varying pH values.

Tafel-extrapolation measurements were done in the potentials region  $\pm 250$  mV from corrosion potential,  $E_{\text{corr}}$ . Figure 4.2 shows the steady-state current voltage curves obtained in seawater at different pH values varying from 5 to 11 in absence of inhibitors. The corresponding  $E_{\text{corr}}$ ,  $I_{\text{corr}}$ , anodic Tafel slopes ( $\beta_a$ ) and cathodic Tafel slopes ( $\beta_c$ ) at different pH values were summarized in Table 4.1.

Tafel extrapolation data were observed with less than 2 chi-square value in order to obtain consistency between the results, minimize the error percentage and standardize the extrapolation range (Table 4.1).

At pH= 9.5, a shift of  $E_{\text{corr}}$  in the anodic direction is observed and  $I_{\text{corr}}$  decreased in comparison with the other pH values.  $I_{\text{corr}}$  obtained from Tafel extrapolation and polarization resistance ( $R_p$ ) data obtained from EIS support each other and show smaller corrosion rate as compare to the other pH values (Table 4.1)

According to Pourbaix diagrams (Figure 2.3), possible reaction associated with iron in aqueous conditions at pH=9.5 is reaction of dissolved iron with hydroxyl ion in solution and formation of a passive film which consist of iron hydroxide on electrode surface. This explain the lower corrosion rate at this pH.

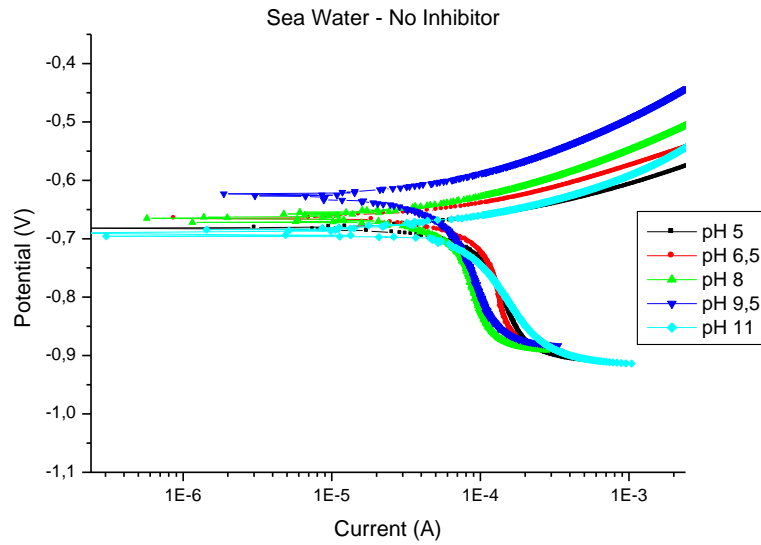


**Figure 4.2 :** Potentiodynamic polarization curves for carbon steel in seawater at 25 °C in absence of inhibitors at different pH values.

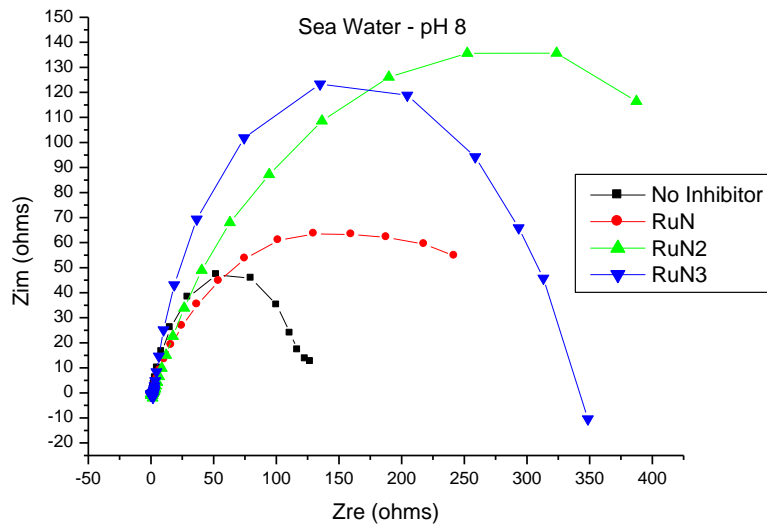
**Table 4.1 :** Polarization parameters for carbon steel in seawater at 25 °C in absence of inhibitors at different pH values.

Seawater		No Inhibitor				
pH	$-E_{corr}$ (mV vs. Ag/AgCl)	$I_{corr}$ ( $\mu A.cm^{-2}$ )	$\beta_a$ (mV)	$\beta_c$ (mV)	$R_p$ ( $\Omega cm^2$ )	Chi-Squ.
5.0	683	26	71	749	277	1.13
6.5	664	28	88	1302	668	1.07
8.0	661	21	99	1573	502	1.06
9.5	626	19	105	1473	1556	0.71
11.0	684	20	75	405	596	1.24

#### 4.1.2. Measurements in Seawater in the presence of inhibitors at pH=8

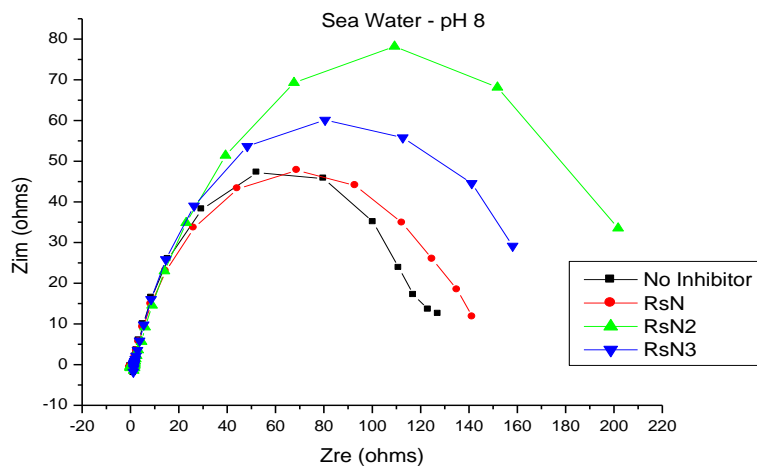
Inhibitors with different chemical structure are studied in order to observe the effect of chemical structure at constant pH (pH=8).

Figure 4.3 presents the impedance diagrams plotted for the unsaturated amines with the same concentration at pH=8 in order to compare them more clearly.  $R_{UN_2}$  has higher inhibition efficiency when compared with  $R_{UN_3}$  and  $R_{UN}$ . Both polarization data (Table 4.2) and impedance data support that the inhibition efficiency sequence is  $R_{UN_2} > R_{UN_3} = R_{UN}$ .



**Figure 4.3 :** Nyquist plot for carbon steel in seawater at 25 °C in absence and with unsaturated filming amines at pH 8.

Figure 4.4 shows the Nyquist diagrams plotted for the saturated amines with the same concentration at pH= 8 in seawater.  $R_S N_2$  has the largest  $R_p$  value which is also complying with the polarization results listed at Table 4.2. In fact, the higher is the  $R_p$  value, the better is the anticorrosion efficiency. The inhibition efficiency sequence is  $R_S N_2 > R_S N_3 > R_S N$  according to EIS data.



**Figure 4.4 :** Nyquist plot for carbon steel in seawater at 25 °C in absence and with saturated filming amines at pH 8.

The impedance response of carbon steel in seawater has significantly changed in the presence of inhibitors.

Polarization resistances were increased according to blank condition showing formation of more resistive layer on electrode surface in the presence of all inhibitor. On the other hand, the capacitive loop has the largest diameter with  $R_{UN_2}$  (Figure 4.5).

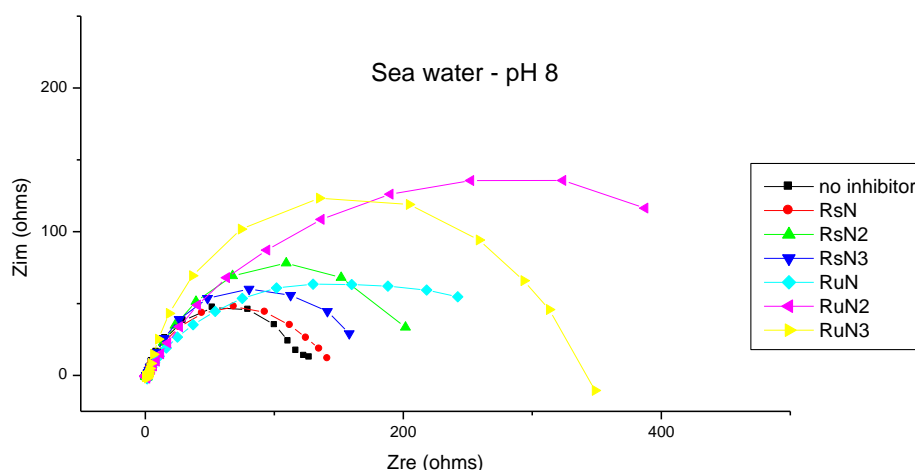


**Figure 4.5:** Nyquist plot for carbon steel in seawater at 25 °C in absence and presence of different inhibitors at pH=8.

From Table 4.2, it can be observed based on EIS data that unsaturated filming amines shows higher  $R_p$  values meaning better anticorrosion efficiency when compared to saturated polyamines, also diamines of both saturated and unsaturated species show the best efficiency compared to mono and triamines at seawater at pH 8.

**Table 4.2 :** Polarization parameters for carbon steel in seawater at 25 °C in absence and with different inhibitors at pH 8.

Seawater	pH 8					
	-E <sub>corr</sub> (mV vs. Ag/AgCl)	I <sub>corr</sub> ( $\mu\text{A}\cdot\text{cm}^{-2}$ )	$\beta_a$ (mV)	$\beta_c$ (mV)	$R_p^*$ ( $\Omega\text{cm}^2$ )	Chi-Squ.
<b>no inhibitor</b>	661	21	99	1573	502	<b>1.06</b>
<b><math>R_{S N_3}</math></b>	743	9	72	304	632	<b>0.90</b>
<b><math>R_{S N_2}</math></b>	745	10	72	250	790	<b>0.60</b>
<b><math>R_{S N}</math></b>	694	17	75	589	557	<b>0.92</b>
<b><math>R_{U N_3}</math></b>	565	17	91	734	1375	<b>0.54</b>
<b><math>R_{U N_2}</math></b>	530	11	86	476	1529	<b>0.92</b>
<b><math>R_{U N}</math></b>	622	16	89	548	1086	<b>0.78</b>

Inhibition efficiency expected to increase with decrease in amine number i.e  $RN > RN_2 > RN_3$ . Although second amin group shows expected effect in both saturated and unsaturated cases ( $R_U N_2$ ,  $R_s N_2$ ), further increase in amine number ( $RN_3$ ) does not have further increase in efficiency. It can be concluded that the inhibition efficiency is not proportional to the amine number in seawater. On the other hand unsaturated amines ( $R_U N_x$ ) have better inhibition effect than the saturated ones ( $R_s N_x$ ), may be due to better interaction of  $\pi$ -bonds of unsaturated inhibitors with metal surface.

EIS data is also analyzed by fitting it to an equivalent electrical circuit model. As the Nyquist plot obtained for all inhibitors present a depressed loop, such behavior is characteristic for solid electrodes and often referred to as frequency dispersion which has been attributed to the surface heterogeneity [58-61].

Figure 4.6 depicts the equivalent circuits to model electrochemical behavior belonging to the absence of the inhibitors after 1 hour immersion in seawater. The simplified Randles circuit with a CPE is used to represent the corroding system where  $R_s$  represents solution resistance,  $R_{ct}$  charge transfer resistance,  $CPE_{dl}$  a constant phase element, non ideal double layer capacitive element to give a more accurate fit [62].

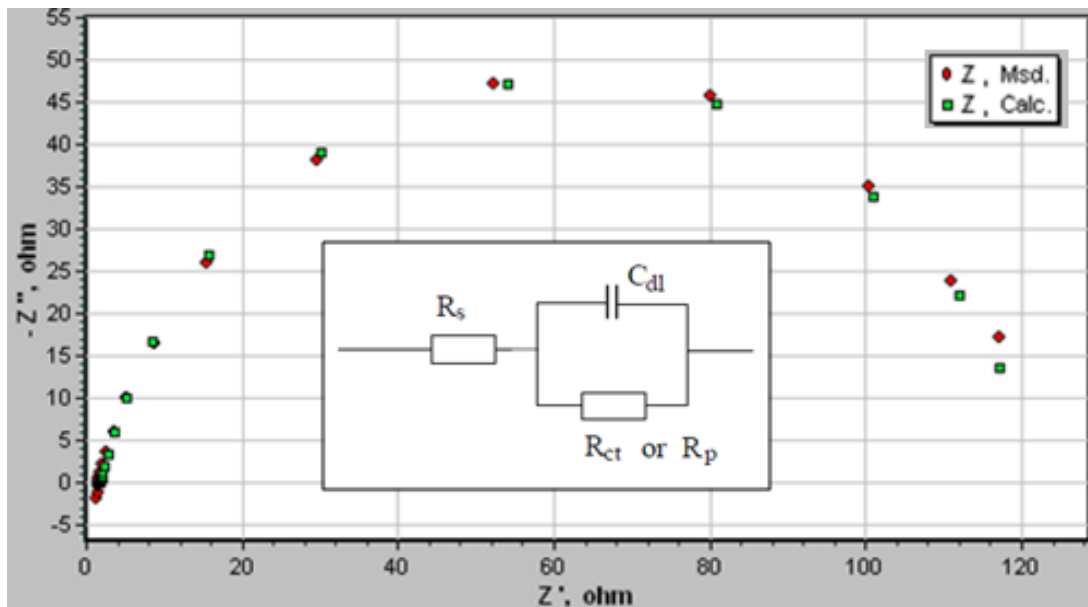


**Figure 4.6 :** Values of the elements of equivalent circuit required for fitting the EIS of carbon steel in seawater in absence of inhibitors at pH=8.

On the other hand, Figure 4.7 shows the equivalent circuits to model electrochemical behavior in the presence of the inhibitors after 1 hour immersion in seawater. The



electrochemical circuit model is represented by two time constant where the capacitance of the intact coating is represented by  $C_c$ . Its value is much smaller than a typical double layer capacitance.  $R_{po}$  (pore resistance) is the resistance of ion conducting paths that develop in the coating. These paths may not be physical pores filled with electrolyte. On the metal side of the pore, it is assumed that an area of the coating has delaminated and a pocket filled with an electrolyte solution has formed. This electrolyte solution can be very different than the bulk solution outside of the coating. The interface between this pocket of solution and the bare metal is modeled as a double layer capacitance in parallel with a kinetically controlled charge transfer reaction [62].

It is observed that a reasonable accuracy of the fitting was obtained, as evidence by chi-square in the order of  $10^{-3}$  and  $10^{-4}$  for all the experimental data.

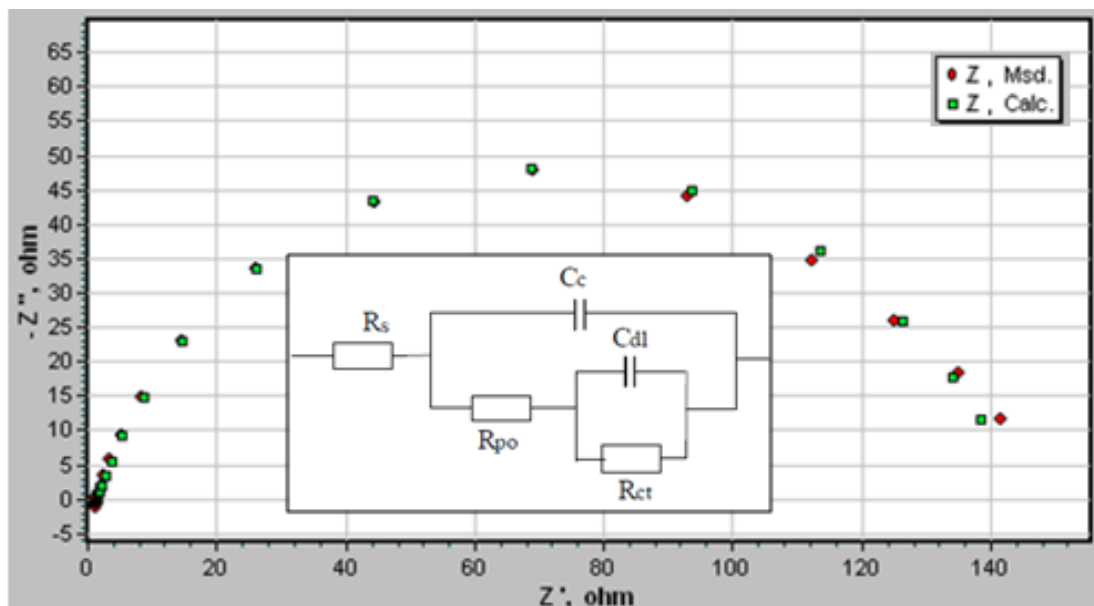


**Figure 4.7 :** Values of the elements of equivalent circuit required for fitting the EIS of carbon steel in seawater in presence of different inhibitors at pH=8.

Table 4.3 contains all the impedance parameters obtained from the simulation of experimental impedance data, including  $R_s$ ,  $R_{ct}$ ,  $Y_o$  and  $n$ . In the Table 4.3, also the calculated “double layer capacitance” values,  $C_{dl}$ , are shown using the equation 4.1.

$$C_{dl} = (Y_o \cdot R_{ct}^{1-n})^{1/n} \quad (4.1)$$

where  $Y_0$  is the CPE constant,  $n$  is a CPE exponent which can be used as a gauge of the heterogeneity or roughness of the surface. Inhibitor efficiency based on impedance data are calculated (Equation 4.2) and listed at Table 4.3 [56,57,58]

$$IE\% = \theta = \frac{R_{ct}(inh) - R_{ct}}{R_{ct}(inh)} \quad (4.2)$$

From Table 4.3, it is clear that the addition of inhibitors causes an increase in  $R_{ct}$  in seawater as the  $R_{ct}$  increases inhibitor efficiency increases and gets the highest value with  $R_{U}N_2$  when compared with the other species.

The value of the proportional factor  $Y_0$  of CPE varies in a regular manner with inhibitor concentration. The change of  $R_{ct}$  and  $Y_0$  values can be related to the gradual replacement of water molecules by inhibitor molecules on the surface and consequently to a decrease in the number of active sites necessary for the corrosion reaction.

**Table 4.3 :** Values of the elements of equivalent circuit required for fitting the EIS of carbon steel in seawater in absence and presence of different inhibitors at pH 8.

Seawater pH 8	$R_s$ $\Omega\text{cm}^2$	$R_{ct}$ $\Omega\text{cm}^2$	CPE, $Y_{odl}.10^5$ $\Omega^{-1}\text{s}^n\text{cm}^{-2}$	$n_{dl}$	$C_{dl}\mu\text{Fcm}^{-2}$	$R_{po}$ $\Omega\text{cm}^2$	CPE, $Y_{oc}.10^5$ $\Omega^{-1}\text{s}^n\text{cm}^{-2}$	$n_c$	IE %
No inh.	8	474	29	0.86	211				
$R_sN_3$	6	664	149	0.75	1.489	10	42	1	29
$R_sN_2$	7	909	194	0.71	2.453	12	42	1	48
$R_sN$	6	557	44	0.69	236	10	7	1	15
$R_U N_3$	8	1,311	29	0.77	216	10	9	1	64
$R_U N_2$	8	1,888	2	0.96	13	83	78	0.62	75
$R_U N$	8	1,169	53	0.51	340	6	4	0.87	59

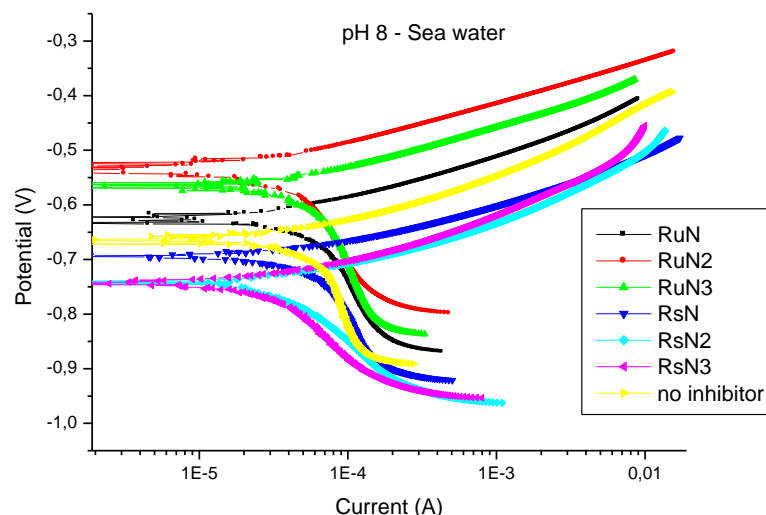


**Figure 4.8 :** Potentiodynamic polarization curves for carbon steel in seawater at 25 °C in absence and with different inhibitors at pH 8.

As it can be seen from Figure 4.8, the anodic and cathodic reactions are affected by the inhibitors. Meaning that, the addition of even saturated or unsaturated alkyl amines to seawater reduces the anodic dissolution of steel and also retards the cathodic hydrogen evolution reaction. Regarding the potentiodynamic polarization curves, it can be clearly seen that the  $E_{\text{corr}}$  values shifted to more positive potentials in the presence of unsaturated polyamines on the other hand to more negative potentials in the presence of saturated polyamines. There was not a specific relation between  $E_{\text{corr}}$  and inhibitors efficiency (Table 4.2). However, this can be related to alkyl chain chemistry.

As a result of these polarization data,  $I_{\text{corr}}$  values decrease considerably in the presence of all inhibitors which is more observable at  $R_{\text{UN}}_2$  and  $R_{\text{SN}}_2$ . The anodic Tafel slope ( $\beta_a$ ) change is less than when it is compared with the cathodic Tafel slope ( $\beta_c$ ) of all inhibitors, indicating that the all inhibitors controlled both anodic and cathodic reactions however more observable in cathodic side in seawater at pH 8.

The inhibition efficiency (IE%) can be calculated both from polarization and EIS measurements as given below with Equation 4.3. Calculated IE% were given in Table 4.4. Although values obtained from polarization and EIS have different values due to different methods (i.e DC and AC current measurements), they have similar trends. The polarization resistance ( $R_p$ ) was calculated from the EIS data.

$$IE\% = \left(\frac{I_{corr} - I_{inh}}{I_{corr}}\right) \times 100 = \left(\frac{R_{pinh} - R_{pcorr}}{R_{pinh}}\right) \times 100 \quad (4.3)$$

IE(%) reaches a maximum value with diamines for both of unsaturated and saturated amines when compared with mono and triamines. It is found that, saturated and unsaturated diamines present slightly better performances than mono and triamines.

**Table 4.4 :** Polarization parameters and the corresponding inhibition efficiency for the corrosion of carbon steel in seawater in absence and with different inhibitors at pH 8.

Seawater	pH 8				
	$-E_{corr}$ (mV vs. Ag/AgCl)	$I_{corr}$ ( $\mu A.cm^{-2}$ )	$R_p$ ( $\Omega cm^2$ )	$IE_{I_{corr}}$ (%)	$IE_{R_p}$ (%)
<b>no inhibitor</b>	661	21	502		
<b><math>R_S N_3</math></b>	743	9	632	56	21
<b><math>R_S N_2</math></b>	745	10	790	52	37
<b><math>R_S N</math></b>	694	17	557	17	10
<b><math>R_U N_3</math></b>	565	17	1375	19	64
<b><math>R_U N_2</math></b>	530	11	1529	46	67
<b><math>R_U N</math></b>	622	16	1086	21	54

#### 4.1.3. Measurements in seawater in the presence of $R_U N_2$

Saturated and unsaturated diamines showed better inhibition than the other amines. Therefore, they were investigated at different pH in seawater. Figure 4.9 presents the impedance diagrams obtained at the corrosion potential in the presence of 100 ppm  $R_U N_2$  in seawater at different pH values. It is obvious that the inhibitor has the largest loop size at pH=11. However, a phase formation occurred at pH=11 with addition of 100 ppm  $R_U N_2$  into seawater that has approx. 60.000  $\mu s/cm$  conductivity.

Addition of NaOH in order to pH adjustment causes phase formation at the end of 1 hour measurement which was not observed in the other pH measurements. Therefore, the measurement at pH=11 was not conducted under the same conditions with the others.

When pH=11 measurements eliminated,  $R_U N_2$  has the largest loop size at pH=9.5 when compared with the other pH values. Also, there is a noticeable increase at  $R_p$  value compared to in absence of inhibitor at pH 9.5 which enables the protection of the material.

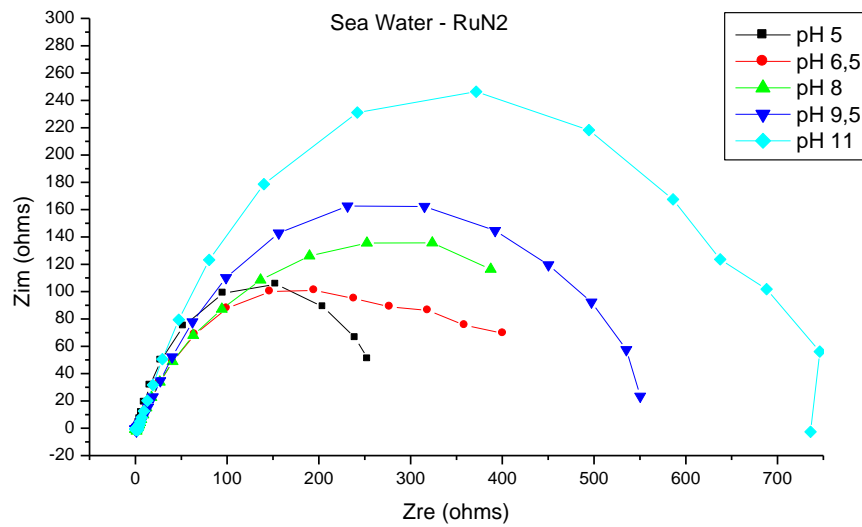


**Figure 4.9** : Nyquist plot for carbon steel in seawater at 25 °C with  $R_{UN_2}$  at different pH values.

Potentiodynamic polarization curves in the presence of  $R_{UN_2}$ , were given in Figure 4.10. Addition of  $R_{UN_2}$  caused a shift in positive direction meaning more positive  $E_{corr}$  values (Figure 4.9) as compared to in the absence of inhibitors. At higher pH than 5.0 potential shift to anodic direction which shows inhibition of anodic reaction due to formation of a passive film.

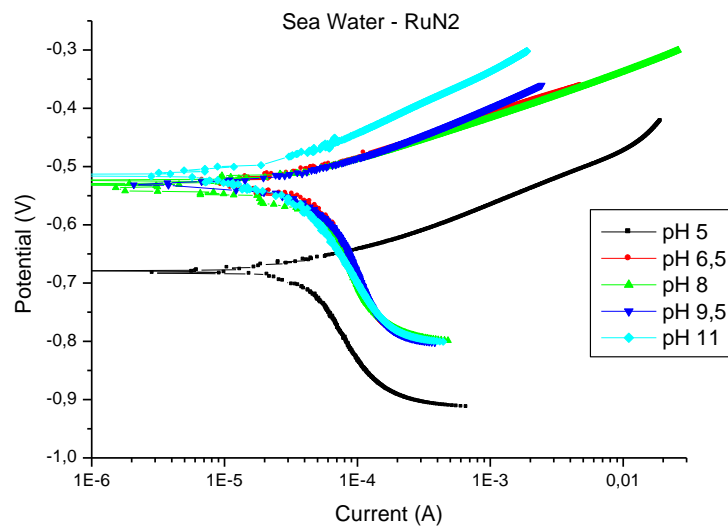


**Figure 4.10** : Potentiodynamic polarization curves for carbon steel in seawater at 25 °C with  $R_{UN_2}$  at varying pH values.

The corresponding  $E_{\text{corr}}$ ,  $I_{\text{corr}}$ ,  $IE\%$ ,  $\beta_a$  and  $\beta_c$  at different pH values for  $R_{\text{UN}_2}$  are listed in Table 4.5. The polarization resistance ( $R_p$ ) values are derived from the EIS data. When the data compared with the absence and presence of  $R_{\text{UN}_2}$  (Table 4.1 and Table 4.5 respectively), it can be seen that  $I_{\text{corr}}$  values were significantly changed in the pH range of 6.5- 9.5 according to both polarization and EIS results. We can conclude that  $R_{\text{UN}_2}$  has high anticorrosion efficiency in a range of 6.5-9.5 in seawater. Also,  $IE\%$  values calculated from both polarization EIS data comply with the conclusion that  $R_{\text{UN}_2}$  has high anticorrosion efficiency in a range of 6.5-9.5 in seawater.

**Table 4.5 :** Polarization parameters for carbon steel in seawater at 25 °C with  $R_{\text{UN}_2}$  at different pH values.

Seawater		$R_{\text{UN}_2}$						
pH	-E <sub>corr</sub> (mV vs. Ag/AgCl)	I <sub>corr</sub> ( $\mu\text{A}\cdot\text{cm}^{-2}$ )	$\beta_a$ (mV)	$\beta_c$ (mV)	R <sub>p</sub> ( $\Omega\text{cm}^2$ )	IE <sub>I<sub>corr</sub></sub> (%)	IE <sub>R<sub>p</sub></sub> (%)	Chi-Squ.
5.0	682	12	84	466	988	53	72	1.25
6.5	529	11	87	454	1580	55	58	1.42
8.0	530	11	86	476	1529	46	67	0.92
9.5	530	14	102	551	2173	27	28	1.13
11.0	513	9	131	430	2907	53	79	1.13

#### 4.1.4. Measurements in seawater in the presence of $R_{\text{SN}_2}$

Figure 4.11 reports the impedance diagrams obtained at the corrosion potential in the presence of 100 ppm  $R_{\text{SN}_2}$  in seawater at different pH values. Again, phase formation with addition of 100 ppm  $R_{\text{SN}_2}$  occurred at pH 11 in seawater. The largest loop size is obtained at pH 9.5 ( $R_p = 1,047 \Omega\cdot\text{cm}^2$ ). Meaning that better corrosion inhibition is enabled with  $R_{\text{SN}_2}$  at pH 9.5 which is also supported by polarization data listed in Table 4.6.

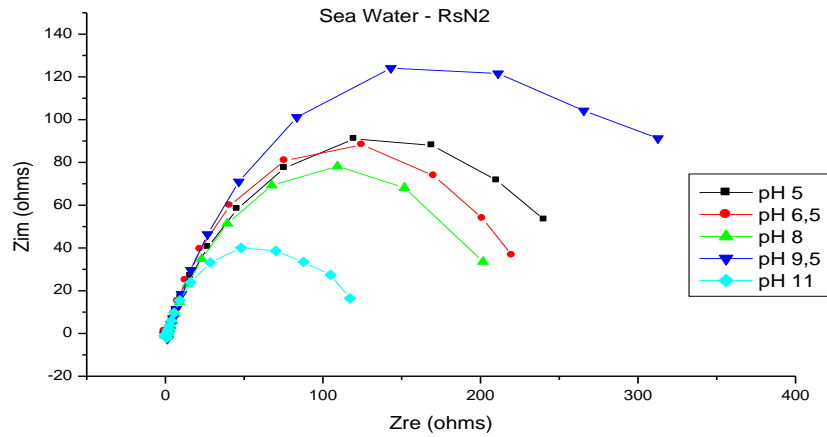


**Figure 4.11** : Nyquist plot for carbon steel in seawater at 25 °C with  $R_S N_2$  at different pH values.

Potentiodynamic polarization curves in the presence of  $R_S N_2$ , were given in Figure 4.12. Corrosion potential were shifted in the cathodic range as compared to in absence of inhibitors (Figure 4.11 and Figure 4.2 respectively).

The corresponding  $E_{corr}$ ,  $I_{corr}$ ,  $IE\%$ ,  $\beta_a$  and  $\beta_c$  at different pH values for  $R_S N_2$  are listed in Table 4.6. It can be observed that both polarization and impedans data supporting each other and suggest that the better corrosion inhibition is enabled in a pH range of 6.5- 9.5 with  $R_S N_2$  in seawater similarly to  $R_U N_2$ .  $IE\%$  values based on polarization results also support this pH range. While  $E_{corr}$  values shifted in the anodic range with  $R_U N_2$  they were shifted in cathodic direction with  $R_S N_2$  in seawater.

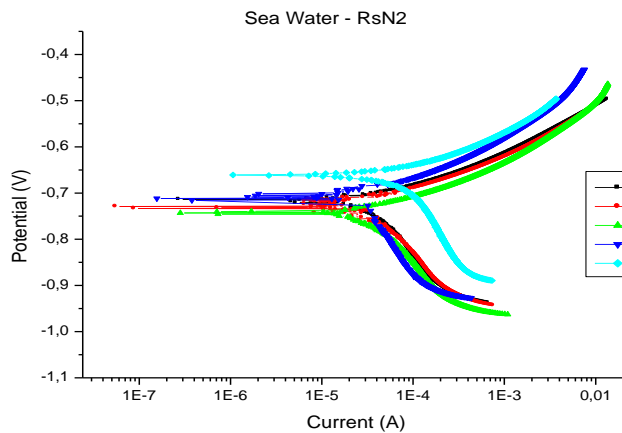


**Figure 4.12** : Potentiodynamic polarization curves for carbon steel in seawater at 25 °C with  $R_S N_2$  at different pH values.

**Table 4.6 :** Polarization parameters for carbon steel in seawater at 25 °C with  $R_sN_2$  at varying pH values.

Seawater		$R_sN_2$						
pH	-E <sub>corr</sub> (mV vs. Ag/AgCl)	I <sub>corr</sub> ( $\mu A \cdot cm^{-2}$ )	$\beta_a$ (mV)	$\beta_c$ (mV)	R <sub>p</sub> ( $\Omega cm^2$ )	IE <sub>I<sub>corr</sub></sub> (%)	IE <sub>R<sub>p</sub></sub> (%)	Chi-Squ.
5.0	719	10	67	273	948	62	71	0,99
6.5	727	9	70	230	869	62	23	1,06
8.0	745	10	72	250	790	52	37	0,60
9.5	717	7	78	277	1047	64	-49	0,99
11.0	662	26	86	429	462	-30	-29	0,94

## 4.2. Measurements in Decarbonised Water

In this part of the work, corrosion phenomena of carbon steel is examined by polarization curves and EIS data in absence and presence of inhibitor at different pH values from 5 to 11 in decarbonised water. Similarly to the measurements in seawater at constant pH (pH= 8), corrosion inhibition of inhibitors for carbon steel were also investigated. In addition inhibition effect of  $R_U N_2$  and  $R_S N_2$  were also investigated at different pH comparatively with the absence of inhibitors.

### 4.2.1. Measurements in decarbonised water in the absence of inhibitor

Figure 4.13 shows the Nyquist diagrams obtained after 1h immersion in absence of inhibitors at different pH. When the diameter of semicircle obtained at different pH compared with each other significant changes as in the case of seawater measurements (Figure 4.1) were not observed in decarbonised water.

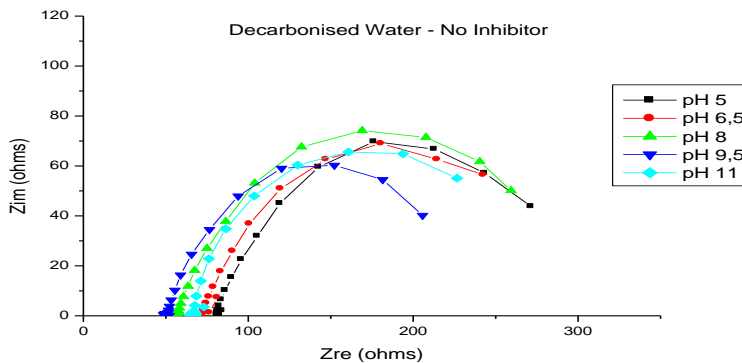


**Figure 4.13 :** Nyquist plot for carbon steel in decarbonised water at 25 °C in absence of inhibitors at varying pH values.



Anodic and cathodic polarization curves obtained at different pH in decarbonized water were given in Figure 4.14. Data collected from these curves were summarized in Table 4.7. It can be seen that anodic and cathodic slopes are very similar for all pH values. However, at pH=8,  $I_{corr}$ ,  $\beta_a$  and  $\beta_c$  have the lowest values as compared to the other pH values suggested more stable behaviour of carbon steel.

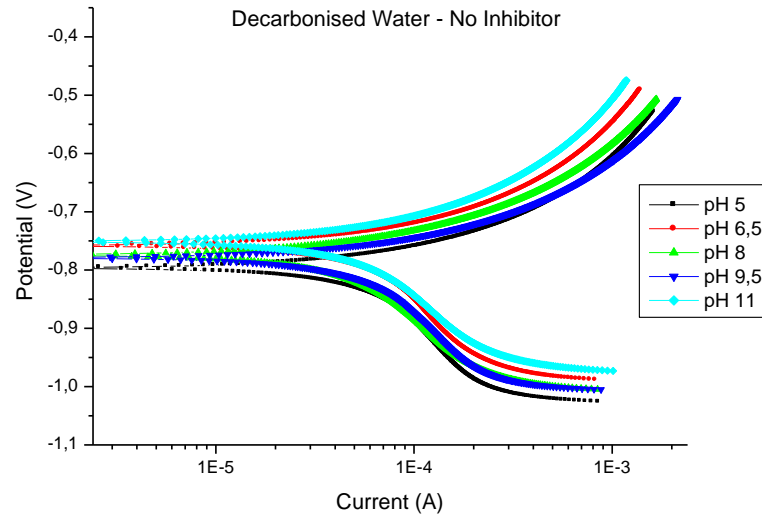


**Figure 4.14** : Potentiodynamic polarization curves for carbon steel in decarbonised water at 25 °C in absence of inhibitors at varying pH values.

The polarization resistances ( $R_p$ ) were obtained from the EIS measurements and compared with polarization measurements (Table 4.7).  $R_p$  values are very close to each other.

**Table 4.7** : Polarization parameters for carbon steel in decarbonised water at 25 °C in absence of inhibitors.

Decarbonised Water		No Inhibitor				
pH	- $E_{corr}$ (mV vs. Ag/AgCl)	$I_{corr}$ ( $\mu A.cm^{-2}$ )	$\beta_a$ (mV)	$\beta_c$ (mV)	$R_p$ ( $\Omega cm^2$ )	Chi-Squ.
5.0	797	25	135	886	790	1.08
6.5	758	24	131	824	810	0.71
8.0	775	13	104	373	790	1.06
9.5	780	21	112	774	672	1.08
11.0	751	25	161	864	711	1.11

#### 4.2.2. Measurements in decarbonised water in the presence of inhibitors at pH=8

pH stayed constant at 8 and, inhibitors added in decarbonized water in order to observe the effect of chemical structure polarization and EIS measurements were performed. The impedance response of carbon steel in decarbonised water has significantly changed after the addition of inhibitors. The capacitive loop has the largest shape with  $R_{UN_2}$  (Figure 4.15) which is similar to the behaviour in seawater. It means that  $R_{UN_2}$  has greatest anticorrosion efficiency in decarbonised water when compared with the other inhibitors which is also supported by polarization results given in Table 4.8.  $R_{S_2N_2}$  shows the similar behavior with  $R_{UN_2}$  and it has the highest  $R_p$  values in saturated amines. For both saturated and unsaturated amines, the inhibition efficiency is not proportional to the amine number. Moreover, alkyl chain structure is also effective on corrosion inhibition that unsaturated diamine has greater efficiency than saturated diamine which is also supported by the results observed in seawater.

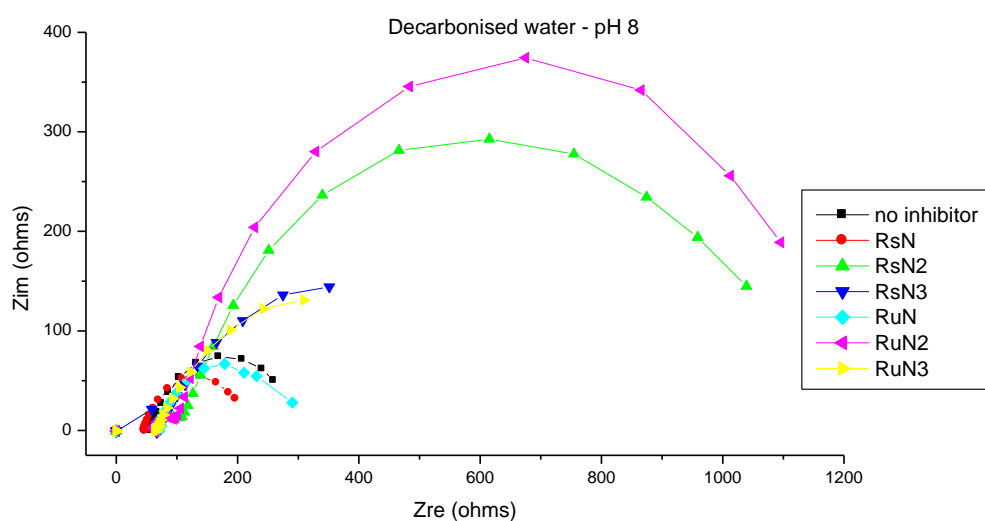


**Figure 4.15** : Nyquist plot for carbon steel in decarbonised water at 25 °C in absence and with different inhibitors at pH 8.

Figure 4.16 presents comparison of saturated and unsaturated diamines and triamines. As it can be seen diamines show better anticorrosion efficiency as compared to triamines and unsaturated diamines effect better than saturated at pH=8.

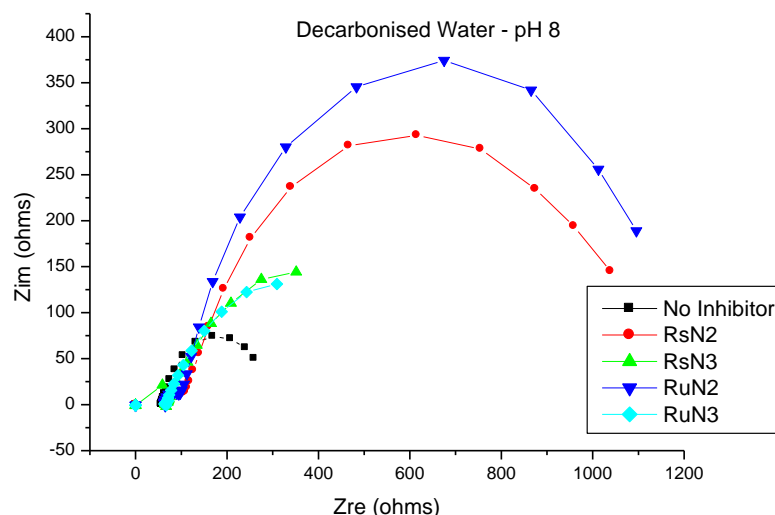


**Figure 4.16** : Nyquist plot for carbon steel in decarbonised water at 25 °C in absence and presence unsaturated and saturated di- and triamines at pH=8.

**Table 4.8** : Polarization parameters for carbon steel in decarbonised water at 25 °C in absence and presence of inhibitors at pH=8.

Decarbonised Water	pH 8					
	-E <sub>corr</sub> (mV vs. Ag/AgCl)	I <sub>corr</sub> ( $\mu\text{A}\cdot\text{cm}^{-2}$ )	$\beta_a$ (mV)	$\beta_c$ (mV)	R <sub>p</sub> ( $\Omega\text{cm}^2$ )	Chi-Squ.
no inhibitor	775	13	104	373	<b>790</b>	<b>1.06</b>
R <sub>S</sub> N <sub>3</sub>	681	13	158	690	<b>1.185</b>	<b>1.03</b>
R <sub>S</sub> N <sub>2</sub>	560	10	195	435	<b>3.950</b>	<b>0.18</b>
R <sub>S</sub> N	804	19	97	392	<b>593</b>	<b>0.8</b>
R <sub>U</sub> N <sub>3</sub>	689	13	151	565	<b>1.067</b>	<b>1.65</b>
R <sub>U</sub> N <sub>2</sub>	547	7	181	321	<b>4.069</b>	<b>0.99</b>
R <sub>U</sub> N	775	17	107	705	<b>869</b>	<b>1.09</b>

Figure 4.17 defines the equivalent circuits to model electrochemical behavior in absence of the inhibitors after 1 hour immersion in decarbonised water. The simplified Randles circuit with a CPE is used to represent the corroding system where R<sub>s</sub> represents solution resistance, R<sub>ct</sub> charge transfer resistance, CPE<sub>dl</sub> a constant phase element, non ideal double layer capacitive element to give a more accurate fit.

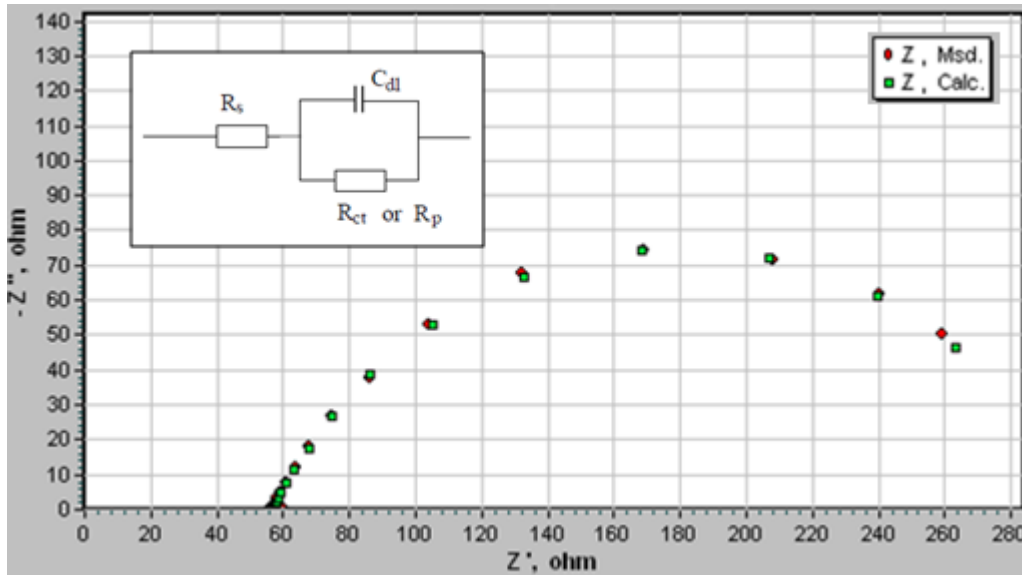


**Figure 4.17 :** Values of the elements of equivalent circuit required for fitting the EIS of carbon steel in decarbonised water in absence of inhibitors at pH 8.

Moreover, Figure 4.18 presents the equivalent circuits to model electrochemical behavior in the presence of the inhibitors after 1 hour immersion in decarbonised water. The electrochemical circuit model is represented by two time constant where the capacitance of the intact coating is represented by  $C_c$ .  $R_{po}$  (pore resistance) is the resistance of ion conducting paths the develop in the coating. These paths may not be physical pores filled with electrolyte. On the metal side of the pore, it is assumed that an area of the coating has delaminated and a pocket filled with an electrolyte solution has formed. This electrolyte solution can be very different than the bulk solution outside of the coating. The interface between this pocket of solution and the bare metal is modeled as a double layer capacitance in parallel with a kinetically controlled charge transfer reaction [62].

All the experimental data was observed by a reasonable accuracy of the fitting by chi-square in the order of  $10^{-4}$ .

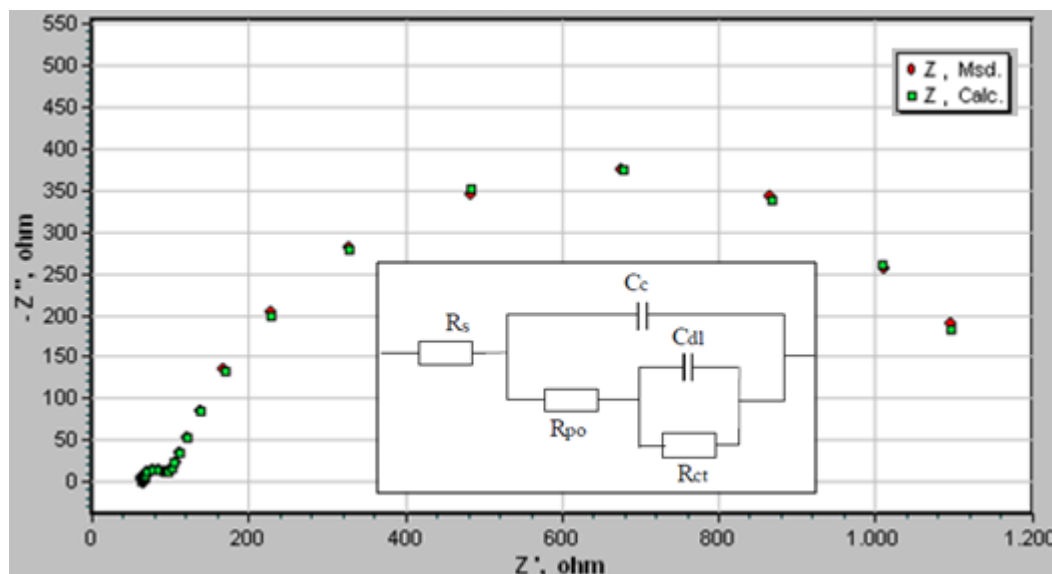


**Figure 4.18 :** Values of the elements of equivalent circuit required for fitting the EIS of carbon steel in decarbonised water in presence of different inhibitors at pH=8.

Table 4.9 contains all the impedance parameters obtained from the simulation of experimental impedance data, including  $R_s$ ,  $R_{ct}$ ,  $Y_o$ ,  $n$  and also the calculated “double layer capacitance” values ( $C_{dl}$ ) are shown, using the Equation 4.1.

From Table 4.9, it is clear that the addition of inhibitors causes an increase in  $R_{ct}$  in decarbonised water except  $R_sN$  and  $R_uN$  and this can be attributed as negligible corrosion inhibition of these inhibitors. As the  $R_{ct}$  increases inhibitor efficiency increases and gets the highest value with  $R_{uN_2}$  when compared with the others.

Inhibitor efficiency based on impedance data are calculated (Equation 4.2) and listed at Table 4.9.  $R_{uN_2}$  has the highest inhibitor efficiency which is also supported by polarization data. It can be said that alkyl chain structure is effective on corrosion inhibition and unsaturated ones shows better performance.

**Table 4.9 :** Values of the elements of equivalent circuit required for fitting the EIS of carbon steel in decarbonised water in absence and presence of different inhibitors at pH=8.

Decarb. pH 8	$R_s$ $\Omega\text{cm}^2$	$R_{ct}$ $\Omega\text{cm}^2$	CPE, $Y_{odl} \cdot 10^5$ $\Omega^{-1}\text{s}^n\text{cm}^{-2}$	$n_{dl}$	$C_{dl}$ $\mu\text{Fcm}^{-2}$	$R_{po}$ $\Omega\text{cm}^2$	CPE, $Y_{oc} \cdot 10^5$ $\Omega^{-1}\text{s}^n\text{cm}^{-2}$	$n_c$	IE %
No inh.	224	969	204	0.7	2,734				
$R_sN_3$	0	2,674	173	0.56	5,792	265	0	1	64
$R_sN_2$	169	4,294	20	0.75	184	332	9	0.4	77
$R_sN$	186	608	237	0.69	2,788	65	74	1	-59
$R_uN_3$	0	2,149	198	0.59	5,438	261	0	1	55
$R_uN_2$	250	4,400	23,26	0.75	234	142	0	0.8	78
$R_uN$	269	845	202	0.66	2,651	71	49	1	-15

Anodic and cathodic polarization curves obtained in the absence and presence of inhibitors at pH=8 in decarbonized water were given in Figure 4.19. As it can be seen, with addition of the inhibitors, shift of  $E_{corr}$  in anodic region was observed. The highest positive shift in  $E_{corr}$  was observed in the case of  $R_{UN_2}$  and  $R_{SN_2}$ . In the presence of monoamines the  $I_{corr}$  values increased as compared to in absence of inhibitors. This results also supported by EIS data (Table 4.9 and Table 4.10).

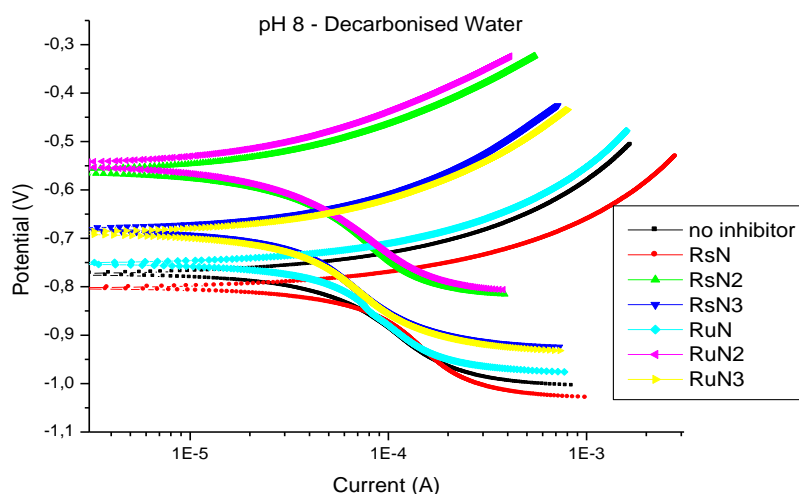


**Figure 4.19** : Potentiodynamic polarization curves for carbon steel in decarbonised water at 25 °C in absence and with different inhibitors at pH 8.

The inhibition efficiency (IE%) are calculated from the Equation 4.3 also given in Table 4.10.

**Table 4.10** : Polarization parameters and the corresponding inhibition efficiency for the corrosion of carbon steel in decarbonised water in absence and with different inhibitors at pH=8.

Decarbonised Water	pH 8				
	-E <sub>corr</sub> (mV vs. Ag/AgCl)	I <sub>corr</sub> (μA.cm <sup>-2</sup> )	R <sub>p</sub> (Ωcm <sup>2</sup> )	E <sub>I<sub>corr</sub></sub> (%)	E <sub>R<sub>p</sub></sub> (%)
no inhibitor	775	13	790		
R <sub>S</sub> N <sub>3</sub>	681	13	1.185	4	33
R <sub>S</sub> N <sub>2</sub>	560	10	3.950	27	80
R <sub>S</sub> N	804	19	593	-41	-33
R <sub>U</sub> N <sub>3</sub>	689	13	1.067	6	26
R <sub>U</sub> N <sub>2</sub>	547	7	4.069	47	81
R <sub>U</sub> N	775	17	869	-24	9

### 4.2.3. Measurements in Decarbonised Water in the presence of $R_{U}N_2$ at different pH

Figure 4.20 presents the impedance diagrams plotted for  $R_{U}N_2$  at varying pH values in decarbonised water. The impedance diagrams are characterized by a single time constant. Comparison of the polarization resistance values,  $R_p$ , determined from this loop has the largest size at pH 8 in presence of  $R_{U}N_2$ .

The distorted shape of the high-frequency part of the impedance diagram (Figure 4.20) can be attributed to the formation of a relatively thick and compact protective film on the metal surface [63].

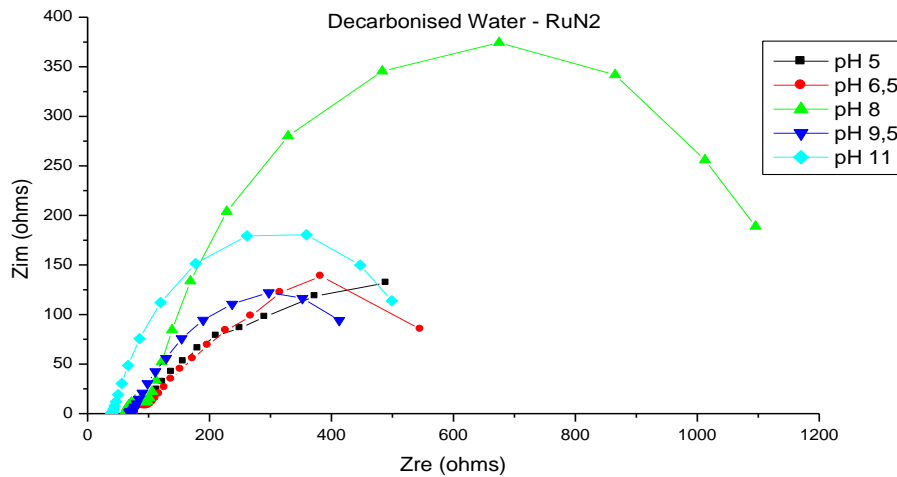


**Figure 4.20** : Nyquist plot for carbon steel in decarbonised water at 25 °C with  $R_{U}N_2$  at varying pH values.

As it can be seen from Figure 4.21, the anodic and cathodic reactions are affected by the addition of  $R_{U}N_2$ .  $E_{corr}$  values (Table 4.11) shifted to more positive potentials in the presence of  $R_{U}N_2$ . At pH 11,  $E_{corr}$  shifted to more positive region compared to the other pH values although there was not a specific relation between  $E_{corr}$  and inhibitors efficiency. Since, at pH 11,  $\beta_a$  got the highest value compared to no inhibitor case which resulted in the highest  $I_{corr}$ .

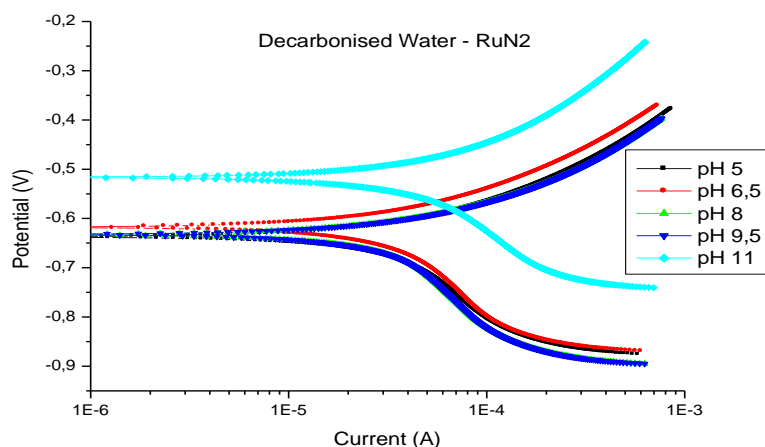


**Figure 4.21** : Potentiodynamic polarization curves for carbon steel in decarbonised water at 25 °C with RuN<sub>2</sub> at varying pH values.

Values of associated electrochemical parameters obtained by extrapolation of the Tafel lines and EIS data and also IE% based on Tafel and EIS data are presented in Table 4.11. The polarization resistance (Rp) was calculated from the EIS data. Both Tafel and EIS support each other that at pH 8, I<sub>corr</sub> got the lowest value and Rp gets the highest value meaning higher anticorrosion efficiency. Moreover, inhibitor efficiency is higher at pH= 8 when compared to the other pH values.

**Table 4.11** : Polarization parameters for carbon steel in decarbonised water at 25 °C with R<sub>U</sub>N<sub>2</sub> at varying pH values.

Decarbonised Water		R <sub>U</sub> N <sub>2</sub>						
pH	-E <sub>corr</sub> (mV vs. Ag/AgCl)	I <sub>corr</sub> (μA.cm <sup>-2</sup> )	β <sub>a</sub> (mV)	β <sub>c</sub> (mV)	R <sub>p</sub> (Ωcm <sup>2</sup> )	E <sub>I<sub>corr</sub></sub> (%)	E <sub>R<sub>p</sub></sub> (%)	Chi-Squ.
5.0	638	16	192	843	1,699	34	53	0.95
6.5	617	14	181	642	1,857	42	55	1.49
8.0	547	7	181	321	3,950	47	80	0.99
9.5	632	18	174	3,262	1,462	14	54	1.51
11.0	516	33	330	1,029	1,817	-32	61	1.55

#### 4.2.4. Measurements in Decarbonised Water in the presence of R<sub>S</sub>N<sub>2</sub> at different pH

Corrosion behaviour of saturated diamine was investigated at different pH in decarbonized water. The Nyquist diagrams obtained at different pH are shown in Figure 4.22. Although there is only one capacitive loop in absence of inhibitor (Figure 4.13) and in the R<sub>U</sub>N<sub>2</sub> (Figure 4.20), in the presence of R<sub>S</sub>N<sub>2</sub> two separated capacitive loops observed. These loops are more observable at pH 5, 6.5 and 9.5



values (Figure A.1). The capacity associated with the high frequency loop observed in the presence of  $R_5N_2$  is very low compared to low frequency that can be ascribed to either a) the change of the dielectric constant of the double layer, resulting from the strong hydrophobic nature of the inhibitor compound thus involving a double layer capacity value of the same order of magnitude to those obtained in less polar solvents, or b) the formation of a more compact and protective film, similar to a paint film [63]. In this case, it can be attributed to formation of more compact and protective film.

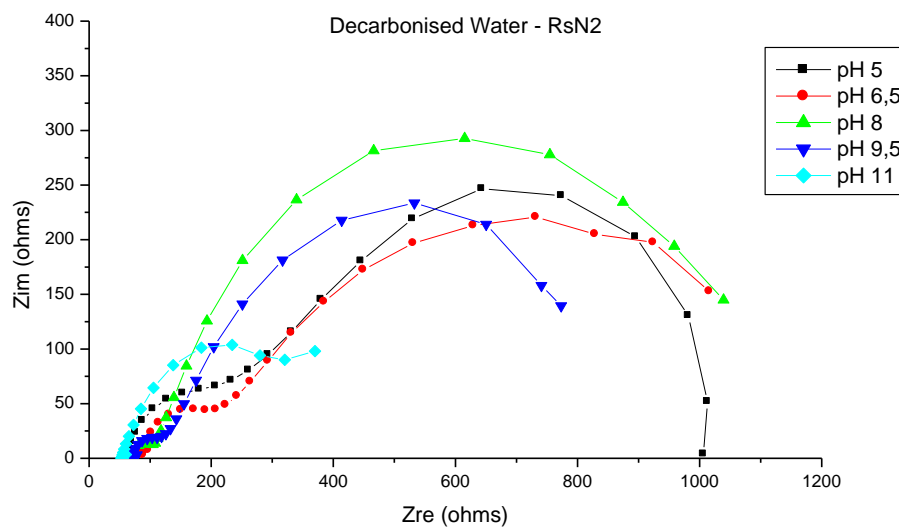


**Figure 4.22** : Nyquist plot for carbon steel in decarbonised water at 25 °C with  $R_5N_2$  at varying pH values.

Anodic and cathodic polarization curves obtained at different pH for  $R_5N_2$  were given in Figure 4.23. Corrosion parameters obtained from these curves summarized in Table 4.12. It can be seen that anodic and cathodic slopes are very close for all pH values and also shifted to more positive potentials except pH=11. At pH=11, there is a drastic increase in  $\beta_c$  the and highest  $I_{corr}$  was obtained as compared to the other pH values. Increase in  $OH^-$  ion concentration exchanged the cathodic reaction and cause the increase in corrosion rate.

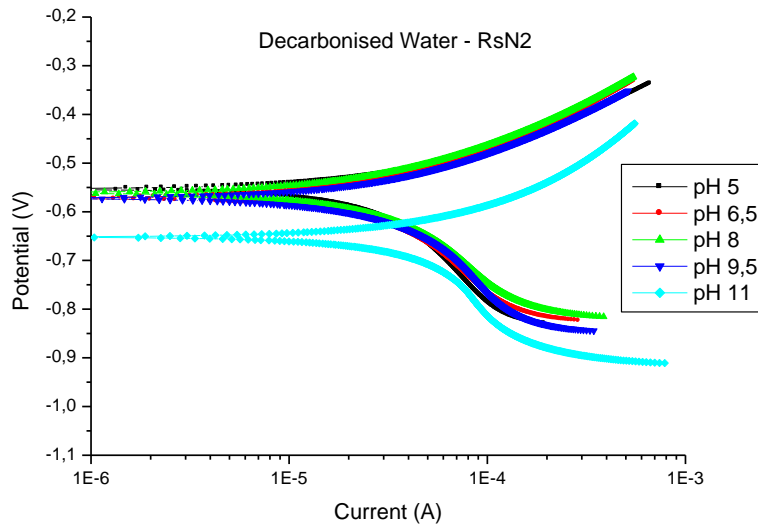


**Figure 4.23** : Potentiodynamic polarization curves for carbon steel in decarbonised water at 25 °C with  $R_5N_2$  at varying pH values.

The polarization resistance ( $R_p$ ) was calculated from the EIS data and given in Table 4.12. Both polarization and EIS results have the same trend and at pH=6.5 and 8.0 the lowest  $I_{corr}$  and the highest  $R_p$  values were observed. Additionally, the IE% values listed in the Table 4.12 show that at pH 6.5 and 8, highest inhibitor efficiencies were observed.

**Table 4.12** : Polarization parameters for carbon steel in decarbonised water at 25 °C with  $R_5N_2$  at different pH values.

Decarbonised Water		$R_5N_2$						
pH	-E <sub>corr</sub> (mV vs. Ag/AgCl)	I <sub>corr</sub> ( $\mu A \cdot cm^{-2}$ )	$\beta_a$ (mV)	$\beta_c$ (mV)	R <sub>p</sub> ( $\Omega cm^2$ )	IE <sub>I<sub>corr</sub></sub> (%)	IE <sub>R<sub>p</sub></sub> (%)	Chi-Squ.
5.0	556	11	173	664	3,753	56	79	1.0
6.5	572	10	197	461	3,950	57	79	1.1
8.0	560	10	195	435	3,950	23	80	0.18
9.5	572	12	204	541	2,765	43	76	0.71
11.0	651	26	227	2,576	1,225	-3	42	1.21

In this part of the work,  $R_{UN}$ ,  $R_{UN_3}$ ,  $R_{SN}$ ,  $R_{SN_3}$  are additionally investigated in decarbonised water at different pH values from 5 to 11. Further detailed informations on these measurements are given in Appendices.

Corrosion behaviour of saturated monoamine ( $R_5N$ ) was studied at different pH in decarbonized water. Anodic and cathodic polarization curves observed at different pH were given in Figure A.3. Corrosion parameters obtained from these curves were

summarized in Table A.1. It can be seen that anodic and cathodic slopes are very close for all pH values and also shifted to more positive potentials except pH=11 which has the same behavior with  $R_S N_2$ . The Nyquist diagrams obtained at different pH for  $R_S N$  are shown in Figure A.4. It can be seen that with obtained polarization and EIS data which is summarized at Table A.1, with addition of  $R_S N$ , not an observable anticorrosion efficiency was obtained.

Corrosion behaviour of saturated monoamine ( $R_S N_3$ ) was investigated at different pH in decarbonized water. Anodic and cathodic polarization curves observed at different pH were given in Figure A.5. Corrosion parameters obtained from these curves were listed in Table A.2. It can be seen that anodic and cathodic slopes are very close for all pH values except pH=5 and pH=11 at which there was a drastic increase in cathodic slopes. At pH= 6.5, corrosion potential shifted to more positive potentials which resulted in the highest inhibitor efficiency compared to the other pH values. The Nyquist diagrams obtained at different pH for  $R_S N_3$  are shown in Figure A.6.

From Figure A.7, the anodic and cathodic reactions are affected by the addition of unsaturated monoamine,  $R_U N$ .  $E_{corr}$  values (Table A.3) shifted to more positive potentials in the presence of  $R_U N$ . At pH=6.5 and pH=11,  $E_{corr}$  shifted to more positive region compared to the other pH values although there was not a specific relation between  $E_{corr}$  and inhibitors efficiency. Since, at pH 11,  $\beta_a$  got the highest value compared to no inhibitor case which resulted in the highest  $I_{corr}$ . Figure A.8 presents the impedance diagrams plotted for  $R_U N$  at varying pH values in decarbonised water. Comparison of the polarization resistance values,  $R_p$ , determined from this loop has the largest size at pH 6.5 in presence of  $R_U N$ .

Anodic and cathodic polarization curves obtained at different pH for  $R_U N_3$  were given in Figure A.9. Corrosion parameters obtained from these curves summarized in Table A.4. It can be seen that anodic slopes are very close for all pH values and got the lowest values at pH= 8 which resulted in the lowest  $I_{corr}$ . The Nyquist diagrams obtained at different pH for  $R_U N_3$  are shown in Figure A.10. It can be seen that with obtained EIS data which is summarized at Table A.4, higher inhibitor efficiency was obtained at around pH=8.

### 4.3. Measurements in Deionised Water

This part of study is composed of the investigated of carbon steel corrosion by polarization curves and EIS data in absence of inhibitor, at different pH values from 5 to 11 in deionised water. Additionally, at the same pH value (pH=8), corrosion inhibition of inhibitors for carbon steel in deionised water were compared. Effect of pH in the presence of  $R_{UN_2}$  and  $R_{SN_2}$  was also investigated as in the case of sea and decarbonized water.

#### 4.3.1. Measurements in Deionised Water in the Absence of Inhibitor

Figure 4.24 reports the Nyquist diagrams plotted at the corrosion potential for the different pH values in deionised water in absence of inhibitors. The impedance diagrams are characterized by two time constant which is more significant at pH=11 (Figure 4.25). Polarization resistance values obtained from Nyquist diagram listed in Table 4.24.  $R_p$  value at pH 9.5 is higher than the other pH values meaning higher anticorrosion efficiency.

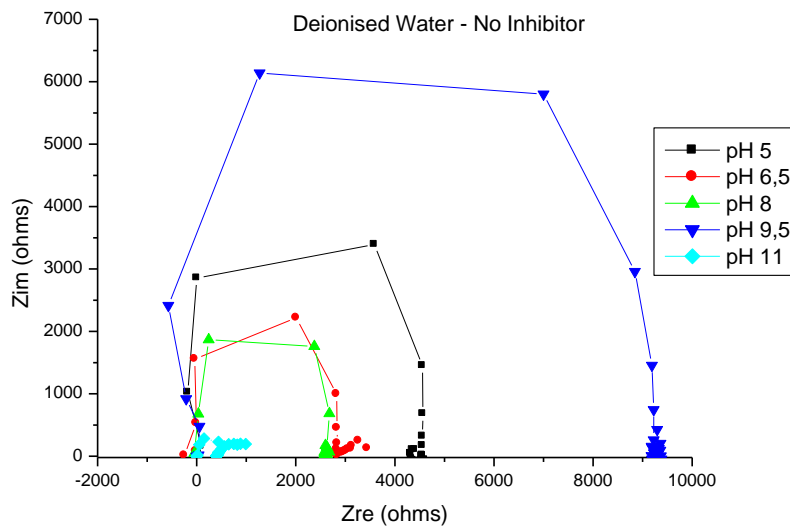


**Figure 4.24** : Nyquist plot for carbon steel in deionised water at 25 °C in absence of inhibitors at varying pH values.

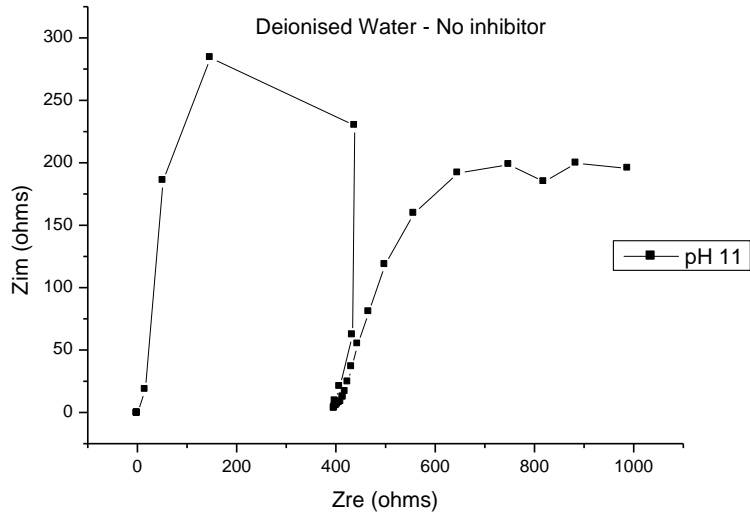


**Figure 4.25** : Nyquist plot for carbon steel in deionised water at 25 °C in absence of inhibitors at pH 11.

Potentiodynamic polarization curves for carbon steel in deionised water in the absence of inhibitors at different pH values were given in Figure 4.26. Corrosion parameters obtained from these curves were summarized in Table 4.13. It can be seen that anodic and cathodic slopes ( $\beta_a$  and  $\beta_c$ ) and positive shift in  $E_{corr}$  at pH 9.5 have the highest values. The polarization resistance ( $R_p$ ) was obtained from the EIS measurements and given in Table 4.13. It has the highest value at pH 9.5 which is in agreement with polarization measurements .

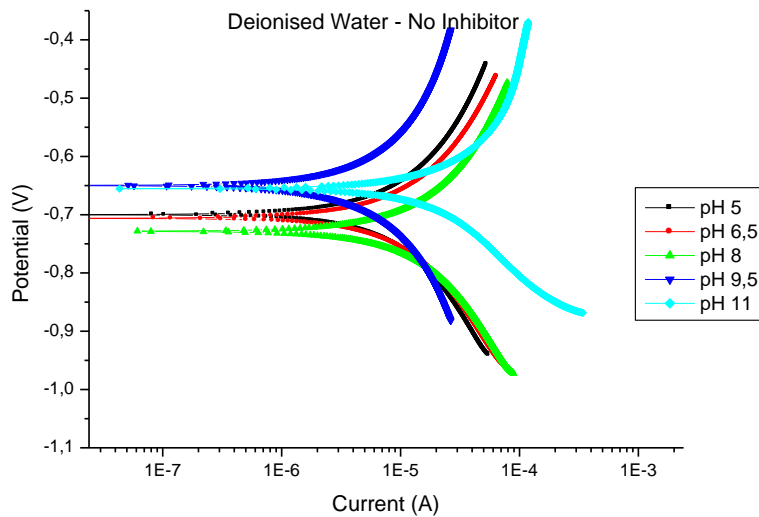


**Figure 4.26** :Potentiodynamic polarization curves for carbon steel in deionised water at 25 °C in absence of inhibitors at different pH values.

**Table 4.13 :** Polarization parameters for carbon steel in deionised water at 25 °C in absence of inhibitors at pH 8.

Deionised Water		No Inhibitor				
pH	-E <sub>corr</sub> (mV vs. Ag/AgCl)	I <sub>corr</sub> ( $\mu\text{A}\cdot\text{cm}^{-2}$ )	$\beta_a$ (mV)	$\beta_c$ (mV)	R <sub>p</sub> ( $\Omega\text{cm}^2$ )	Chi-Squ.
5.0	700	12	575	563	17,143	<b>0.64</b>
6.5	706	11	432	462	12,561	<b>0.68</b>
8.0	729	11	568	564	9,926	<b>0.42</b>
9.5	650	14	2,026	1,430	36,170	<b>1.1</b>
11.0	655	9	432	501	3,753	<b>0.57</b>

#### 4.3.2. Measurements in Deionised Water in the Presence of Inhibitors at pH=8

The effect of addition of different amin derivatives on the carbon steel corrosion at pH= 8 carbon steel in deionised water was investigated similarly to sea and decarbonized water. The impedance response of steel in deionised water significantly changed after the addition of inhibitors. On the other hand, the highest capacitive loop was observed in the case of RuN (Figure 4.27). It means that RuN has greatest anticorrosion efficiency in deionised water when compared to the other inhibitors. RuN<sub>2</sub> and RuN<sub>3</sub> show almost similar behaviour. Moreover, alkyl chain structure is also effective on corrosion inhibition and unsaturated diamine has greater efficiency than saturated diamine which is in agreement with the results observed for sea and decarbonised water.

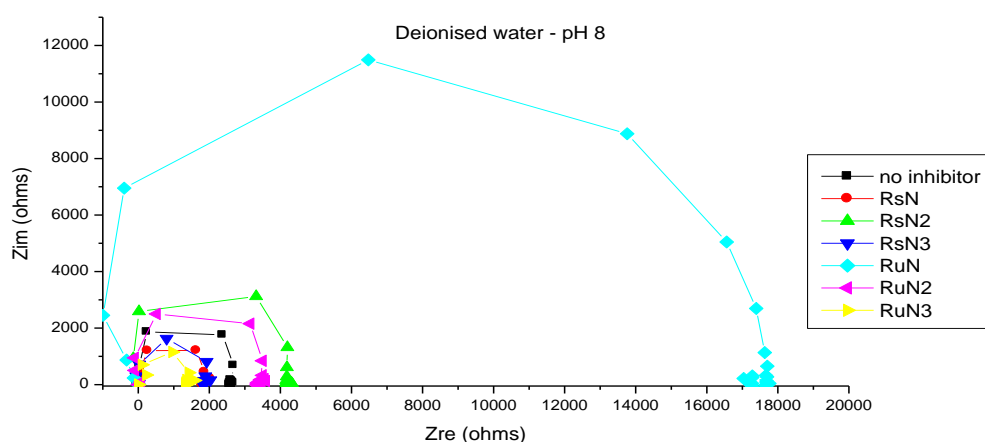


**Figure 4.27 :** Nyquist plot for carbon steel in deionised water at 25 °C in absence and with different inhibitors at pH 8.

Figure 4.28 shows the cathodic and anodic polarization plots of carbon steel immersed in deionized water the absence and the presence of inhibitors. Electrochemical parameters such as  $E_{corr}$ , Tafel slopes and  $i_{corr}$  as well as percentage of inhibition efficiency (IE%) are listed in Table 4.14.

Corrosion potential in Fig. 4.28, shifts with no definite trend with the addition of the inhibitors indicating that amine derivatives act as mixed type inhibitor. Only positive shift of  $E_{corr}$  was observed in the case of RuN and it shows lower  $i_{corr}$  than the others and this result also supported with EIS data (Table 4.14) Triamines seem to have negligible effects on the corrosion behaviour of carbon steel in deionized water.

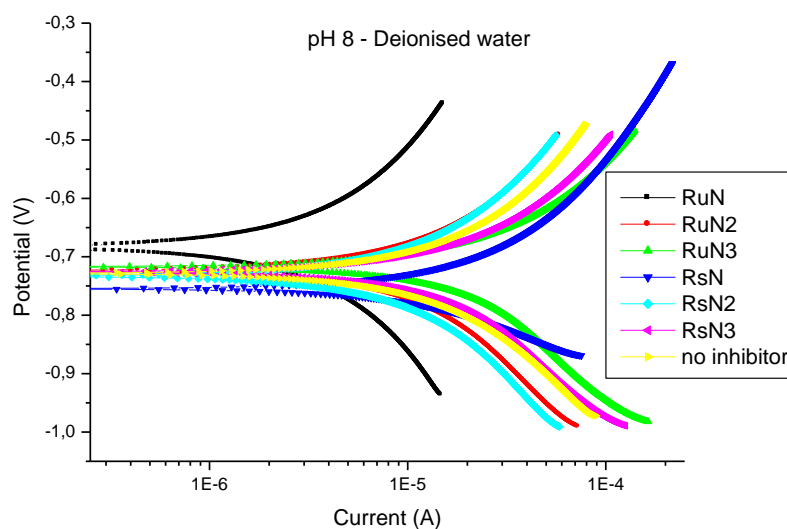


**Figure 4.28** :Potentiodynamic polarization curves for carbon steel in deionised water at 25 °C in absence and with different inhibitors at pH 8.

$R_p$  values obtained from Nyquist plot were also listed in Table 4.14 and they are in agreement with the polarization results.

**Table 4.14 :** Polarization parameters for carbon steel in deionised water at 25 °C in absence and presence of different inhibitors at pH 8.

Deionised Water	pH 8					
	-E <sub>corr</sub> (mV vs. Ag/AgCl)	I <sub>corr</sub> ( $\mu\text{A}\cdot\text{cm}^{-2}$ )	$\beta_a$ (mV)	$\beta_c$ (mV)	R <sub>p</sub> ( $\Omega\text{cm}^2$ )	Chi-Squ.
no inhibitor	729	8	568	564	9,926	<b>0.42</b>
R <sub>S</sub> N <sub>3</sub>	726	9	401	681	7,505	<b>0.86</b>
R <sub>S</sub> N <sub>2</sub>	734	6	530	650	16,590	<b>0.85</b>
R <sub>S</sub> N	756	7	343	255	7,308	<b>0.86</b>
R <sub>U</sub> N <sub>3</sub>	718	12	403	794	5,372	<b>0.94</b>
R <sub>U</sub> N <sub>2</sub>	724	6	495	636	13,430	<b>0.91</b>
R <sub>U</sub> N	685	4	1100	1243	67,150	<b>0.02</b>

All results from polarization and EIS measurements were compared in Table 4.15 and they suggest that most effective inhibitors are R<sub>U</sub>N, R<sub>S</sub>N<sub>2</sub>, R<sub>U</sub>N<sub>2</sub>, respectively.

**Table 4.15 :** Polarization parameters and the corresponding inhibition efficiency for the corrosion of carbon steel in deionised water in absence and presence of different inhibitors at pH 8.

Deionised Water	pH 8				
	-E <sub>corr</sub> (mV vs. Ag/AgCl)	I <sub>corr</sub> ( $\mu\text{A}\cdot\text{cm}^{-2}$ )	R <sub>p</sub> ( $\Omega\text{cm}^2$ )	E <sub>I<sub>corr</sub></sub> (%)	E <sub>R<sub>p</sub></sub> (%)
no inhibitor	729	8	9,926		
R <sub>S</sub> N <sub>3</sub>	726	9	7,505	<b>-8</b>	<b>- 32</b>
R <sub>S</sub> N <sub>2</sub>	734	6	16,590	<b>29</b>	<b>40</b>
R <sub>S</sub> N	756	7	7,308	<b>22</b>	<b>-36</b>
R <sub>U</sub> N <sub>3</sub>	718	12	5,372	<b>- 47</b>	<b>-85</b>
R <sub>U</sub> N <sub>2</sub>	724	6	13,430	<b>25</b>	<b>26</b>
R <sub>U</sub> N	685	4	67,150	<b>57</b>	<b>85</b>

#### 4.3.3. Measurements in Deionised Water in the presence of R<sub>U</sub>N<sub>2</sub> at Different pH

Electrochemical impedance spectroscopy measurements are performed to study the effect of pH for R<sub>U</sub>N<sub>2</sub> similarly to sea and decarbonized water (Figure 4.29). They are characterized by two separated capacitive loops where LF (low frequency) loop size is more significant at pH 9.5 and 11.0.



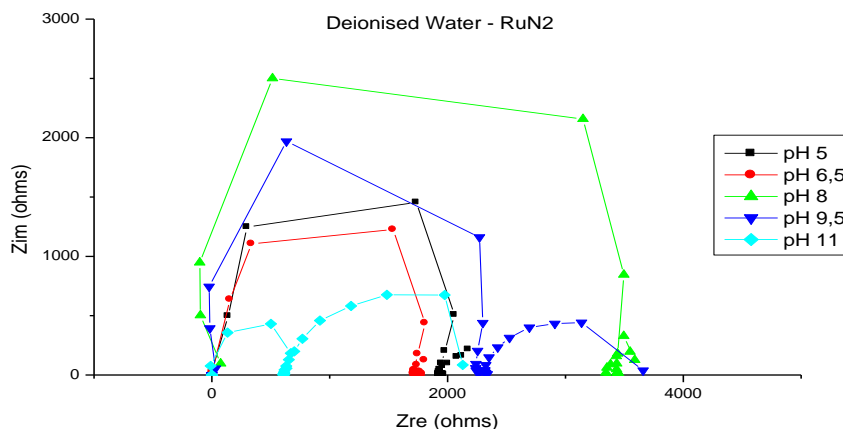


**Figure 4.29** : Nyquist plot for carbon steel in deionised water at 25 °C with  $R_{UN_2}$  at varying pH values.

Potentiodynamic polarization curves for carbon steel in deionised water in the presence of  $RuN_2$  at different pH values were given in Figure 4.30. It can be seen that there is a drastic increase in  $\beta_a$  and  $\beta_c$  at pH 11 and positive shift of  $E_{corr}$  is observed. Moreover, at pH= 8.0 and 9.5, different  $E_{corr}$  and lower  $I_{corr}$  values are observed with similar  $\beta_a$  and  $\beta_c$  as compared to the other pH values. Associated electrochemical parameters obtained by extrapolation of the Tafel lines and EIS data and also IE% based on Tafel and EIS data are presented in Table 4.16. The polarization resistance ( $R_p$ ) was calculated from the EIS data and the highest value was observed in the case of pH 9.5. On the other hand, based on polarization data, inhibitor efficiency (IE%) is obtained in a range from pH= 6.5 to pH=9.5.

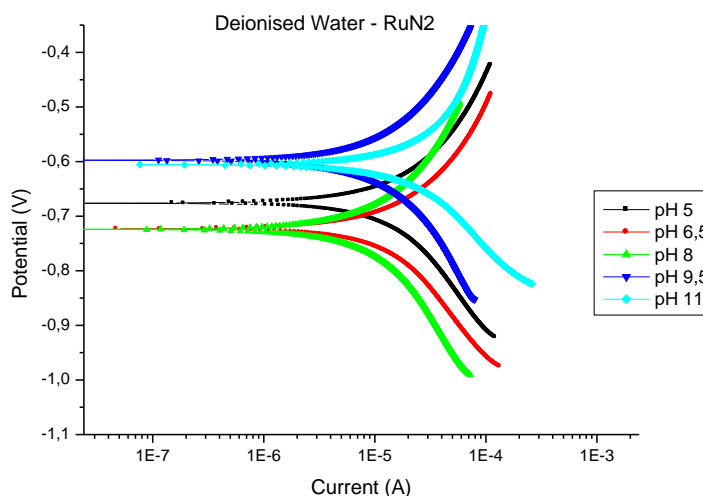


**Figure 4.30** : Potentiodynamic polarization curves for carbon steel in deionised

water at 25 °C with RuN<sub>2</sub> at varying pH values.

**Table 4.16 :** Polarization parameters for carbon steel in deionised water at 25 °C with R<sub>U</sub>N<sub>2</sub> at different pH values.

Deionised Water		R <sub>U</sub> N <sub>2</sub>						
pH	-E <sub>corr</sub> (mV vs. Ag/AgCl)	I <sub>corr</sub> (μA.cm <sup>-2</sup> )	β <sub>a</sub> (mV)	β <sub>c</sub> (mV)	R <sub>p</sub> (Ωcm <sup>2</sup> )	E <sub>I<sub>corr</sub></sub> (%)	E <sub>R<sub>p</sub></sub> (%)	Chi-Squ.
5.0	677	10	457	615	8,295	-71	-107	0.87
6.5	724	8	374	595	7,110	64	-77	0.88
8.0	724	6	495	636	13,825	25	28	0.91
9.5	597	7	510	565	14,418	31	-151	0.07
11.0	606	31	1570	759	8,295	-116	55	0.78

#### 4.3.4. Measurements in Deionised Water in the presence of R<sub>S</sub>N<sub>2</sub> at different pH

Figure 4.31 reports the impedance diagrams obtained at the corrosion potential in the presence of 100 ppm R<sub>S</sub>N<sub>2</sub> in deionised water at different pH values. The largest loop size (R<sub>p</sub> = 21,330 Ω.cm<sup>2</sup>) is obtained at pH=9.5. Meaning that better corrosion inhibition is enabled with R<sub>S</sub>N<sub>2</sub> at pH=9.5 which is also supported by polarization data listed in Table 4.17.

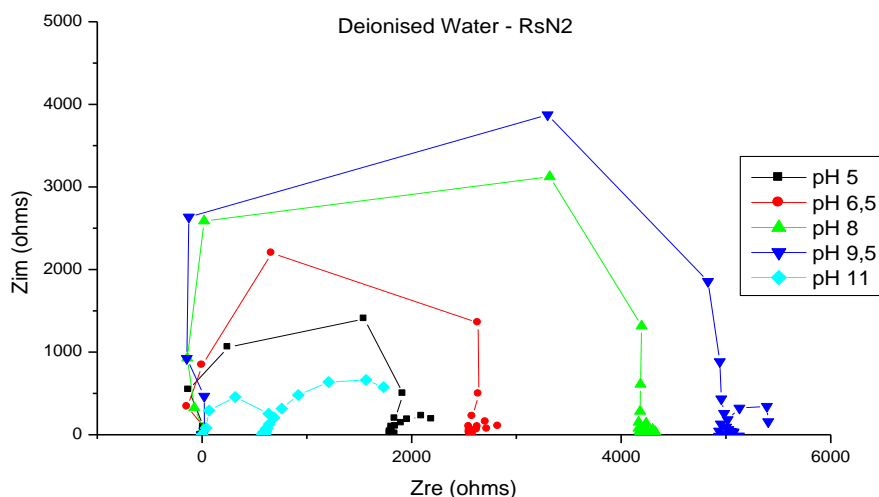


**Figure 4.31 :** Nyquist plot for carbon steel in deionised water at 25 °C with R<sub>S</sub>N<sub>2</sub> at varying pH values.

In the presence of R<sub>S</sub>N<sub>2</sub>, the highest positive shift in E<sub>corr</sub> is obtained at pH 11 (Figure 4.32). Associated electrochemical parameters obtained by extrapolation of the Tafel

lines and EIS data are presented in Table 4.17. There is abrupt increase in  $\beta_a$  and decrease in  $\beta_c$  and the highest  $I_{corr}$  values was observed in the case of pH=11.

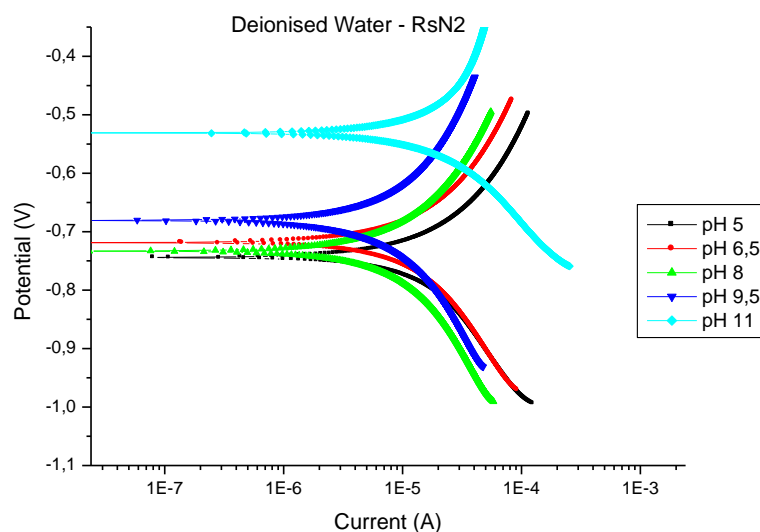


**Figure 4.32** : Potentiodynamic polarization curves for carbon steel in deionised water at 25 °C with  $R_5N_2$  at varying pH values.

The polarization resistance ( $R_p$ ) was calculated from the EIS data and has the highest value at pH 9.5. According to both EIS and polarization data, it can be concluded that  $R_5N_2$  has better anticorrosion efficiency in the range of pH= 6.5-9.5. However, at pH=8, inhibitor efficiency which is observed based on both polarization and EIS data is the highest compared to the other pH values.

**Table 4.17** : Polarization parameters for carbon steel in deionised water at 25 °C with  $R_5N_2$  at different pH values.

Deionised Water		$R_5N_2$						
pH	-E <sub>corr</sub> (mV vs. Ag/AgCl)	I <sub>corr</sub> ( $\mu A \cdot cm^{-2}$ )	$\beta_a$ (mV)	$\beta_c$ (mV)	R <sub>p</sub> * ( $\Omega cm^2$ )	E <sub>Icorr</sub> (%)	E <sub>Rp</sub> (%)	Chi-Squ.
5.0	745	10	411	687	8,690	-77	-97	0.84
6.5	719	6	396	493	10,665	-27	-18	0.87
8.0	734	6	530	650	16,748	29	41	0.85
9.5	682	8	902	914	21,330	25	-70	0.89
11.0	531	13	1.087	319	6,834	11	45	0.84

In deionised water at pH= 11, most significant two capacitive loops were observed with  $R_U N_2$  and  $R_S N_2$  (Figure A.2) meaning two time constants. Figure 4.33 depicts the equivalent circuit to model electrochemical behavior of the inhibitors after 1 hour immersion in deionised water at pH= 11 which is the pH value with most significant

two capacitive loops.  $R_s$ , solution resistance is a property of the test solution and the test cell geometry, not a property of the coating. It is, therefore, not interested.

The capacitance of the intact coating is represented by  $C_c$ . Its value is much smaller than a typical double layer capacitance.  $R_{po}$  (pore resistance) is the resistance of ion conducting paths the develop in the coating. These paths may not be physical pores filled with electrolyte. On the metal side of the pore, it can be assumed that an area of the coating has delaminated and a pocket filled with an electrolyte solution has formed. This electrolyte solution can be very different than the bulk solution outside of the coating. The interface between this pocket of solution and the bare metal is modeled as a double layer capacitance in parallel with a kinetically controlled charge transfer reaction.  $R_{ct}$  charge transfer resistance and  $C_{dl}$  double layer capacitive element.

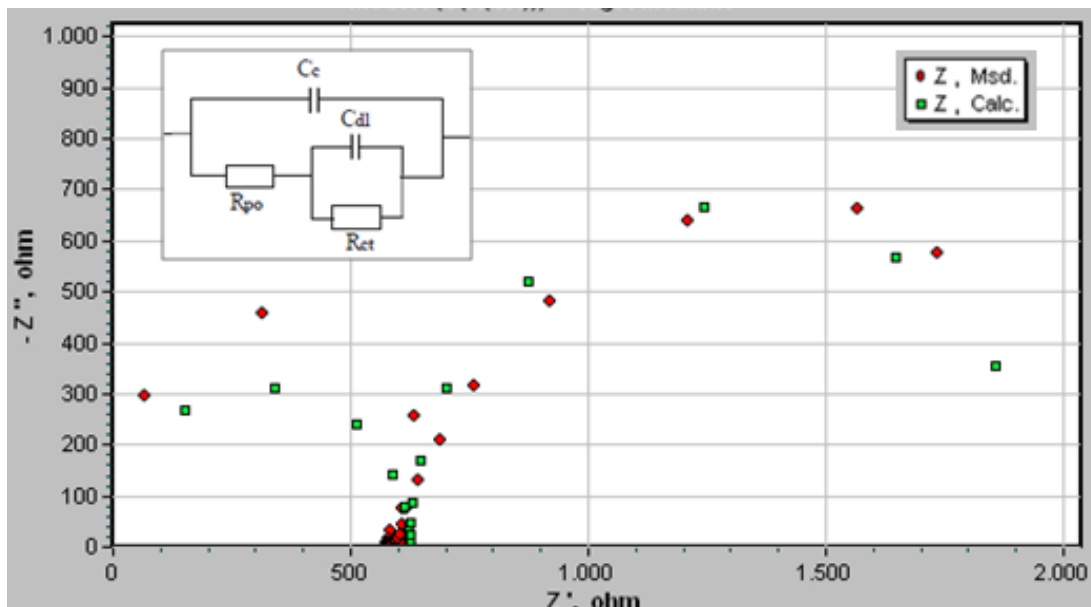


**Figure 4.33 :** Values of the elements of equivalent circuit required for fitting the EIS of carbon steel in deionised water with  $R_5N_2$  at pH 11.

Values of the elements of equivalent circuit were given in Table 4.18. It is clear that the addition of inhibitors causes an increase in  $R_{ct}$  in deionised water. As the  $R_{ct}$  increases inhibitor efficiency increases and gets higher value with  $R_U N_2$  when compared with  $R_S N_2$ .

Inhibitor efficiency based on impedance data are calculated (Equation 4.2) and listed at Table 4.18.  $R_U N_2$  has the highest inhibitor efficiency which is also supported by polarization data. It can be said that alkyl chain structure is effective on corrosion inhibition and unsaturated ones shows better performance.

**Table 4.18 :** Values of the elements of equivalent circuit required for fitting the EIS of carbon steel in deionised water in absence and presence of  $R_{UN_2}$  and  $R_{SN_2}$  at pH=11.

Deionised water pH 8	$R_s$ ( $\Omega.cm^2$ )	$R_{ct}$ ( $\Omega.cm^2$ )	CPE, $Y_0.10^5$ ( $\Omega^{-1}.s^n.cm^{-2}$ )	$n_{dl}$	$C_{dl}$ ( $\mu F.cm^{-2}$ )	IE%
no inhibitor	7	474	29	0.86	210	
$R_{SN_2}$	7	883	221	0.77	2,693	46
$R_{UN_2}$	9	1,945	78	0.64	984	76

#### 4.4 Adsorption Mechanisms

Electrochemical impedance spectroscopy provides a new method to characterize the film coverage on the electrode, which is related to charge transfer resistance ( $R_{ct}$ ). The interface capacitance can also be used to determine the film quality. It is known that the coverage of an organic substance on the metal surface depends not only on the structure of the organic substance and the nature of the metal, but also on the experimental conditions such as immersion time and concentration of adsorbent [60]. The adsorption isotherms can provide basic information on the interaction of inhibitor and metal surface [64].

The adsorption on corroding surfaces never reaches the real equilibrium and tends to reach an adsorption steady state. When corrosion rate is sufficiently decreased in the presence of inhibitor, the adsorption steady state has a tendency to attain quasi-equilibrium state.

It is known that the adsorption isotherms are very important for the understanding of the mechanism of corrosion inhibition [65]. The most frequently used isotherms are Langmuir, Freundlich, Temkin and Frumkin equations. Because impedance measurements are based on small amplitude perturbations, they are non-destructive and well suited to continuous monitoring of the corrosion [66].

In this work, the influence of concentration on the surface coverage in decarbonised water with  $R_{SN_2}$  and  $R_{UN_2}$  was carried out. Therefore, EIS measurement data were used to evaluate the surface coverage ( $\theta$ ), which was given by Equation 4.4.

$$IE\% = \theta = \frac{R_{ct}(inh) - R_{ct}}{R_{ct}(inh)} \quad (4.4)$$

It is assumed that the adsorption of these inhibitors follows the Langmuir adsorption isotherm model, and can be described by the following Equation 4.5 [64].

$$\frac{\theta}{1-\theta} = K_{ads}.c \quad (4.5)$$

The plot of  $C/\Theta$  versus  $C$  (Equation 4.6) yield s a straight line with correlation coefficients of 0.998 and 0.993 for  $R_S N_2$  and  $R_U N_2$ , respectively, providing that the adsorption of these inhibitors in decarbonised water on the carbon steel surface obeys Langmuir adsorption isotherm, which is presented by Equation 4.5.

$$\frac{c}{\theta} = \frac{1}{K_{ads}} + c \quad (4.6)$$

where  $C$  is inhibitor concentration,  $\Theta$  is the degree of coverage on the metal surface and  $K_{ads}$  is the equilibrium constant for adsorption-desorption process.

From the intercepts of the straight lines on the  $C/\Theta$  axis,  $K_{ads}$  can be calculated that relates to the standard free energy of adsorption,  $\Delta G_{ads}^0$  as given by the Equation 4.7.

$$\Delta G_{ads}^0 = -RT \ln(55.5 K_{ads}) \quad (4.7)$$

At Table 4.19, Langmuir isotherm adsorption parameters for  $R_S N_2$  in decarbonised water at pH 8 are listed.  $R_{ct}$  is increasing as the concentration of  $R_S N_2$  is increased.

**Table 4.19 :** Langmuir isotherm adsorption parameters for  $R_S N_2$  in decarbonised water at pH=8 at 25 °C.

$R_S N_2$	$R_s$ $\Omega cm^2$	$R_{ct}$ $\Omega cm^2$	CPE, $Y_{odl}.10^5$ $\Omega^{-1} s^n cm^{-2}$	$n_{dl}$	$C_{dl}$ $\mu F cm^{-2}$	$R_{po}$ $\Omega cm^2$	CPE, $Y_{oc}.10^5$ $\Omega^{-1} s^n cm^{-2}$	$n_c$	IE %
No inh.	224	969	204	0.7	2,734				
50 ppm	119	3,990	19	0.7	170	115	1	0.8	76
100 ppm	169	4,294	20	0.8	184	332	9	0.4	77
150 ppm	277	4,993	35	0.6	532	324	1	0.8	81
200 ppm	249	6,162	16	0.7	158	423	1	0.7	84

Regarding the obtained  $R_{ct}$  values, corresponding  $\Theta$  the degree of coverage on the metal surface are calculated and reported at Table 4.20.

**Table 4.20 :** Concentration and degree of coverage values for  $R_S N_2$  in decarbonised water at pH=8 at 25 °C.

$c$ (ppm)	$c$ (mol/L)	$\Theta$	$c/\Theta$
50	0.000153	0.76	0.00020
100	0.000307	0.77	0.00040
150	0.000460	0.81	0.00057
200	0.000613	0.84	0.00073

Figure 4.34 shows The plot of  $C/\theta$  versus  $C$  for  $R_S N_2$  in decarbonised water at varying concentration from 50 ppm to 200 ppm. From the interception of the Y axis,  $K_{ads}$  is observed as 0,00004 mol/L for  $R_S N_2$ .

At Table 4.21, Langmuir isotherm adsorption parameters for  $R_U N_2$  in decarbonised water at pH 8 are listed.  $R_{ct}$  is decreasing as the concentration of  $R_U N_2$  is increased from 50 ppm to 200 ppm.

Regarding the obtained  $R_{ct}$  values, corresponding  $\theta$  the degree of coverage on the metal surface are calculated for  $R_U N_2$  and reported at Table 4.22.

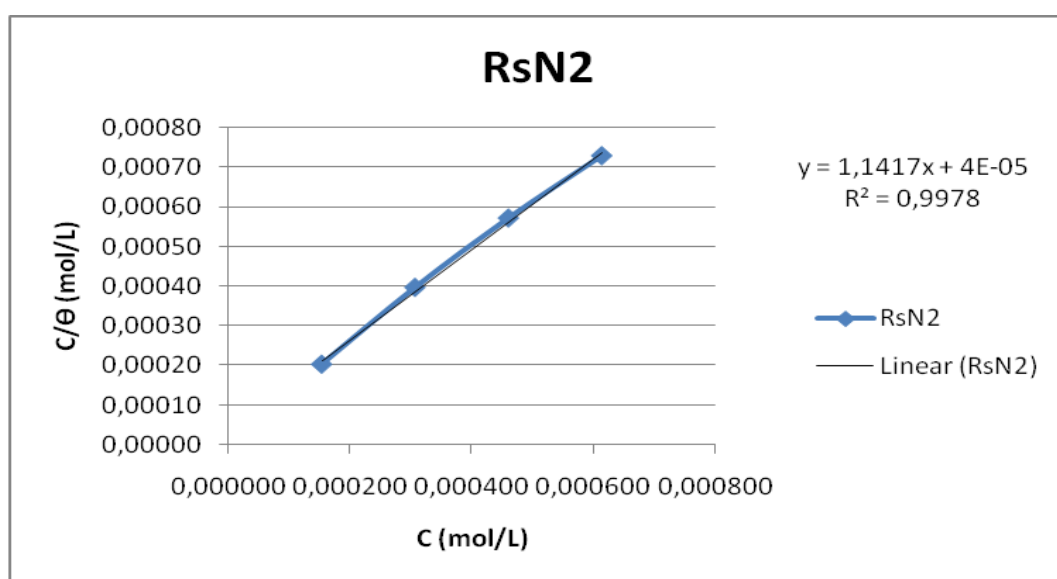


**Figure 4.34 :** Langmuir isotherm adsorption plot for adsorption of  $R_S N_2$  in decarbonised water at pH 8 at 25 °C.

**Table 4.21 :** Langmuir isotherm adsorption parameters for  $R_U N_2$  in decarbonised water at pH 8 at 25 °C.

$R_U N_2$	$R_s$ $\Omega cm^2$	$R_{ct}$ $\Omega cm^2$	CPE, $Y_{odl} \cdot 10^5$ $\Omega^{-1} s^n cm^{-2}$	$n_{dl}$	$C_{dl}$ $\mu F cm^{-2}$	$R_{po}$ $\Omega cm^2$	CPE, $Y_{oc} \cdot 10^5$ $\Omega^{-1} s^n cm^{-2}$	$n_c$	IE %
No inh.	224	969	204	0.7	2.734				
50 ppm	257	5,672	19	0.72	192	201	1	0.8	83
100 ppm	250	4,400	23	0.75	234	142	0	0.8	78
150 ppm	142	4,357	25	0.71	256	126	1	0.8	78
200 ppm	150	3,231	33	0.67	339	119	0	0.9	70

**Table 4.22 :** Concentration and degree of coverage values for RuN<sub>2</sub> in decarbonised water at pH 8 at 25 °C.

c (ppm)	c(mol/L)	θ	c/θ
50	0.000154	0.83	0.00019
100	0.000309	0.78	0.00040
150	0.000463	0.78	0.00060
200	0.000617	0.70	0.00088

Figure 4.35 shows The plot of C/θ versus C for RuN<sub>2</sub> in decarbonised water at varying concentration from 50 ppm to 200 ppm. From the interception of the Y axis, K<sub>ads</sub> is observed as 0,00006 mol/L for RuN<sub>2</sub>.

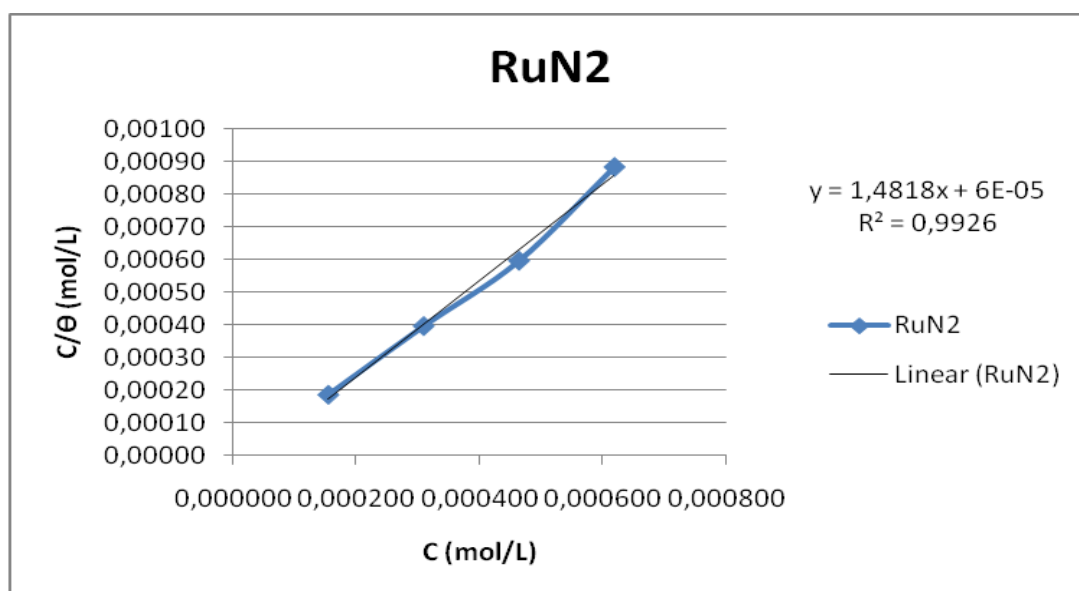


**Figure 4.35 :** Langmuir isotherm adsorption plot for adsorption of RuN<sub>2</sub> in decarbonised water at pH 8 at 25 °C.

Free energies ( $\Delta G^0_{ads}$ ) were calculated to be -34 and -35 kJ/mol for RuN<sub>2</sub> and R<sub>S</sub>N<sub>2</sub> respectively; the negative value of  $\Delta G^0_{ads}$  indicates spontaneous adsorption of these inhibitors on the mild steel surface and also the strong interaction between inhibitors molecules and metal surface. Generally, values of  $\Delta G^0_{ads}$  up to -20 kJ/mol are consistent with physisorption, while those around -40 kJ/mol or higher are associated with chemisorptions as a result of the sharing or transfer of electrons from organic molecules to the metal surface to form a co-ordinate.

The basic character of inhibitors affects the adsorption of cation on the surface of carbon steel (electrostatic attraction). In the presence of Cl<sup>-</sup> which are strongly



adsorbed on the metal surface, the metal surface becomes negatively charged hence favoured the adsorption of cation type inhibitors. Thus, all the inhibitors studied in this work adsorbed through electrostatic interactions between the positively charged molecules and negatively charged metal surface [65].

Thus, the value of  $\Delta G_{\text{ads}}^0$  for  $R_{\text{U}}\text{N}_2$  and  $R_{\text{S}}\text{N}_2$  on carbon steel in decarbonised water is in the range of -30-40 kJ/mol indicated that they are all adsorbed by mixed mode (physisorption and chemisorptions) of adsorption on the metal surface [34,65].

#### 4.5 SEM (Scanning Electron Microscopy) Measurements

Morphology of carbon steel electrode that left in corrosion environment in the presence and absence of inhibitors was investigated in three of corrosion media (decarbonized, sea and deionized water) (Figure 4.36 - 4.38). In the presence of  $R_{\text{U}}\text{N}_2$  and  $R_{\text{S}}\text{N}_2$  surface became more smooth than the case of blank, showing the adsorption of the inhibitors on the electrode surface in decarbonised water (Figure 4.36).

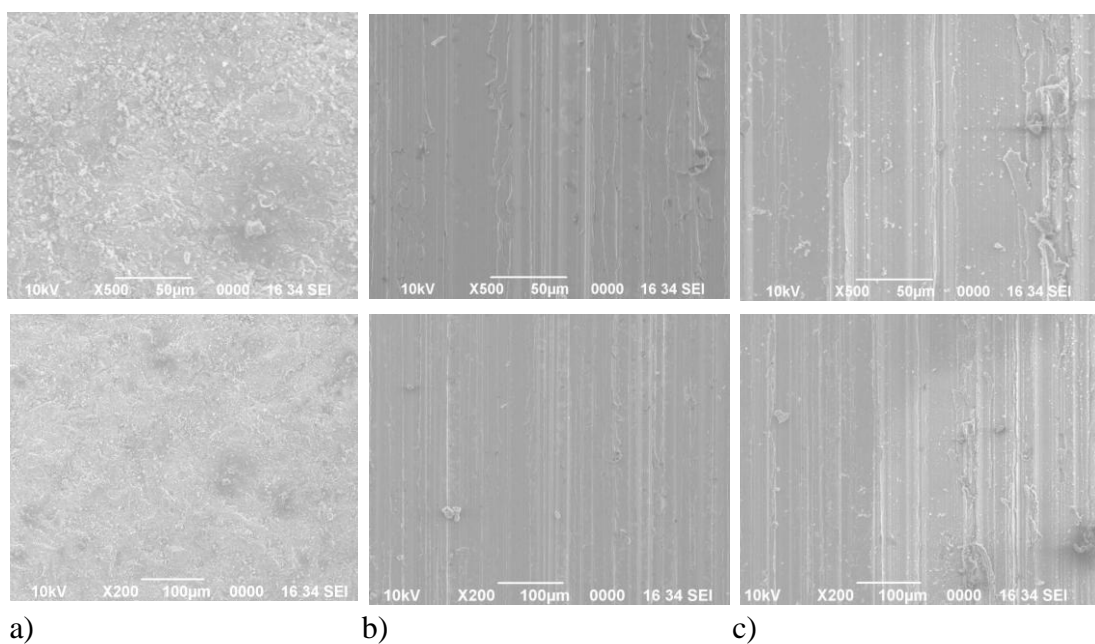


**Figure 4.36 :** SEM image ( x 500, x 200) of the carbon steel electrode obtained after 1 h immersion a) without inhibitor b) in the presence of  $R_{\text{U}}\text{N}_2$  c) in the presence of  $R_{\text{S}}\text{N}_2$  in decarbonised water at pH=8 at 25 °C.

In seawater, corrosion products are more pronounced than other corrosion environment due to aggressiveness of chloride ion (Figure 4.37). A denser and smoother film adsorbed on the steel surface for  $R_{\text{U}}\text{N}_2$  inhibited mild steel than that for the  $R_{\text{S}}\text{N}_2$ .

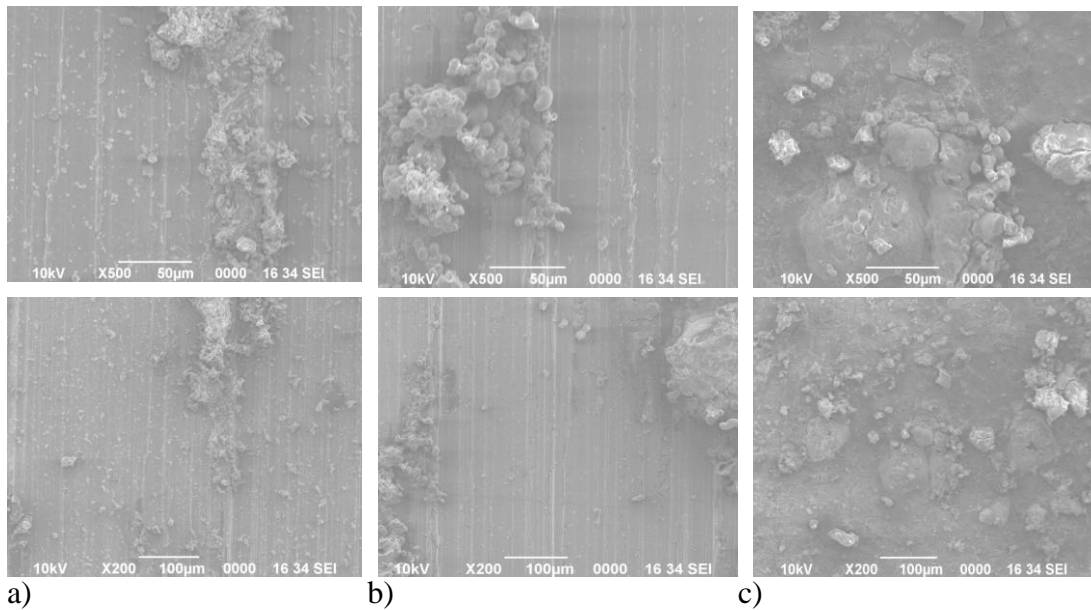


**Figure 4.37 :** SEM image ( x 500, x 200) of the carbon steel electrode obtained after 1 h immersion a) without inhibitor b) in the presence of  $R_U N_2$  c) in the presence of  $R_S N_2$  in seawater at pH=8 at 25 °C.

SEM photographs in deionised water at pH=8 in the absence and presence of inhibitors are shown in Figure 4.38. It can be seen from Figure 4.38- a that the surface is strongly damaged in the absence of the inhibitors. In the presence of  $R_U N$  and  $R_U N_2$  it can be seen that the rate of corrosion is suppressed, and there is little acid corrosion product on the steel surface, suggesting an adsorbed layer is formed on the surface, which inhibits corrosion. In the presence of  $R_S N_2$  inhibitor leads to formation of a stiffly stuck surface cover with irregular pits and adsorption of this inhibitor is not as well as  $R_U N$  and  $R_U N_2$ . This result is in agreement with the polarization measurements (Table 4.14).

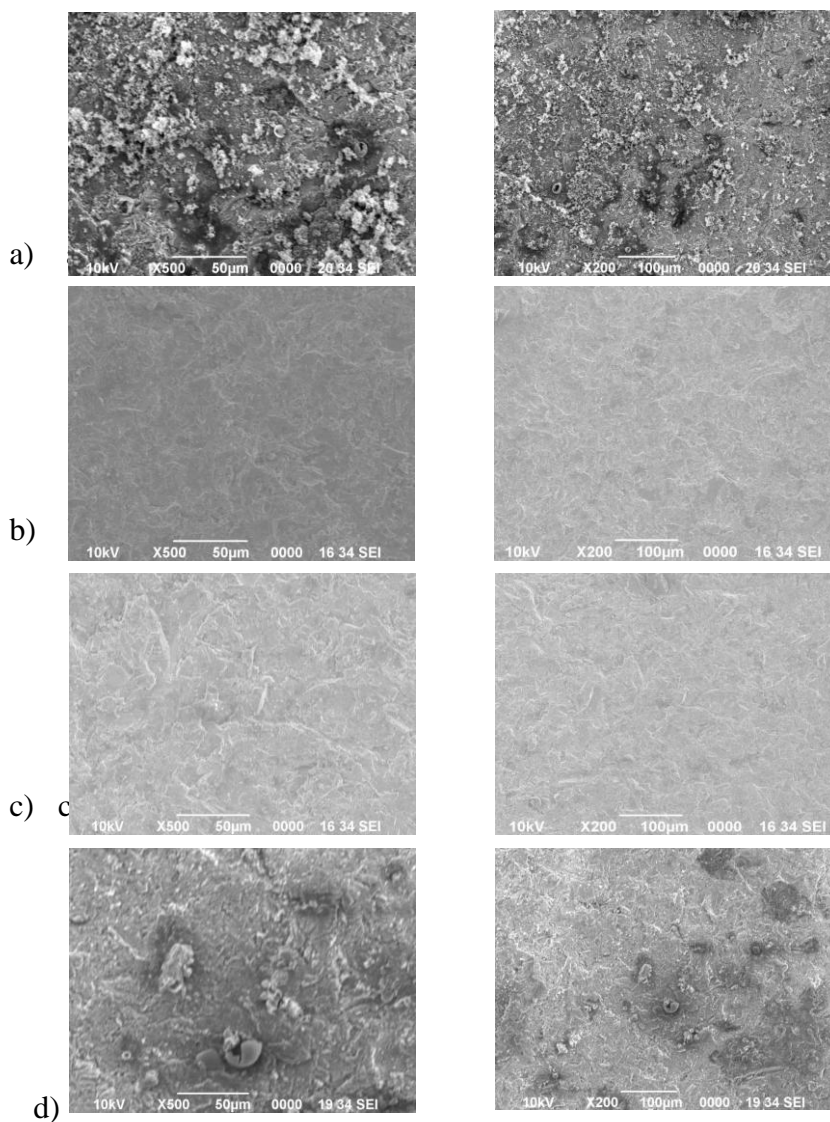


**Figure 4.38** : SEM image ( x 500, x 200) of the carbon steel electrode obtained after 1 h immersion a) without inhibitor b) in the presence of  $R_{UN}$  c) in the presence of  $R_{UN_2}$  d) in the presence of  $R_{S_N_2}$  in deionised water at pH=8 at 25 °C.



## 5. CONCLUSIONS

In this work, the behavior of the carbon steel, in presence of different inhibitors which have different functional group based of FFA of different structures, by steady-state current-voltage curves and impedance spectroscopy measurements was studied. Sea, decarbonised and deionised water qualities were examined in absence of and with inhibitors at different pH values from 5 to 11 in order to observe the pH dependency of the inhibitors on corrosion inhibition. Also, at the same pH value (pH=8), 6 different inhibitors were examined at 3 different water quality in order to obtain the relationship between the inhibitor structure and inhibitor efficiency, additionally by the effect of different corrosive media. In the last part, adsorption isotherm plots were observed by using EIS data at decarbonised water at pH=8 in order to understand the corrosion inhibition mechanism.

In seawater, inhibition efficiency expected to increase with decrease in amine number i.e  $RN_3 < RN_2 < RN$ . Although second amine group shows expected effect in both saturated and unsaturated cases ( $R_U N_2$ ,  $R_S N_2$ ), further increase in amine number ( $RN_3$ ) does not have further increase in efficiency. It can be concluded that the inhibition efficiency is not proportional to the amine number in seawater. On the other hand unsaturated amines ( $R_U N_x$ ) have better inhibition effect than the saturated ones ( $R_S N_x$ ), may be due to better interaction of  $\pi$ -bonds of unsaturated inhibitors with metal surface.

Regarding the potentiodynamic polarization curves obtained in seawater with different inhibitors, it can be clearly seen that the  $E_{corr}$  values shifted to more positive potentials in the presence of unsaturated polyamines on the other hand to more negative potentials in the presence of saturated polyamines. There was not a specific relation between  $E_{corr}$  and inhibitors efficiency. However, this can be related to alkyl chain chemistry.

It can be observed that both polarization and impedans data supporting each other and suggest that the better corrosion inhibition is enabled in a pH range of 6.5- 9.5 for both  $R_U N_2$  and  $R_S N_2$  in seawater where  $R_U N_2$  has higher IE% than  $R_S N_2$  due to the unsaturated alkyl chain chemistry.

Similar results were observed in decarbonised water that for both saturated and unsaturated amines, the inhibition efficiency is not proportional to the amine number. Moreover, alkyl chain structure is also effective on corrosion inhibition that unsaturated diamine has greater efficiency than saturated diamine in decarbonised water which is also supported by the results observed in seawater. Diamines show better anticorrosion efficiency as compared to triamines and unsaturated diamines effect better than saturated ones at pH=8.

The distorted shape of the high-frequency part of the impedance diagrams (Figure 4.20 and Figure 4.22) of both  $R_U N_2$  and  $R_S N_2$  can be attributed to the formation of a relatively thick and compact protective film on the metal surface.

In deionised water, corrosion potential (Fig. 4.28) shifts with no definite trend with the addition of the inhibitors indicating that amine derivatives act as mixed type inhibitors. Also, triamines seem have negligible effects on the corrosion behaviour of carbon steel in deionized water .Both polarization and EIS data (Table 4.15) are supporting each others.

$R_U N$  has greatest anticorrosion efficiency in deionised water when compared to the other inhibitors in deionised water.  $R_U N_2$  and  $R_S N_2$  show almost similar behaviour. Moreover, alkyl chain structure is also effective on corrosion inhibition and unsaturated diamine has greater efficiency than saturated diamine which is in agreement with the results observed for sea and decarbonised water.

In deionised water at pH= 11, most significant two capacitive loops were observed with  $R_U N_2$  and  $R_S N_2$  (Figure A.2) meaning two time constants. This can be attributed to the low conductivity of the medium which is not sufficient for the current flow. Additionally, cation type inhibitors adsorption is affected by the negative charge deposition of the metal surface where the deionised water may not be negatively charged for the adsorption of the inhibitors due to deionised water characteristics. Two time constants can also be attributed to not formation of the film on the metal surface.

Moreover, the influence of concentration on the surface coverage in decarbonised water with  $R_S N_2$  and  $R_U N_2$  was carried out. Assuming that the adsorption of these inhibitors follows the Langmuir adsorption isotherm model, obtained  $\Delta G^0_{ads}$  values indicated that they are all adsorbed by mixed mode (physisorption and chemisorptions) of adsorption on the metal surface.

Table 5.1 reports inhibitor efficiencies of different inhibitors obtained from polarization data in different water qualities 25 °C at pH=8. It is obvious that with saturated and unsaturated diamines, highest anticorrosion efficiencies were obtained in both of sea and decarbonised water. In deionised water, the highest efficiency was observed with unsaturated monoamine which was followed by saturated and unsaturated diamines. There is also a significant observation that , in sea water anticorrosion efficiency is much more dependent on alkyl chain chemistry while amino group number is more important than alkyl chain chemistry in the case of decarbonised water.

**Table 5.1 :** Inhibitor efficiencies of different inhibitors obtained from polarization data in different water qualities 25 °C at pH=8.

	pH=8, IE%Rp		
	Decarbonised Water	Seawater	Deionised Water
$R_S N_3$	33	21	-32
$R_S N_2$	80	37	40
$R_S N$	-33	10	-36
$R_U N_3$	26	64	-85
$R_U N_2$	81	67	26
$R_U N$	9	54	85





## REFERENCES

- [1] **Roberge, P. R.**, 1999. Introduction, in *Handbook of Corrosion Engineering*, p. 1-12, McGraw Hill, New York, USA.
- [2] **Frankel, G.S.**, 2008. Electrochemical Techniques in Corrosion: Status, Limitations, and Needs, *Journal of ASTM International*, Vol. **5**, No. 2, Paper ID JAI101241.
- [3] **Roberge, P. R.**, 1999. Corrosion inhibition, in *Handbook of Corrosion Engineering*, Chapter 10, p.834, McGraw Hill, New York, USA.
- [4] **Kern, P. and Landolt, D.**, 2001. Adsorption of organic corrosion inhibitors on iron in the active and passive state. A replacement reaction between inhibitor and water studied with the rotating quartz crystal microbalance, *Electrochimica Acta*, 47, p. 589–598.
- [5] **Naderi, R., Mahdavian, M. and Attar, M. M.**, 2009. Electrochemical behavior of organic and inorganic complexes of Zn(II) as corrosion inhibitors for mild steel: Solution phase study, *Electrochimica Acta*, **54**, p. 6892–6895
- [6] **Url 1** < [http://www.dhw-ecogreenoleo.de/Fatty\\_Amines.pdf](http://www.dhw-ecogreenoleo.de/Fatty_Amines.pdf) >, accessed at 29.09.2010.
- [7] **Roberge, P. R.**, 1999. Aqueous corrosion, in *Handbook of Corrosion Engineering*, Chapter 1, p.14, McGraw Hill, New York, USA.
- [8] **Url 2** < [http://water.me.vccs.edu/courses/ENV115/lesson19\\_2.htm](http://water.me.vccs.edu/courses/ENV115/lesson19_2.htm) >, accessed at 29.09.2010.
- [9] **Tan, S. W.**, 1991. Organic corrosion inhibitors, Western Australia, *PhD Thesis*, Murdoch University.
- [10] **Zipperian, D.**, 2003. Chemical etching, *Quality Matters Newsletters*, Vol. II, Issue 5.
- [11] **Roberge, P. R.**, 1999. Thermodynamic Data and E-pH Diagrams, in *Handbook of Corrosion Engineering*, Appendix F, p.1109-1110, McGraw Hill, New York, USA.
- [12] **Url 3** < <http://corrosion-doctors.org/Corrosion-Thermodynamics/Potential-pH-diagram-iron.htm> >, accessed at 29.09.2010
- [13] **Roberge, P. R.**, 1999. Aqueous corrosion, in *Handbook of Corrosion Engineering*, Chapter 1, p.16, McGraw Hill, New York, USA.
- [14] **Berg, H. B.**, 2009. Corrosion mechanisms and their consequences for nuclear power plants with light water reactors, *R&RATA # 4*, Vol. **2**, p. 57-68.

- [15] **Rashidi, N., Alavi-Soltani, S. and Asmatulu, R.**, 2007. Crevice Corrosion Theory, Mechanisms and Prevention Methods, *Proceedings of the 3<sup>rd</sup> Annual GRASP Symposium*, Wichita State University.
- [16] **Url 4** < <http://electrochem.cwru.edu/encycl/art-c02-corrosion.htm> >, accessed at 29.09.2010.
- [17] **Url 5** < [http://www.tis-gdv.de/tis\\_e/misc/korro.htm](http://www.tis-gdv.de/tis_e/misc/korro.htm) >, accessed at 29.09.2010.
- [18] **Fekry, A.M. and Ameer, M. A.**, 2010. Corrosion inhibition of mild steel in acidic media using newly synthesized heterocyclic organic molecules, *International journal of hydrogen energy*, **35**, p. 7641 -7651.
- [19] **Url 6** < <http://corrosion-doctors.org/Inhibitors/Introduction.htm> >, accessed at 29.09.2010.
- [20] **Url 7** <<http://140.194.76.129/publications/eng-manuals/em1110-2-3400/c-2.pdf>>, accessed at 29.09.2010.
- [21] **Url 8** < [http://www.arcelormittal.com/sections/fileadmin/redaction/pdf/Brochures/Galvanisation\\_EN.pdf](http://www.arcelormittal.com/sections/fileadmin/redaction/pdf/Brochures/Galvanisation_EN.pdf)>, accessed at 29.09.2010.
- [22] **Url 9** < [http://www.dhw-ecogreenoleo.de/Fatty\\_Amines.pdf](http://www.dhw-ecogreenoleo.de/Fatty_Amines.pdf) >, accessed at 29.09.2010.
- [23] **Musa, A. Y., Kadhum, A. A. H., Mohamad, A. B., Takriff, M. S., Daud, A. R. and Kamarudin, S.K.**, 2010. Adsorption isotherm mechanism of amino organic compounds as mild steel corrosion inhibitors by electrochemical measurement method, *J. Cent. South Univ. Technol.*, **17**, p. 34–39.
- [24] **Baril, G., Moran, F. and Pebere, N.**, 2000. A corrosion inhibition study of a carbon steel in a low conductivity medium by phosphonocarboxylic acid salt/fatty amine association, *Proceedings of the 9<sup>th</sup> European Symposium on Corrosion Inhibitors (9 SEIC)*, Ann. Univ. Ferrara, N.S., Sez. V, Suppl. N. **11**.
- [25] **Herrag, L., Hammouti, B., Elkadiri, S., Aouniti, A., Jama, C., Vezin, H. and Bentiss, F.**, 2010. Adsorption properties and inhibition of mild steel corrosion in hydrochloric solution by some newly synthesized diamine derivatives: Experimental and theoretical investigations, *Corrosion Science*, **52**, p. 3042–3051.
- [26] **Akhmadeeva, G.I. and Zagidullin, R.N.**, 2006. Inhibitor of hydrogen sulfide corrosion of steel based on di- and polypropylene polyamines, ISSN 0033-1732, *Protection of Metals*, Vol. **42**, No. 6, p. 577–582.
- [27] **Url 10** <<http://www.w3c.org/TR/1999/REC-html401-19991224/loose.dtd>>, accessed at 29.09.2010.
- [28] **Ochoa, N., Moran, F., Pebere, N. and Tribollet, B.**, 2005. Influence of flow on the corrosion inhibition of carbon steel by fatty amines in association with phosphonocarboxylic acid salts, *Corrosion Science*, **47**, p. 593–604.
- [29] **Speciality Chemicals Magazine**, 2008. Phosphate esters & alkoxyated amines for severe corrosion, Vol. 28, No.10.

- [30] **Rafiquee, M.Z.A., Khan, S., Saxena, N. and Quraishi, M.A.,** 2009. Investigation of some oleochemicals as green inhibitors on mild steel corrosion in sulfuric acid, *J Appl Electrochem*, 39. p. 1409–1417.
- [31] **Hater, W., Rudschützky, N. and Olivet, D.,** 2008. The chemistry and properties of organic boiler feed water additives based on film forming amines and their use in steam generators, *Technical publication*, p. 1-11.
- [32] **Naraghi, A.,** 1998. Compositions and methods for inhibiting corrosion, *United States Patent*, patent no: 5,779,938, dated 14.07.1998.
- [33] **Roberge, P. R.,** 1999. Corrosion inhibition, in *Handbook of Corrosion Engineering*, Chapter 10, p.837, McGraw Hill, New York, USA.
- [34] **Bahrami, M.J., Hosseini, S.M.A. and Pilvar, P.,** 2010. Experimental and theoretical investigation of organic compounds as inhibitors for mild steel corrosion in sulfuric acid medium, *Corrosion Science*, **52**, p. 2793–2803
- [35] **Morgan, D. M. L.,** Polyamine Protocols, *Methods in Molecular Biology*, Vol **79** Humana Press Inc , Totowa, NJ.
- [36] **Lawrence, S. A.,** 2004. Amines: synthesis, properties and applications, p. 50, Cambridge, United Kingdom.
- [37] **Lawrence, S. A.,** 2004. Amines: synthesis, properties and applications, p. 205, Cambridge, United Kingdom
- [38] **Nmai, C. K.,**2004. Multi-functional organic corrosion inhibitor, *Cement & Concrete Composites* 26, p.199–207, Master Builders, Inc., 23700 Chagrin Boulevard, Cleveland, OH 44122, USA.
- [39] **Abd El Rehim S.S., Sayyah, S.M., El-Deeb, M.M., Kamal, S.M. and Azooz R.E.,** 2010. Poly(o-phenylenediamine) as an inhibitor of mild steel corrosion in HCl solution, *Materials Chemistry and Physics*, **123**, p. 20–27.
- [40] **Niu, L., Zhang, H., Wei, F., Wu, S., Cao, X. and Liu, P.,** 2005. *Appl. Surf. Sci.* 252, 1634.
- [41] **F. Touhami, A. Aouniti, Y. Abed, B. Hammouti, S. Kertit, A. Ramdani, K. Elkacemi,** 2000. *Corros. Sci.* 42 , 929.
- [42] **Url 11** < <http://chemicalland21.com/industrialchem/organic/TALLOW%20AMINES.htm> >, accessed at 29.09.2010.
- [43] **Chernyshev, E.V., Veprov, E.N., Petrov, V.A., Bogdanov, S.L., Levina, T.Y., Petrova, T.I., Kashinskii, V.I., Zonov, A.A. and Verkhovskii, A.E.,** 2006. Increasing the corrosion resistance of equipment due to the use of film forming amines, *Power Technology and Engineering*, Translated from *Élektricheskie Stantsii*, Vol. **40**, No. 1, p. 15 – 18.
- [44] **Baboian, R.,** 2005. Corrosion tests and standards: application and interpretation, *2<sup>nd</sup> edition* , p. 422, Baltimore MD.
- [45] **Url 12** < <http://corrosion-doctors.org/Electrochem/Techniques.htm> >, accessed at 29.09.2010.

- [46] **Stern, M. and Geary, A.L.**, 1957. *J. Electrochem. Soc.*, **104** (56).
- [47] **Pourbaix, M.**, 1973. *Lectures on Electrochemical Corrosion*, Plenum Press, New York.
- [48] **Press, W.H., Flannery, B.P., Teukolsky, S.A. and Vetterling, W.T.**, 1988. *Numerical Recipes in C*, Section **14.4**, Cambridge University Press, Cambridge.
- [49] **Stern, M.**, 1958. A Method For Determining Corrosion Rates From Linear Polarization Data By Milton Stern, *Corrosion*, Vol. **14**, No. 9, p. 440-444.
- [50] **Andrade, C. and Alonso, C.**, 2004. Test methods for on-site corrosion rate measurement of steel reinforcement in concrete by means of the polarization resistance method, *Materials and Structures / Matériaux et Constructions*, Vol. **37**, p. 623-643.
- [51] **Url 13** < [http://www.gamry.com/App\\_Notes/DC\\_Corrosion/GettingStartedWithEchemCorrMeasurements.htm#Calculation of Corrosion Rate from Corrosion Current](http://www.gamry.com/App_Notes/DC_Corrosion/GettingStartedWithEchemCorrMeasurements.htm#Calculation%20of%20Corrosion%20Rate%20from%20Corrosion%20Current) >, accessed at 29.09.2010.
- [52] **Url 14** < [http://www.gamry.com/App\\_Notes/DC\\_Corrosion/GettingStartedWithEchemCorrMeasurements.htm#Current and Voltage Conventions](http://www.gamry.com/App_Notes/DC_Corrosion/GettingStartedWithEchemCorrMeasurements.htm#Current%20and%20Voltage%20Conventions) >, accessed at 29.09.2010.
- [53] **Agarwal, P., Orazem, M.E. and Garcia- Rubio, L.H.**, 1992. *J. Electrochem. Soc.*, 139, 1917.
- [54] **Barsoukov, E. and Macdonald, J.R.**, 2005. *Impedance Spectroscopy; Theory, Experiment, and Applications*, 2nd ed., Wiley Interscience Publications.
- [55] **Scully, J.R., Silverman, D.C. and Kendig, M.W.**, 1993. *Electrochemical Impedance: Analysis and Interpretation*, *ASTM*.
- [56] **Foret, C., Stoianovici, G., Chaussec, G., de Bache, A., zum Kolk, C. and Hater, W.**, 2008. Study of efficiency and stability of film forming amines (FFA) for the corrosion protection of the carbon steel in water circuits, *Eurocorr 2008, European Federation of Corrosion*, Edinburg, United Kingdom.
- [57] **Kester, D. R., Duedall I. W., Connors D. N. and Pytkowicz, R. M.**, 1967. Preparation of Artificial Sea Water, Department of Oceanography, Oregon State University, Corvallis 97331, Vol. 12, Issue 1, p. 178.
- [58] **Growcock, F. B. and Jasinski, R. J.**, 1989. *J. Electrochem. Soc.* **136 - 2310**.
- [59] **Reinhard, G. and Rammelt, U.**, 1985. *6th European Symposium on Corrosion Inhibitors*, Ann. Univ. Ferrara, p. 831.
- [60] **Li, P., Lin, Y.J., Tan, K. L. and Lee, J. Y.**, 1997. *Electrochim. Acta* 42, 605.
- [61] **Lopez, D.A., Simison, S. N. and de Sanchez, S.R.**, 2003. *Electrochim. Acta* 48, 845.
- [62] **Jütner, K.**, 1990. *1501 Electrochim. Acta*, **10**.

- [63] **Duprat, M., Dabosi, F. and Moran, F.**, 1983. Some preliminary experiments regarding the corrosion inhibition of a carbon steel by oleylamino-propylene amine with tri(methyl-phosphonic) acid, *Corrosion Science*, Toulouse Cedex, France, Vol. **23**, No. 9, pp.1047-1050.
- [64] **Musa, A. Y., Kadhum, A. A. H., Mohamad, A. B., Takriff, M. S., Daud, A. R. and Kamarudin, S.K.**, 2010. Adsorption isotherm mechanism of amino organic compounds as mild steel corrosion inhibitors by electrochemical measurement method, *J. Cent. South Univ. Technol.*, **17**, p. 34–39.
- [65] **Singh, A. K. and Quraishi, M. A.**, 2010. Investigation of adsorption of isoniazid derivatives at mild steel/hydrochloric acid interface: Electrochemical and weight loss methods, *Materials Chemistry and Physics*, Vol. **123**, Issue: 2-3, pp. 666-677.
- [66] **Duprat, M., Lafont, M. C., Dabosi, F. and Moran, F.**, 1985. Study of the and inhibition process of carbon steel in a low conductivity medium by electrochemical methods, *Electrochimica Acta*, Toulouse Cedex, France, Vol. **30**, No. 3, pp.353-365.



## **APPENDICES**

**APPENDIX A.1** : Measurements in presence of inhibitors in decarbonised and deionised water





## APPENDIX A.1

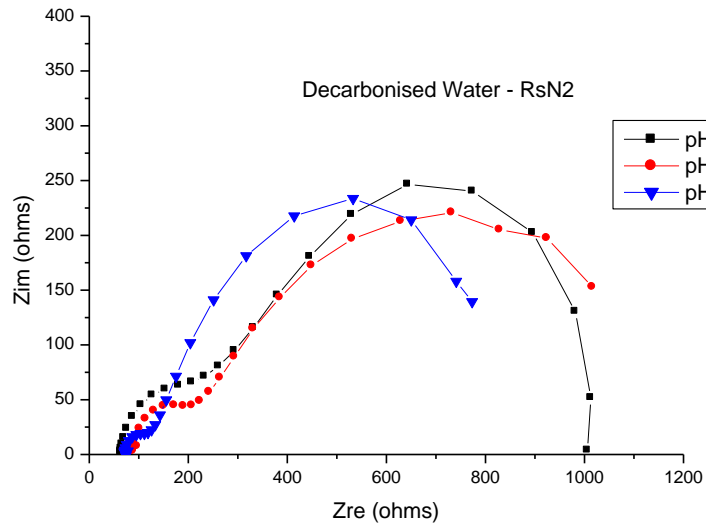


**Figure A.1 :** Nyquist plot for carbon steel in decarbonised water at 25 °C with  $R_sN_2$  at 3 different pH values.

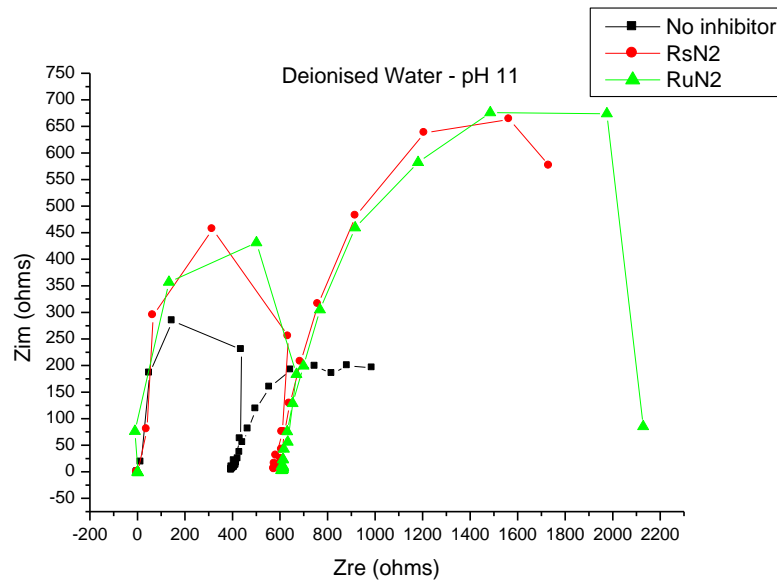


**Figure A.2 :** Nyquist plot for carbon steel in deionised water at 25 °C in absence and presence of  $R_uN_2$  and  $R_sN_2$  at pH=11.

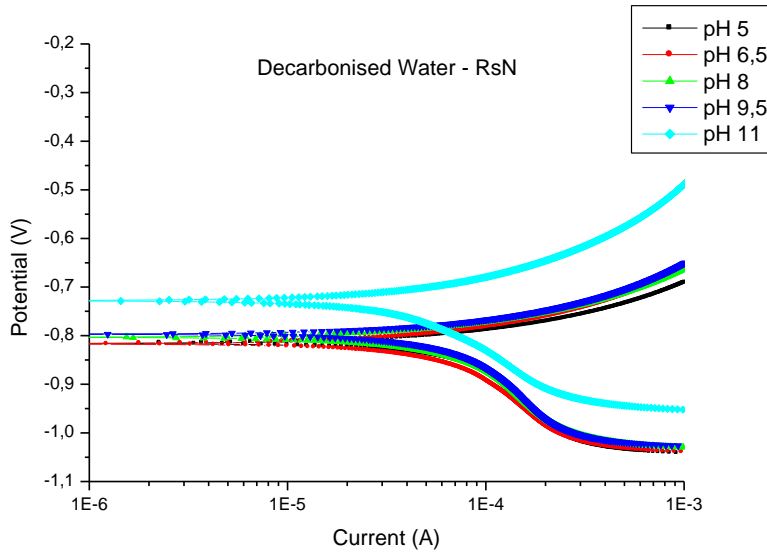


**Figure A.3 :** Potentiodynamic polarization curves for carbon steel in decarbonised water at 25 °C with RsN at different pH values.

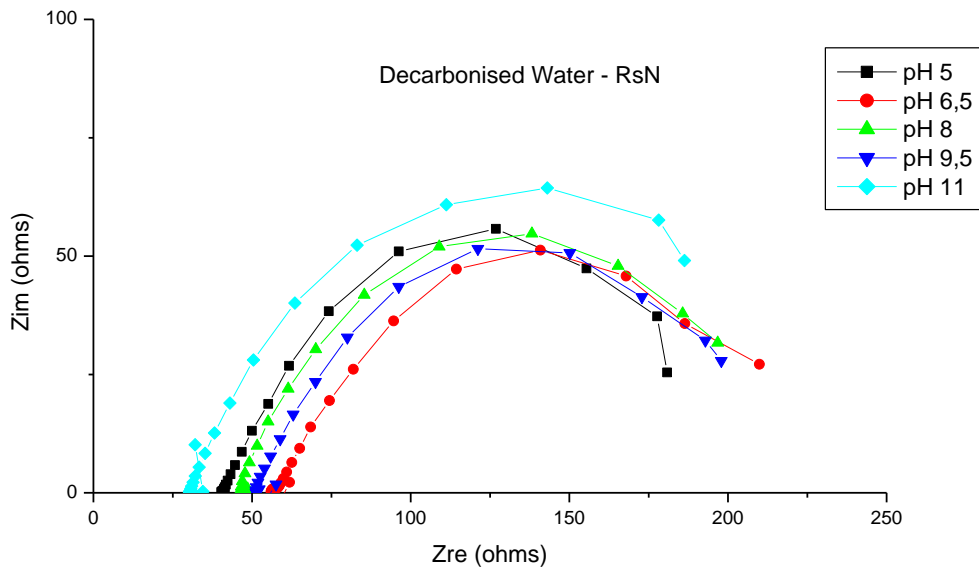


**Figure A.4 :** Nyquist plot for carbon steel in decarbonised water at 25 °C with RsN at different pH values.

**Table A.1** : Polarization parameters for carbon steel in decarbonised water at 25 °C with  $R_sN$  at different pH values.

Decarbonised Water		$R_sN$						
pH	-E <sub>corr</sub> (mV vs. Ag/AgCl)	I <sub>corr</sub> ( $\mu A \cdot cm^{-2}$ )	$\beta_a$ (mV)	$\beta_c$ (mV)	R <sub>p</sub> ( $\Omega cm^2$ )	IE <sub>Icorr</sub> (%)	IE <sub>Rp</sub> (%)	Chi-Squ.
5.0	816	23	91	490	553	6	-43	<b>0.96</b>
6.5	817	21	115	460	514	12	-62	<b>1.03</b>
8.0	804	19	97	392	593	-41	-33	<b>0.8</b>
9.5	797	22	98	549	553	-7	-21	<b>0.98</b>
11.0	731	15	141	362	593	40	-20	<b>0.96</b>

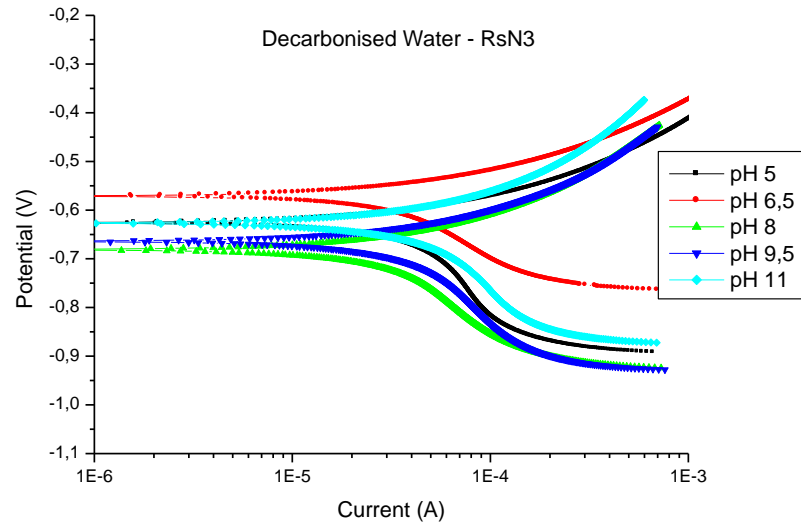


**Figure A.5** : Potentiodynamic polarization curves for carbon steel in decarbonised water at 25 °C with  $R_sN_3$  at different pH values.

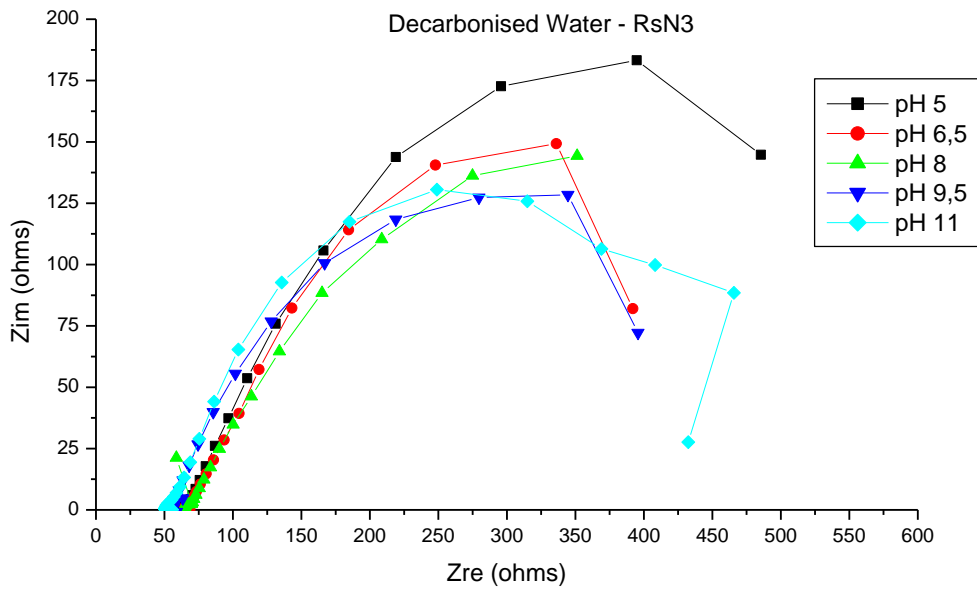


**Figure A.6 :** Nyquist plot for carbon steel in decarbonised water at 25 °C with  $R_sN_3$  at different pH values.

**Table A.2 :** Polarization parameters for carbon steel in decarbonised water at 25 °C with  $R_sN_3$  at different pH values.

Decarbonised Water		$R_sN_3$						
pH	-E <sub>corr</sub> (mV vs. Ag/AgCl)	I <sub>corr</sub> ( $\mu A.cm^{-2}$ )	$\beta_a$ (mV)	$\beta_c$ (mV)	R <sub>p</sub> ( $\Omega cm^2$ )	IE <sub>I<sub>corr</sub></sub> (%)	IE <sub>R<sub>p</sub></sub> (%)	Chi-Squ.
5.0	627	16	143	1145	<b>1,659</b>	<b>33</b>	<b>52</b>	<b>1.07</b>
6.5	571	13	125	496	<b>1,304</b>	<b>43</b>	<b>36</b>	<b>0.97</b>
8.0	681	13	158	690	<b>1,146</b>	<b>4</b>	<b>31</b>	<b>1.03</b>
9.5	664	16	161	789	<b>1,343</b>	<b>26</b>	<b>50</b>	<b>1</b>
11.0	627	32	268	3533	<b>1,620</b>	<b>- 28</b>	<b>56</b>	<b>1.19</b>

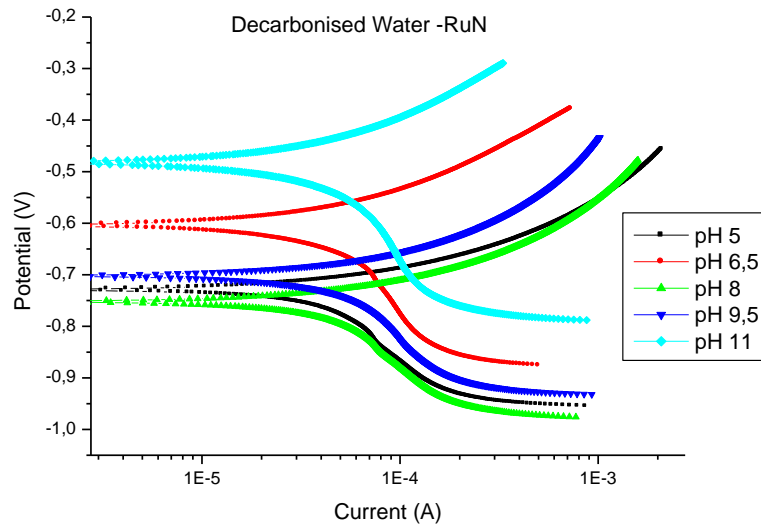


**Figure A.7** : Potentiodynamic polarization curves for carbon steel in decarbonised water at 25 °C with RuN at different pH values.

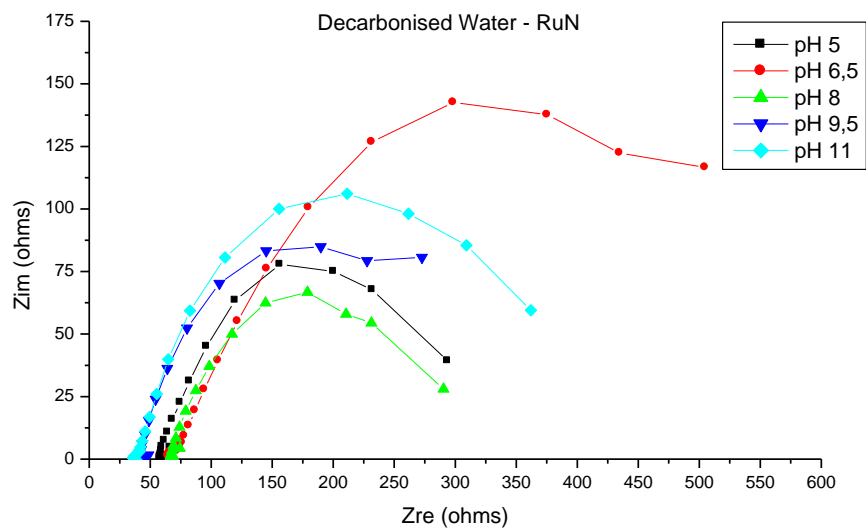


**Figure A.8** : Nyquist plot for carbon steel in decarbonised water at 25 °C with RuN at different pH values.

**Table A.3** : Polarization parameters for carbon steel in decarbonised water at 25 °C with RuN at different pH values.

Decarbonised Water		RuN						
pH	-E <sub>corr</sub> (mV vs. Ag/AgCl)	I <sub>corr</sub> ( $\mu\text{A}\cdot\text{cm}^{-2}$ )	$\beta_a$ (mV)	$\beta_c$ (mV)	R <sub>p</sub> ( $\Omega\text{cm}^2$ )	IE <sub>I<sub>corr</sub></sub> (%)	IE <sub>R<sub>p</sub></sub> (%)	Chi-Squ.
5.0	729	15	99	700	909	38	13	<b>0.5</b>
6.5	604	15	175	457	1.422	37	42	<b>0.05</b>
8.0	752	17	107	705	909	-24	13	<b>1.09</b>
9.5	702	27	157	3866	869	-30	23	<b>1.12</b>
11.0	481	31	369	2130	1.304	-23	45	<b>0.98</b>

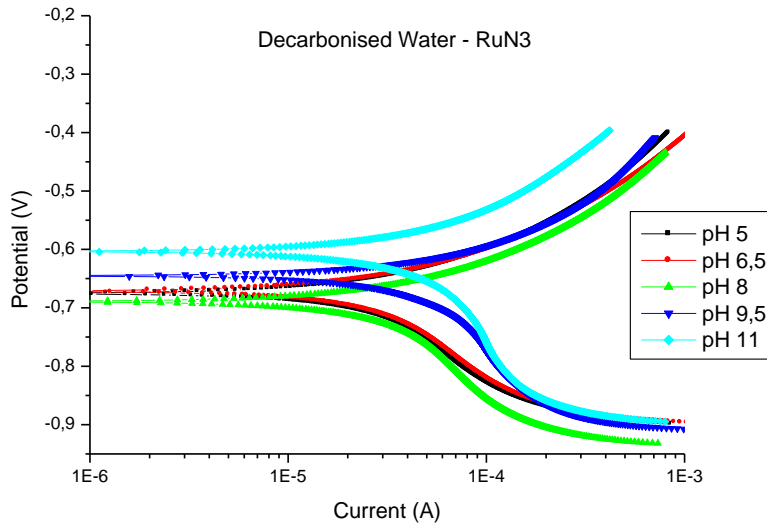


**Figure A.9** : Potentiodynamic polarization curves for carbon steel in decarbonised water at 25 °C with RuN<sub>3</sub> at different pH values.

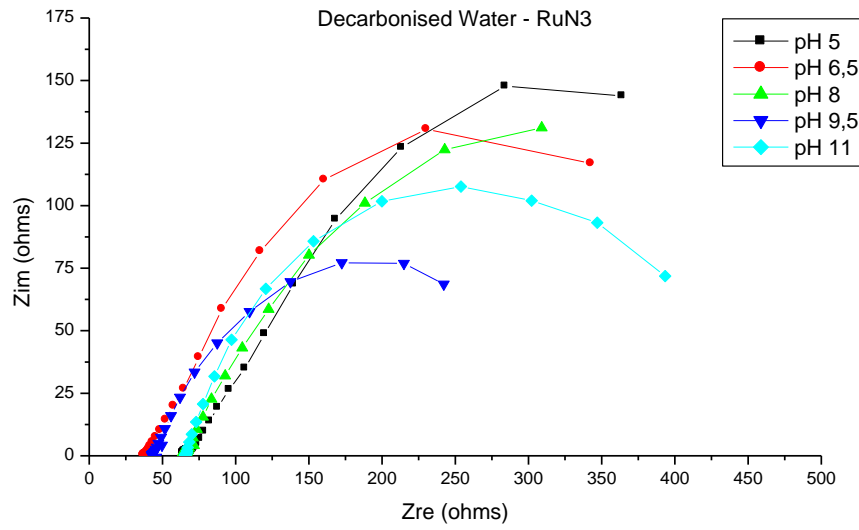


**Figure A.10** : Nyquist plot for carbon steel in decarbonised water at 25 °C with RuN<sub>3</sub> at different pH values.

**Table A.4** : Polarization parameters for carbon steel in decarbonised water at 25 °C with RuN<sub>3</sub> at different pH values.

Decarbonised Water		Ru <sub>3</sub> N <sub>3</sub>						
pH	-E <sub>corr</sub> (mV vs. Ag/AgCl)	I <sub>corr</sub> (μA.cm <sup>-2</sup> )	β <sub>a</sub> (mV)	β <sub>c</sub> (mV)	R <sub>p</sub> (Ωcm <sup>2</sup> )	IE <sub>I<sub>corr</sub></sub> (%)	IE <sub>R<sub>p</sub></sub> (%)	Chi-Squ.
5.0	675	20	218	2,315	553	20	33	<b>0.02</b>
6.5	671	13	164	616	514	44	32	<b>0.33</b>
8.0	689	13	151	565	593	6	66	<b>1.65</b>
9.5	645	24	176	1,168	553	-13	15	<b>1.04</b>
11.0	602	25	222	1,496	593	2	28	<b>1.24</b>





## **CURRICULUM VITA**

### **PERSONAL DETAILS**

**Full name:** İpek Öztürk

**Place and date of birth:** 14th June 1983, Ankara-Turkey

**Permanent Address:** Narcity Konutları A1 Blok Daire 40  
Maltepe- Istanbul

**Telephone:** 00 90 216 372 17 87

**Mobile Phone:** 00 90 533 306 87 26

**E- mail:** ipekztrk@yahoo.com



### **EDUCATION**

**2008- 2010 :** Polymer Science and Technology – Interdisciplinary Master Program at Istanbul Technical University, Istanbul - Turkey

**2001-2006 :** Chemical Engineering at Istanbul Technical University, Istanbul – Turkey (1<sup>st</sup> Degree in Chemical Engineering Department, GPA: 3.77 / 4.0). (1<sup>st</sup> Degree in Chemical and Metallurgy Faculty, GPA: 3.77 / 4.0).

**1994-2001 :** Sırrı Yırcalı Anatolian High School, Balıkesir -Turkey (5<sup>th</sup> Degree).

### **WORK EXPERIENCE**

**Feb. 10 – :** Technical and Marketing Manager at Water Treatment Department of BKG Water Solutions – Turkey & ME.

**June 09 – Feb. 10:** Marketing Manager at Water Treatment Department of BKG Water Solutions – Turkey & ME.

**Jan. 08 – June 09:** Marmara Region Sales Manager at Water Treatment Department of BKG Water Solutions – Turkey (JV of BK Giulini GmbH with Henkel Water Treatment Department).

**July 06 – Jan. 08 :** Marmara Region Sales Engineer at Water Treatment Department of Henkel.

**Summer 2005:** Internship at Anadolu Efes Beer and Malt Industry, Istanbul-Turkey.

**Summer 2005:** Internship at Ege Chemical Company, Istanbul-Turkey.

**Summer 2004:** Internship at Plastifay Chemical Industry, Istanbul - Turkey.

### **PROJECTS**

**Jan. 06 - May 06 :** Production of Modified Lipid with Conjugated Trienoic Acid, Graduation Thesis Project.

**Oct. 05 - May 06:** Design of Hydrogen Fluoride Production Plant-Slurry Process, Graduate Design Course Project.

**Jan. 10 – Dec. 10:** Investigation the Effect of Film Forming Amines on the Corrosion Inhibition of Carbon Steel, M.Sc. Graduation Thesis.